FACULTY OF SCIENCE AND TECHNOLOGY

MASTER'S THESIS

Study programme/specialisation: Petroleum Geosciences Engineering	Spring semester, 2020 Confidential
Author: Bjarte Usken	…………………………………………. (signature of author)

Programme coordinator: Alejandro Escalona, UiS

Supervisor(s):
Bjørn Kåre Lotsberg Bryn, Spirit Energy
Dora Luz Marin Restrepo, UiS
Ingrid Carita Augustsson, UiS

Title of master's thesis:

Provenance Evaluation of Lower Cretaceous in the Stappen High Area and Implications for Reservoir Development

Credits: 30

Keywords: Provenance Barents Sea Fingerdjupet Subbasin Lower Cretaceous	Number of pages: 64 + supplemental material/other: ………… Stavanger, 27.07.2010 / 2020 date/year

Title page for Master's Thesis
Faculty of Science and Technology

Abstract

Southeast directed fluvio-deltaic systems transported across Svalbard during Early Cretaceous are age correlated to southeast progradation deposits in the in Fingerdjupet Subbasin. Both local (few km) and distal (>300 km) source regions has been suggested for this system. The recent exploration well 7321/4-1 drilled on the flank of the basin encountered sandstones in the Lower Cretaceous interval. This well data has not been implemented in the previous studies.

This study uses detrital zircon U/Pb geochronology from well 7321 / 4-1 and 7322 / 7-1 in the Fingerdjupet Subbasin to interpret the source of coarse grain sediments. Palynological analyses, well and seismic data are integrated to interpret the distribution of the sandstones encountered in recent well 7321 / 4-1. The aim of this study is to evaluate the provenance of Lower Cretaceous sandstones in encountered by well 7321 / 4-1 and the implications for reservoir development in the Fingerdjupet Subbasin.

Two seismic units (SU1 and SU2) is defined based on seismic downlap terminations and seismically guided well correlations. The SU1 shows wedge-shaped packages thickening towards fault in the central part of the basin. The SU2 consist of the encountered by well 7321/4-1 and is characterized by shelf-edge clinoforms that prograded southeast into the basin. The dominant detrital zircon age populations in SU2 unit from well 7321 / 4-1 is: (1) 2.6-2.75, (2) 1.7-1.5 Ga and (3) 1.2-1 Ga. Only a few Detrital Zircon ages were measured in well 7322 / 7-1 and it was thus not possible to compare the result with this well. By comparing Detrital Zircon Ages from the SU2 unit with Lower Cretaceous formations on Svalbard and in the Barents shelf, it became clear that both regions contain similar dominant age distribution.

The source of sediment is interpreted to originate from north Greenland and/or Arctic Canada based on the similar detrital age distribution and the southwestern progradation direction of the clinoforms. Seismic interpretation suggests that the well 7321 / 4-1 penetrates the topsets segment of the shelf-edge clinoforms, which interpreted as a potential sandy system in the topsets.

Table of Contents

List of Figures

List of Tables

1 INTRODUCTION

The western Barents shelf borders the mainland of northern Norway in the south, Northeast Atlantic Ocean in the west and is exposed in the Svalbard archipelago in the north-western corner (Fig. 1.1a) (Smelror et al., 2009). The northern margin of the Barents shelf is interpreted to have been uplifted during Cretaceous time (e.g. Maher, 2001; Polteau, 2015). Outcrop studies on Svalbard suggests that a northern tilt of the shelf triggered a southeast evolving paleoshoreline during Barremian (Early Cretaceous, Steel & Worsley, 1984; Gjeldberg & Steel, 1995; Worsley, 2008; Midtkandal and Nystuen, 2009). This regressive system consists of sandy fluvio-deltaic deposits visible in outcrops across Svalbard and are interpreted to extend into the south-western Barents shelf (Fig. 1.1b, e.g. Grundvåg et al., 2017; Midtkandal et al., 2019).

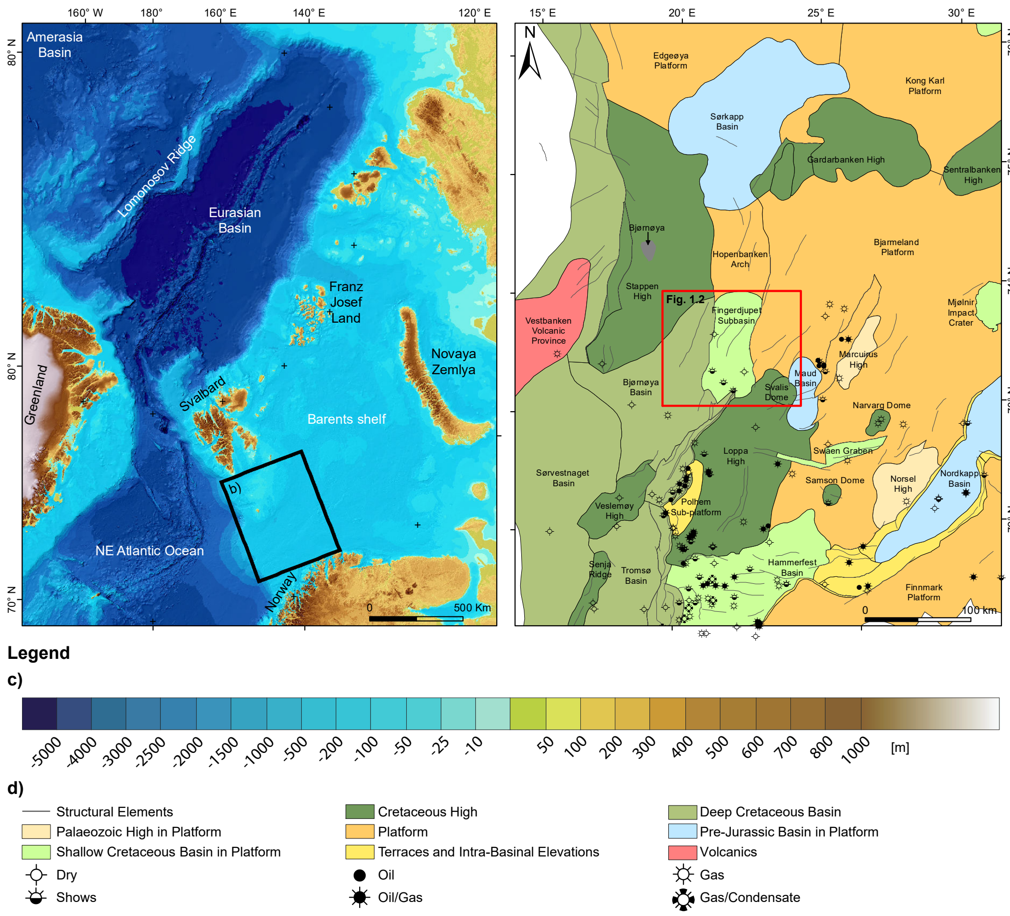

Fig. 1.1 Structural elements in the Arctic and the southwestern Barents shelf *a) Map view of topographic and bathymetric features in the Arctic region after Jakobsson et al., (2012). The coordinate system used is the WGS 1984 with polar stereographic projection. The square marks the map area in Fig. 1b. b) Regional map of the southwestern Barents shelf showing the structural elements based on NPD (2020). The square marks the map area in Fig. 1.2. c) Color coding used in Fig. 1a and the corresponding meters above and below mean sea level. d) Color coding and well symbols used in Fig. 1b.*

The terminal deposits of the regressive system observed on Svalbard is age correlated to a southeast directed clinoform system in the Fingerdjupet Subbasin and on the western Bjarmeland Platform (Grundvåg et al., 2017; Midtkandal et al., 2019). Recent exploration well 7322/7-1 targeted topsets of southeast prograding, delta-scale (25-80 m), clinoforms in the Fingerdjupet Subbasin (Fig. 1.2 , Bryn et al. 2019). The well penetrated the topsets less than one kilometer away from the delta-scale foresets which were interpreted to be of coarse-grianed lithology based on the high angle foresets (10–12°) and modern quantitative clinoform analysis (Bryn et al., 2019, Patruno & Helland-Hansen, 2018). The reservoir proved to be gas-charged siltstones of Barremian age with a non-commercial volume. Bryn et al. (2019) studied the reservoir potential of clinothems in the Fingerdjupet Subbasin and argued that the high angle foresets near the well may still be sand-prone. Thus, the reservoir potential of the Barremian clinoform system in the Fingerdjupet Subbasin remains unproven. Furthermore, Bryn et al. (2019) concluded that linking a coarse-grained source area to clinoforms of coarse grain character can be an important first step towards predicting the reservoir potential of the Barremian clinothems.

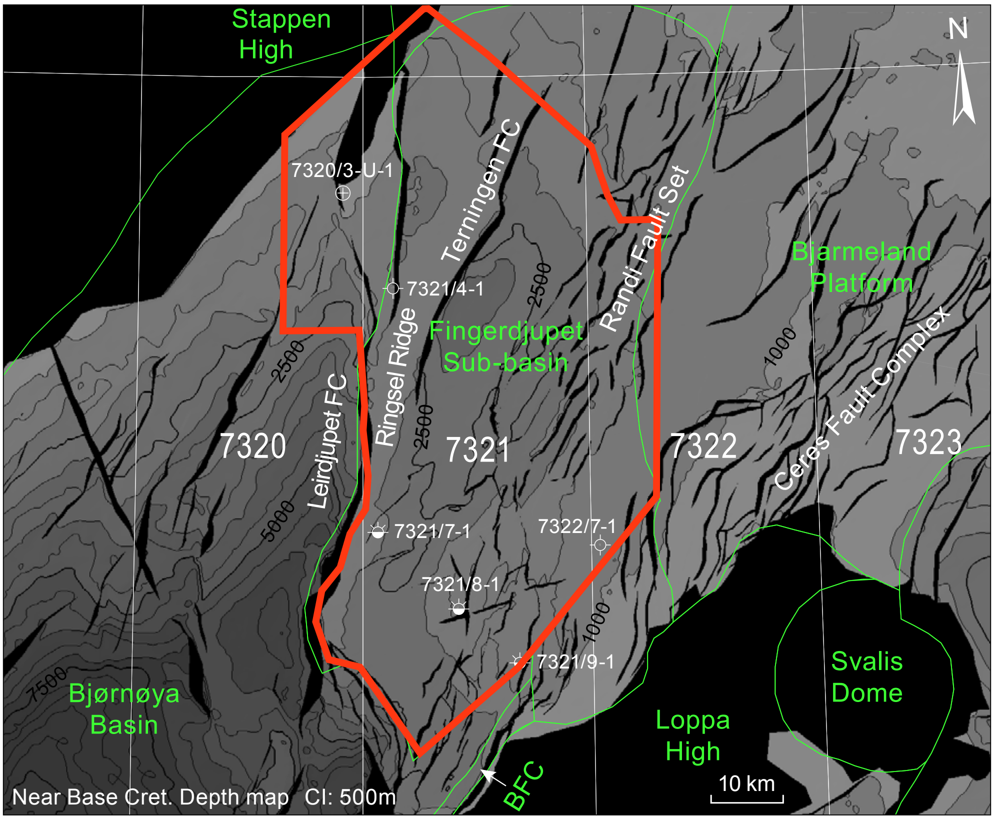

Legend

Structural Elements

Study Area

Fig. 1.2 Study Area. *Depth structure map of a reflector near the Base Cretaceous Unconformity (edited from Bryn et al. (2019)). The study area is illustrated in red color. For location of map see Fig. 1.1b.*

Three source regions have been suggested to supply coarse grain sediments to the southeast directed clinoform system observed in the Barents shelf. (1) A western region corresponding to north-eastern Greenland (Grundvåg et al., 2017), (2) a north-western region corresponding to Crockerland (Paleohigh in northern Canada, Midtkandal et al., 2019) and (3) the Stappen High, located at the western margin of the south-western Barents shelf (Fig. 1.1b, Bryn et al., 2019). Hence, the source of sediments is poorly constrained.

Recent exploration Well 7321/4-1 (2018) was drilled on the Ringsel Ridge, a horst structure defined by the Leirdjupet Fault Complex (LFC) and the Terningen Fault Complex, in the Fingerdjupet Subbasin (Fig. 1.2). This well targeted Jurassic and Triassic sandstones but also encountered sandstones in the Lower Cretaceous interval (B.K. Bryn. 2019. Pers. Comm.). This well data has not been implemented by previous studies.

This study uses biostratigraphic data and detrital zircon U/Pb geochronology (provided by GEUS) to interpret the age and origin of the Lower Cretaceous sandstones in well 7321/4-1 and the siltstones in well 7322/7-1. Biostratigraphy and petrophysical logs from the southern wells (7321/7-1, 7321/8-1 and 7321/9-1, Fig. 1.2) and seismic data is used to interpret the distribution of the sandstones encountered in well 7321/4-1. The aim of this study is to evaluate the provenance of Lower Cretaceous sandstones on the Ringsel Ridge and the implications for reservoir development in the Fingerdjupet Subbasin.

2 GEOLOGICAL SETTING

2.1 Potential Source Areas

During the Early Cretaceous a widespread epicontinental sea (Boreal Sea) covered the present day Barents shelf, parts of northeast Greenland and Sverdrup Basin. The northwest hinterlands facing the Barents shelf were Svalbard, Pearya and Laurentia (Fig. 2.1). The Baltic plate was situated along the south-western margin and Siberia in the south-eastern margin of the Barents shelf (e.g. Torsvik et al., 2002; Torsvik et al., 2012, Fig. 2.1,).

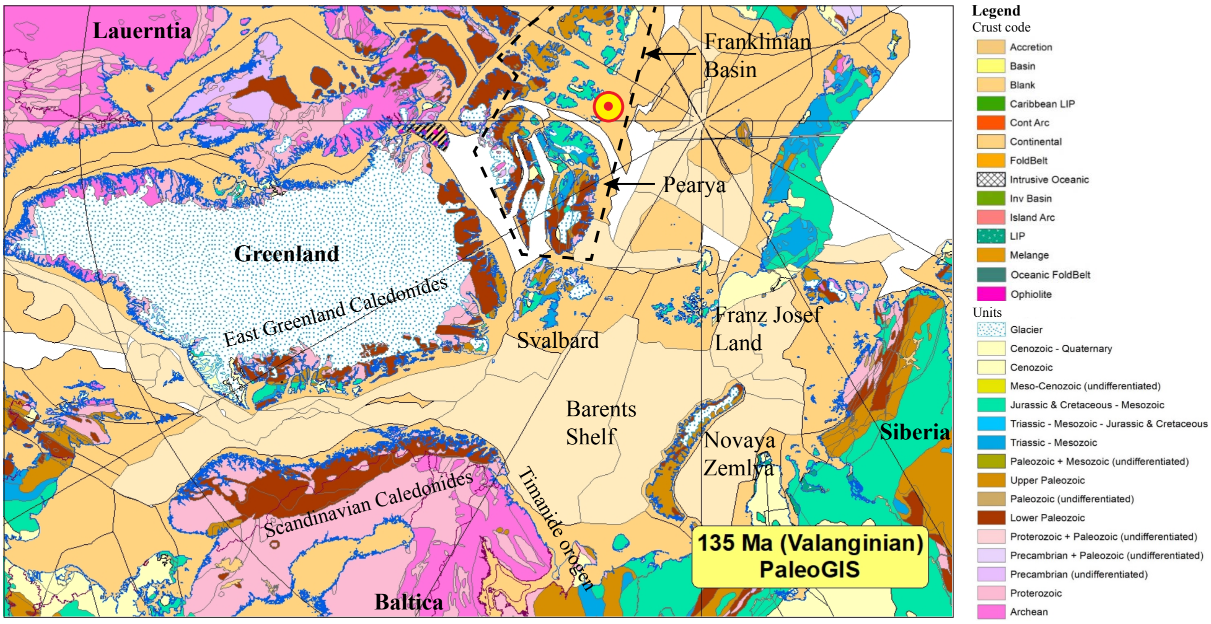

Fig. 2.1 Plate Reconstruction (Valanginian, 135Ma) *Plate tectonic reconstruction of the Barents shelf and basement geology (figure modified from LOCRA Final Report. (2017).*

The crystalline basement of the northeast Laurentia interior consists of Archean cratons, reworked Archean rocks and intervening Palaeoproterozoic orogenic belts (Fig. 2.1, 2006). Towards the boarder of Franklinian Basin (Fig. 2.1), the basement is of Archean to early Proterozoic age with intrusive igneous rocks of mafic to felsic composition, in addition to Proterozoic sedimentary and volcanic rocks (Trettin, 1991). Large parts of the Laurentia basement in the northern part are covered by Neoproterozoic to Devonian silisiclastic and carbonate rocks in the Franklinian Basin (Fig. 2.1), interpreted to represent a passive margin succession (Dewing et al., 2008).

The Pearya Terrane (Fig. 2.1) is located in the northernmost region of Ellesmere Island (Canada) and has been characterized as an accreted or exotic terrane(relative to the adjacent terranes) along the northern margin of Laurentia (Trettin, 1991). Accretion against the Franklinian Basin has been inferred to occur during the middle Palaeozoic Ellesmerian Orogeny (Malone et al., 2017; Piepjohn & Von Gosen, 2017), interpreted as being the equivalent to the Caledonian Orogeny along the North Canada and Greenland margins (Gasser, 2014; Gee, 2015). The basement in the Pearya Terrane is dominated by metasedimentary rocks and granitoid gneiss (Trettin et al., 1991) of Tonian age (972–962 Ma) (Malone et al., 2017). The basement is overlaid by Neoproterozoic to Middle Ordovician metasedimentary and metavolcanic rocks (Fig. 2.1). These deposits also includes igneous intrusions of ultramafic-mafic composition aged 481 Ma and younger felsic intrusions of 462 Ma age. The intrusions were followed by nearly unmetamorphosed volcanic, siliciclastic and carbonate sedimentary rocks of middle Ordovician to late Silurian age (Trettin, 1991).

The northeastern margin of Laurentia is dominated by the 1300 km long East Greenland Caledonides (Fig. 2.1, Gee et al., 2008; Higgins et at., 2008). As a result of the collision of Laurentia and Baltica which culminated during the latest Silurian–early Devonian (Gee et al., 2008). The East Greenland Caledonides can be divided into three segments: northern (80–82°N), central (76–80°N) and southern (70–76°N) (Gasser, 2014). The crystalline basement is dominated by gneisses and metagranitic rocks (2 - 1.85 Ga) which are exposed in the central segment (Kalsbeek et al., 1999; 2008). Caledonian thrust sheets are composed of Paleoproterozic to Neoproterozoic rocks of mainly siliciclastic and sedimentary carbonate, volcanic and metasedimentary rocks (Fig. 2.1, Higgins et al., 2008). While Lower Paleozoic sediments occupies large parts of western foreland and the upper sheets of the orogenic belt in the northern and southern segments (Smith and Rasmussen, 2008). Caledonian granites is only present in the southern segment of the orogen (Gasser, 2014).

Svalbard (Fig. 1.1a, Fig. 2.1) can be divided into the Eastern (Western Ny Friesland and Nordaustlandet terranes), Northwestern and Southwestern basement terranes (Gee and Teben'kov, 2004). The relative origins of the different terranes are poorly constrained (e.g. Gasser, 2014). The oldest rocks on Svalbard are late Archean to late Paleoproterozoic (c. 2.71 - 1.75 Ga) granitic gneisses found in the Eastern terrane (Western Ny Friesland) (Johansson et al. 1995; Wellman al., 2001;). Apart from the gneisses, the Eastern terrane is dominated by Mesoproterozoic metasedimentary and metavolanic rocks, intruded by Tonian and subsequent Silurian aged granitoids (McClelland et al., 2019), overlain by Neoproterozoic to Early Palaeozoic siliciclastic and carbonate sedimentary rocks (Witt-Nilsson et al., 1998; Sandelin et al., 2001). The Northwestern Terrane is dominated by late Mesoproterozoic to Neoproterozoic metasedimentary rocks intruded by Tonian (c. 0.96 Ga) and Silurian (c. 0.42 Ga) aged granitoids (Petterson et al., 2009). The Southwestern Terrane constitutes Mesoproterozoic and Neoproterozoic ortho gneisses (c. 1.2 Ga and 0.95Ga) (Majka et al., 2014) and metaclastic rocks subjected to metamorphism reaching upper amphibolite facies conditions during Torellian (c. 640 Ma) (e.g., Majka et al 2010) and eclogite facies during Ordovician (e.g., Kosminska et al., 2014). These units are followed by Ordovician to Silurian siliciclastic and carbonate sedimentary rocks with no evidence of Silurian magmatism or high-grade metamorphism (Gasser & Andresen, 2013).

The interior of north-western part of Baltica (Fig. 2.1) is dominated by Archean (3.5 – 2.73 Ga) granitoid–gneiss (Holtta et al, 2012), Paleoproterozoic (2.44 - 1.92 Ga) metavolcanic and metasedimentary rocks (Fig. 2.1, Lahtinen et al., 2010; Koykka et al., 2019). During the latest Neoproterozoic Timanide orogen (610-640 Ma), the northeastern margin of the Baltica experienced subduction and accretion (Pease, 2011). Late Neoproterozoic metaclastic rocks along the orogenic belt and granitoids of same age are common along the Timanide segment in Arctic Russia (Lorenz et al., 2004). The Timanide structures in the northern Norway are overprinted by the Scandinavian Caledonides in the north-western margin of Baltica (Fig. 2.1, Pease et al., 2014). The Scandinavian Caledonides are interpreted to extends into the Barents Sea region (e.g. Corfu et al., 2014). Along the length of Scandinavian Caledonides, Archaean to Neoproterozoic rocks of Baltica are followed by metaigneous and metasedimentary rocks of Neopoterozoic and younger age, interpreted to represent the thrust sheets of the orogenic belt. During the closure of the Iapetus Ocean (paleoocean between Laurentia and Baltica), the Batic plate is interpreted to be subducted below Laurentia, stacking the Baltica crust, followed by Iapetan oceanic crust and Laurentia crust (Roberts and Gee, 1985; Corfu et al., 2014). The subduction phase is constrained to Mid-Silurian and the continent–continent collision phase, referred to as the Scandian Orogeny, to mid-Silurian to late Devonian (430-380 Ma, Corfu et al., 2014).

The Uralian Orogeny closed the Uralian Ocean along the eastern margin of Baltica (Fig. 2.1, Arctic Russia) during the Carboniferous-Early Triassic times. By the end of Triassic, erosional products covered the entire eastern Barents shelf (Petrov et al., 2008). The Pai-Khoi-Novaya Zemlya fold belt is a segment of the orogenesis (Korago et al., 2004) and was deformed during thrusting of Novaya Zemlya (Fig. 1.1a, Fig. 2.1) above the Barents plate in the Triassic times (Petrov et al., 2008). The basement of the Novaya Zemlya Archipelago is dominated by Meso- to Neoproterozoic metasedimentary rocks and associated igneous intrusions. The igneous intrusions are of mafic to felsic composition and the oldest granite is dated as 1300 Ma (Korago et al., 2004).

2.2 Tectonic Framework

North-northwest-oriented structural trends of the Scandinavian Caledonides are inherited in the basement of the Barents shelf (e.g Gernigon and Brønner, 2012). These lineaments are interpreted to have played a significant role in the generation of the present-day rift systems in the Barents shelf (Fig. 1.1b, Doré et al., 1991; Gudlaugsson et al., 1998; Ritzmann and Faleide., 2009; Faleide et al., 2010; Gernigon and Brønner, 2012). The post-Caledonian evolution of the shelf can be divided into three main extensional phases: late Paleozoic, Late Jurassic to Early Cretaceous and early Cenozoic. In addition to two uplift phases during Early Cretaceous and Palaeogene to recent (Faleide et al., 1993; Dore,1995; Anell et al., 2014;Faleide et al., 2015; Riis & Fjeldskaar 1992; Riis 1996; Henriksen et al., 2011).

The tectonic setting during the Early Cretaceous was influenced by the opening of the Amerasia Basin (Grantz et al., 2011) and the North Atlantic rift system (Faleide et al., 1993). The breakup of the Amerasia Basin and the associated High Arctic Large Igneous Province (HALIP, Petrov et al., 2016) is interpreted to cause uplift of the northern margin of the Barents shelf (Gjelberg & Steel, 1995; 2012; Worsley, 2008; Midtkandal & Nystuen, 2009). This is supported by southeast directed fluvio-deltaic and clinoform systems on Svalbard and in the south-western Barents shelf, respectively (e.g. Midtkandal & Nystuen, 2009; Midtkandal, 2019). Intrusive and extrusive igneous rocks on Svalbard and Franz Josef Land suggest that the uplift peaked around latest Barremian (Maher, 2001; Corfu et al., 2013; Polteau, 2015).

The North Atlantic rift system, between Greenland and Baltica (Fig. 2.1), continued into the present day south-western Barents shelf during the Late Jurassic to Early Cretaceous. The earliest Cretaceous (Berresian–Hauterivian) structuring is characterized by north-northeast trending normal faults. Large throws and deep depocenters defined by the Harstad, Tromsø and Bjørnøya basins at the present day western margin (Fig. 2.2b, Faleide et al., 1993). Strike-slipe movements accompanying the normal displacement are also recognized, especially in the eastern margin of the Bjørnøya Basin (Bjørnøyrenna Fault Complex). Further east, the north to northeast trending faults delveloped significant subsidence in the estern flank of the Bjørnøya Basin and established the Fingerdjupet Subbasin (Fig. 1.1b,Fig. 2.2, Serck et al., 2017). Minor fault activity is also recognized in the Hoop Fault Complex on the Bjarmeland Platform (Fig. 2.2a, Faleide et al., 2019). The fault activity is suggested to have terminated in the northernmost part of the Barents shelf (Faleide et al., 1993), where compressional tectonic activity occurred (Kairanov et al., 2018). North oriented fault activity on Svalbard is suggested to be expressed as collapse structures within delta fronts on the eastern Spitsbergen (Onderdonk & Midtkandal, 2010).

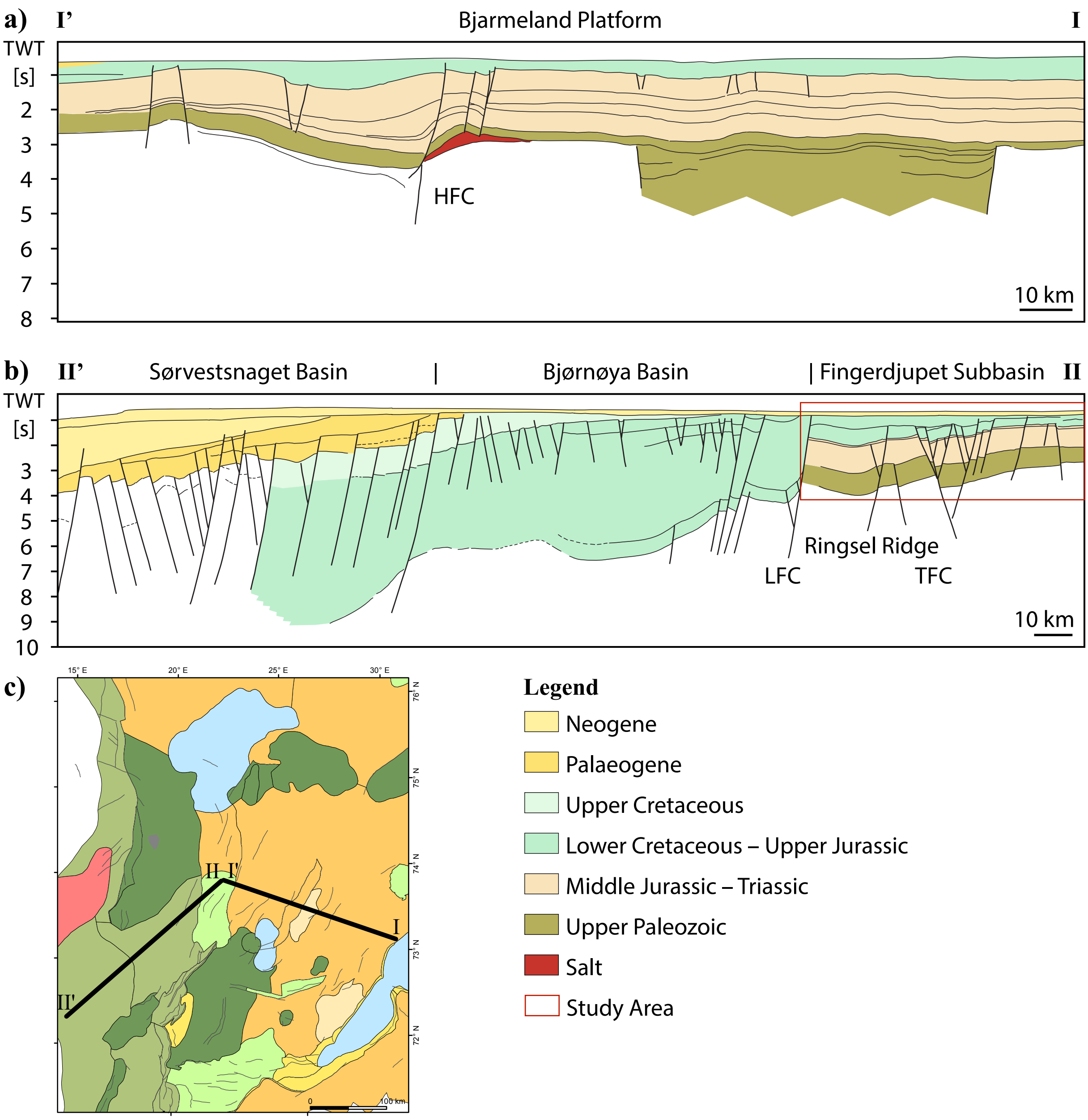

Fig. 2.2 Regional Seismic Line *Regional seismic line showing the structural elements of the Fingerdjupet Subbasin in a regional context (figure modified from Faleide et al., 2015).*

Tectonic quiescence is inferred during the Barremian in the Bjørnøya Basin (Blaich et al., 2017), Fingerdjupet Subbasin (Fig. 1.1b, Fig. 2.2b, Serck et al., 2017) and in the Hoop area on the Bjarmeland Platform (Fig. 2.2a, Faleide et al., 2019). Crustal stretching and thinning in Tromsø and Bjørnøya basins from the earliest Cretaceous fault activity is inferred to have caused uplift and sub-aerial exposure of the Loppa High during early Barremian (Indrevær et al., 2016). The uplift has been suggested to have occurred through different stages from Late Jurassic/earliest Cretaceous times (Gabrielsen et al., 1990; Glørstad-clark, 2011) and to have reached its peak during the Barremian (Indrevær et al., 2016). The differential uplift was accompanied by inversion tectonics in the faults surrounding the Loppa High and in the adjacent Hammerfest Basin (Fig. 1.1b, Indrevær et al., 2016). Indrevær et al. (2017) suggests that the uplift model for the Loppa High (phase change driven vertical movements) also could explain the uplift of the Stappen High, but the timing of the uplift phase developing the present-day Stappen High is poorly constrained (Anell et al., 2016). The present structural configuration of the Stappen High is suggested to have developed during Cretaceous–Cenozoic (Anell et al., 2016) and early Cenozoic (Faleide, 1993; Worsley et al., 2001, Blaich et al., 2017).

A second extensional event occurred during Aptian, caused renewed fault activity along north-northeast trending faults. Previous established depocenters such as the Tromsø Basin, Bjørnøya Basin and Fingerdjupet Subbasin experienced subsidence (Fig. 1.1b, Fig. 2.2b, Faleide et al., 1993; Blaich et al., 2017; Serck et al., 2017) , as well as the Hoop area on Bjarmeland Platform (Fig. 2.2a, Faleide et al., 2019). The Albian succession is characterized by post-rift subsidence and rapid infill of previous established paleotopography with increasing magnitude towards the western basins (Faleide et al., 1993).

2.3 Stratigraphy

Svalbard

The Lower Cretaceous succession in Svalbard consists of Rurikfjellet (Valanginian–Hauterivian/early Barremian), Helvetiafjellet (Barremian–early Aptian) and Carolinefjellet formations (early Aptian–Albian) (Mørk et al., 1999, Fig. 2.3). The base of the Lower Cretaceous succession is a regional marker (Dypvik et al., 2017) interpreted to be age equivalent to the Base Cretaceous Unconformity (BCU) offshore in the Barents shelf (Fig. 2.3, Grundvåg et al., 2017). The Rurikfjellet Formation (Fig. 2.3) is dominated by open marine shales that pass vertically into shallow marine, delta-front sandstones in the southeast Svalbard. The coarsening upwards trend are interpreted as a regression induced by the uplift and southern tilt of Svalbard (Gjelberg and Steel, 1995). The source of coarse-grained sediments is linked to the west-northwest hinterlands based on the southeast directed paleocurrents and thinning of the unit (Grundvåg et al., 2017). The lower boundary of Helvetiafjellet Formation (Fig. 2.3) is a regional unconformity of Barremian age (Fig. 2.3, ranging from 129−117Ma, Midtkandal et al., 2016; Vicker et al., 2016). The Barremian unconformity has been inferred to represent a subaerial unconformity associated with deep incisions in the south-west Svalbard (Nathorst Land) as a result of increased slope gradient caused by the emerging northern margin of Svalbard (Midtkandal and Nystuen, 2009). The Helvetiafjellet Formation (Fig. 2.3) is subdivided into an extensive sand sheet of the Festningen member followed by the heterolithic Glitrefjellet Member (Midtkandal et al., 2008). The Festingen Member (Fig. 2.3) consists of coarse grain fluvial braided-plain deposits interpreted as a forced regressive unit extending across the entire southern

Spitsbergen (Gjelberg & Steel, 1995). At the southern edge of Spitsbergen, these sandstone packages are interpreted to either pass laterally into marine mudstone (Gjelberg & Steel 1995, 2012) or continue into the Barents shelf (Midtkandal et al. 2009). Southeast paleocurrents indicate that a north-western source region also existed for the Festingen Member (Grundvåg et al., 2017; Midtkanal et al., 2019a). Glitrefjellet Member consists of fluvio-deltaic deposits with alternating mudstones, sandstones and thin coal beds reflecting a tide dominated coast (Gjelberg and Steel, 1995; Midtkandal and Nystuen, 2009). The base of the Carolinefjellet Formation (Fig. 2.3) forms an regional flooding event marking a return from a coast to an open marine shelf environment (Grundvåg et al, 2017). This unit consists of storm-influenced and storm-dominated sand sheets alternating with outer shelf mudstone(e.g. Hurum et al., 2016).

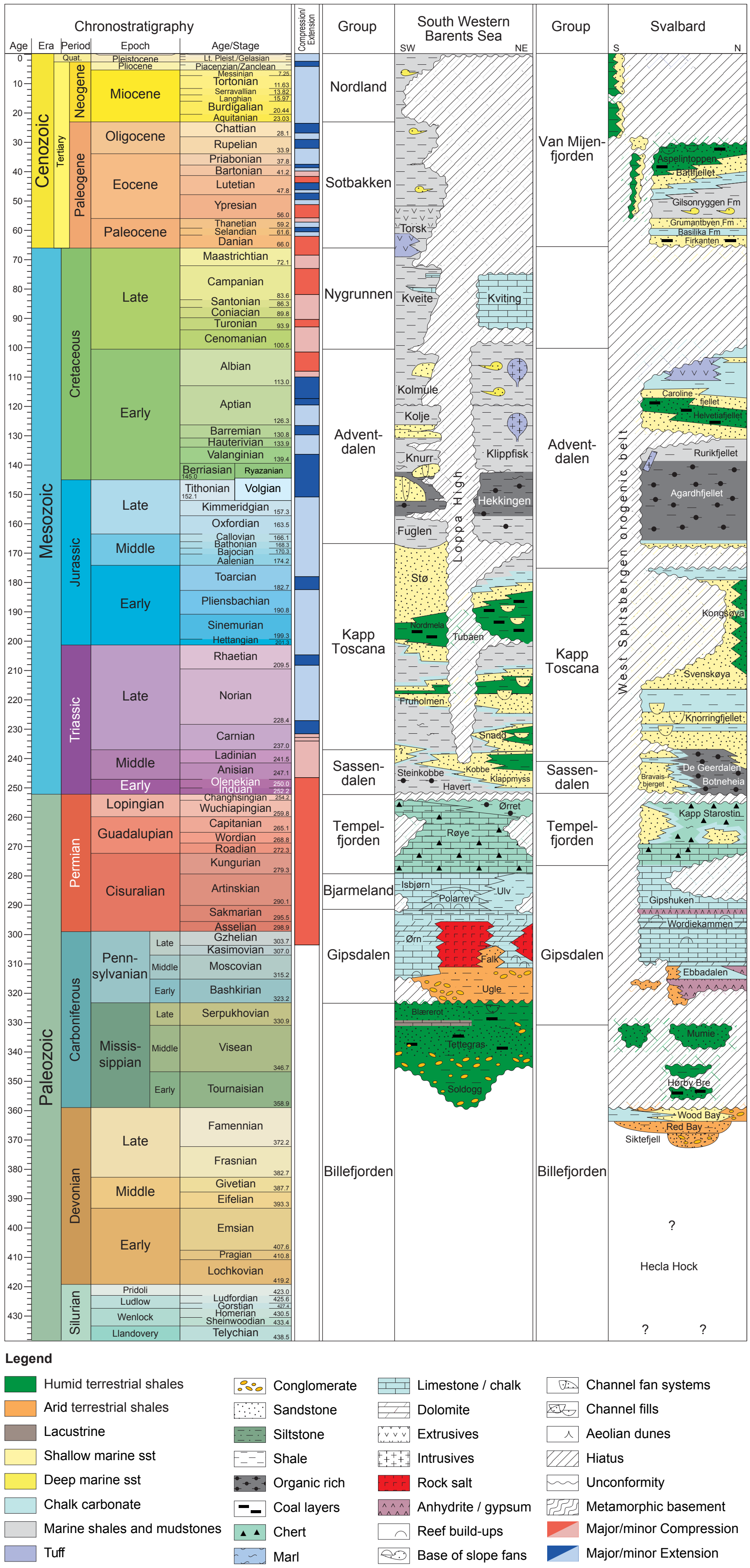

*Fig. 2.3 **Lithostratigraphic chart** Lithostratigraphy of the southwestern Barents shelf and Svalbard (figure modified from Gradstein et al., 2010)*

Barents shelf

The Lower Cretaceous succession in the south-western Barents shelf is divided into the time-equivalent Knurr and Klippfisk formations (Berriasian to early Barremian age), overlain by Kolje Fomation (early Barremian to late Barremian/early Aptian age), followed by Kolmule Formation (Aptian to mid-Cenomanian, Fig. 2.3, Dalland et al., 1988; Mørk et al., 1999). The base of the Lower Cretaceous succession is referred to as the Base Cretaceous Unconformity (BCU), representing a regional unconformity and a correlative conformity (e.g. Mørk et al., 1999). The BCU separates the deep marine deposits of the Upper Jurassic Hekkingen formation and shallow to open marine deposits of the Klippfisk and Knurr formations (Fig. 2.3, Arhus et al., 1990; Faleide et al., 1993; Mørk et al., 1999). The shallow marine Klippfisk formation consists of limestone and marl interpreted as a transgressive condensed deposits on the western platforms and highs, such as on the Ringsel Ridge and on the Bjarmeland Platform (Fig. 1.1b, Fig. 2.2a, Smelror et al., 1998; Århus and Kelly, 1990). The Klippfisk Formation passes laterally into the Knurr Formation (Fig. 2.3) which is composed of open-marine claystone interbedded with thin limestone and dolomite beds (Mørk et al., 1999). Sandstones and conglomerates are also present within the Knurr Formation in shallow marine wedges (well 7120/1-2 and 7122/2-1), deep marine wedges and fans (well 7120/10-1 and 7120/10-2) in the Hammerfest Basin (Fig. 1.1b, e.g. Seldal, 2005; Marin et al., 2018). The coarse grained deposits are interpreted to be erosional products of older rocks on the adjacent Loppa High and the Troms–Finnmark Platform (Fig. 1.1b, Seldal, 2005; Marin et al., 2018). The Klippfisk and Knurr formations are age correlated to the Rurikfjellet Formation in Svalbard (Fig. 2.3, Grundvåg et al., 2017; Midtkandal et al., 2019). The base of the Kolje Formation (Fig. 2.3) has been interpreted as a regional unconformity and correlative conformity (Smelror et al., 1998) referred to as Lower Cretaceous Unconfirmity (LCU) (Midtkanal et al., 2019). The LCU is inferred to represent a regressive surface of marine erosion (Midtkandal et al., 2019). The Kolje Formation is dominated by shales and claystones with minor interbeds of limestone and dolomite interpreted as open marine deposits. Sandstones and siltstones also occur in the upper part of the formation (Dalland et al., 1998). The Kolje Formation is age correlated to the Helvetiafjellet Formation on Svalbard (Fig. 2.3, Grundvåg et al., 2017; Midtkanal et al., 2019a). Kolmule Formation (Fig. 2.3) is also considered to be open marine deposits of claystone and shale, with minor interbeds of thin siltstones in addition to limestone and dolomite stringers (Dalland et al., 1998). Sandstones (well 7120/6-3S, 7120/2-3S and 7220/10-1) and conglomerates (well 7120/6-3S) are also encountered within this unit (NPD, 2020). The Kolmule Formation is considered to be time equivalent to the Carolinefjellet Formation on Svalbard (Fig. 2.3, Grundvåg et al., 2017; Midtkanal et al., 2019).

Lower Cretaceous Clinoforms

Clinoforms within the Lower Cretaceous succession in the south-western Barents shelf are characterized as two large scale progradation systems; a system with an dominant southeast direction and a system with south-west direction.

The southeast-directed system in the south-western Barents shelf extends from the Bjørnøya Basin (Midtkadnal et al., 2019), across Fingerdjupet Subbasin and onto the Bjarmeland platform (Grundvåg et al., 2017; Hinna, 2017; Marin et al., 2017; Bryn et al., 2019; Faleide et al., 2019; Midtkandal et al., 2019). The clinoforms on the eastern Bjarmeland Platform are interpreted to be older than on the western part of the platform and in the Fingerdjupet Subbasin based on onlap relations (Faleide, 2017; Faleide et al., 2019). The southeast-directed system has been interpreted to be of Hauterivian–early Barremian (Grundvåg et al., 2017), Barremian–Aptian (Marine et al., 2017) and Barremian age (Bryn et al., 2019; Faleide et al., 2019; Midtkandal et al., 2019). Several sources located to the west-northwest of the Barents shelf have been suggested for the southeast-directed system, including northeastern Greenland, the Lomonosov high, Chukchi Borderland and Crockerland (Grundvåg et al., 2017; Midtkandal et al., 2019).

The southwest-directed system advanced across almost the entire Bjarmeland Platform and Nordkapp Basin in the estern part of the Barents shelf during Hauterivian–Albian (Grundvåg et al., 2017), Valanginian to middle Cenomanian (Marine et al., 2017), or Aptian–Cenomanian time (Midtkandal et al., 2019) age. The source regions are suggested to be in the east-northeast (Marin et al., 2017; Midtkandal et al., 2019), such as the Taimyr and North Kara region in north Russia (Midtkandal et al., 2019).

3 DATA AND METHODOLOGY

3.1 Data

Well and seismic data

The wells used in this study include five exploration wells (7321/4-1, 7321/7-1, 7321/8-1, 7321/9-1 and 7322/7-1, Fig. 3.1 and) located in the southern and in the north-western part of the study area (Fig. 3.2). All of the wells have chechk shot survey, petrophysical well logs and cuttings descriptions (Table 3.1). Well 7321/4-1 and 7322/7-1 were used for the provenance analysis (detrital zircon U/Pb geochronology) and all of the wells were included for biostratigraphic age dating (Table 3.1). The caliper log (hole diameter) relative to the bit size shows large size difference for wells 7321/7-1, 7321/8-1 and intervals in well 7321/9-1 (Fig. 3.1). Irregular boreholes and large spacing between the tool and borehole wall may cause inaccurate well log readings. Therefore, the readings from 7321/7-1, 7321/8-1, and parts of 7321/9-1, are considered to be less reliable than those from wells 7321/4-1 and 7322/7-1(Fig. 3.1).

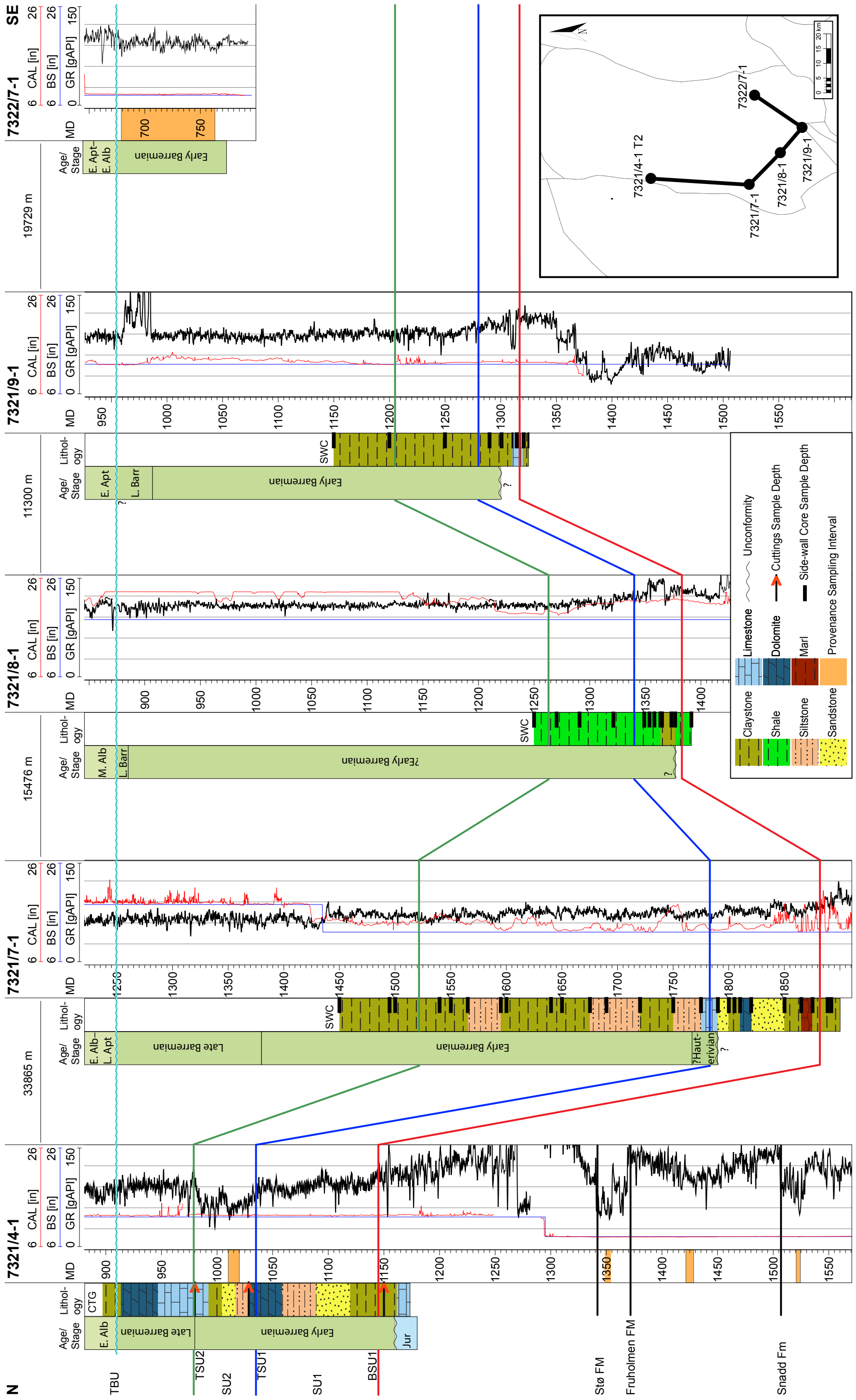

Fig. 3.1 Well Correlation *North-Southeast Well Correlation. MD = Measured Depth, CAL = Caliper, BS = Bit Size, GR = Gamma Ray, TBU = Top Barremian Unconformity, TSU2 = Top Seismic Unit 2, SU2 = Seismic Unit 2, TSU1 = Top Seismic Unit 1, SU1 = Seismic Unit 1, BSU1= Base Seismic Unit 1, FM = Formation, E. Alb = Early Albian, Jur = Jurassic, L. Apt = Late Aptian, M. Albian = Middle Albian, L. Barr = Late Barremian, E. Apt = Early Aptian, CTG = Cuttings, SWC = Side-wall Core. The well logs are flattened on TBU and include Age/Stage columns showing the result of the palynological analyses. Lithology columns are included for well 7321/4-1 (based on cutting descriptions), 7321/7-1, 7321/8-1 (based on side-wall core descriptions). The MD column for well 7321/4-1 and 7322/7-1 display intervals used for provenance sampling. Inset map in the lower right shows the location of the wells. The seismic units (SU1 and SU2) are penetrated by four of the wells and not well 7322/7-1.*

Table 3.1 Well Data *PL= Petrophysical Logs (caliper, gamma ray, neutron porosity, sonic velocity and resistivity), L = Lithostratigraphic Information, CTG = Cuttings, SWC = Side-wall Core, C = Conventional Core, DML = Dip-meter Log, IL = Image Log, B = Biostratigraphic Information, P = Provenance Data, CS = Check-shot*

Well	Year of completion	Oldest penetrated age	Type									
			PL	L	CTG	SWC	C	DML	IL	B	P	CS
7321/8-1	1987	Late Permian	√	√	√	√		√		√		√
7321/7-1	1988	Middle Triassic	√	√	√	√	√	√		√		√
7321/9-1	1988	Late Triassic	√	√	√	√		√		√		√
7322/7-1	2018	Early Cretaceous	√	√	√	√			√	√	√	√
7321/4-1	2018	Late Triassic	√	√	√					√	√	√

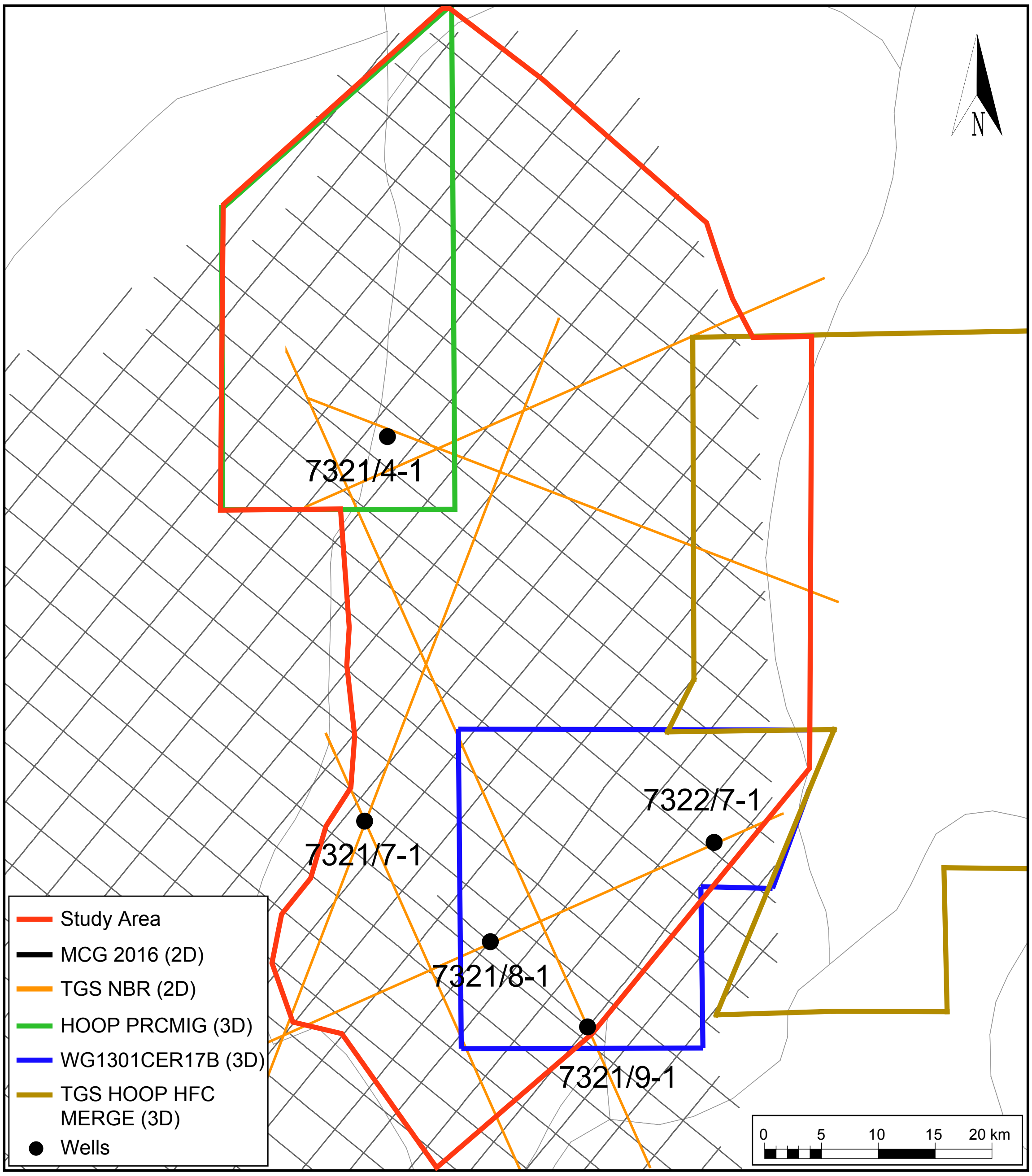

Fig. 3.2 Wells and seismic data *Map of well data and seismic data within the study area.*

The seismic data covering the study area consist of 2D and 3D reflection seismic data (, , Fig. 3.2). The 2D dataset includes four TGS NBR 2D lines and the MCG2016 survey which consists of a dense grid of 2D lines, with around 4 km spacing, covering the study area. The 3D dataset covers the north-western corner (HOOP PRCMIG) and south-eastern part of the study area (WG1301CER17B and TGS Hoop HFC Merge). Average seismic velocities in the Lower Createaceous, between horizon TBU and BSU1, Fig. 3.1, interval ranges from 2761 m/s to 3362 m/s (). The measured dominant frequency in the same interval and calculated wavelength indicates that the vertical resolution range from 23-35m ().

Table 3.2 Seismic Dataset *The five different seismic surveys used in this study.*

Name	Type	Year	Courtesy
MCG2016	2D	2016	TGS/Searcher/Spectrum/PGS/ VBPR
TGS NBR	2D	2008, 2009 and 2011	TGS
HOOP PRCMIG	3D	2017	TGS
WG1301CER17B	3D	2017	Spirit Energy
TGS Hoop HFC Merge	3D	2016	TGS/Searcher/Spectrum/PGS/VBPR

Table 3.3 Average Seismic Velocity *Table with calculated average velocities at four of the wells. MD = Measured Depth, TWT = Two-way-time, D = Difference (e.g. MD top - MD base).*

Well	MD top [m]	MD base [m]	TWT top [s]	TWT base [s]	D MD [m]	D TWT [s]	Average Velocity (v=2xDMD/DTWT) [m/s]
7321/4-1	910	1145	0,962	1,105	235	0,143	3287
7321/7-1	1250	1882	1,232	1,608	632	0,376	3362
7321/8-1	875	1383	0,985	1,353	508	0,368	2761
7321/9-1	955	1317	1,039	1,299	362	0,260	2785

Table 3.4 Vertical Resolution *Table with approximate dominant frequency measured in the seismic, calculated wavelength and vertical resolution.*

Seismic Survey	Well	Approximate Dominant Frequency (fd) [Hz]	Wavelength (wl) (v/fd) [m]	Vertical Resolution, (wl/4) [m]
HOOP PRCMIG	7321/4-1	25-35	131-94	33-23
TGS NBR	7321/7-1	25-35	134-96	33-24
MCG1401	7321/8-1	20-30	138-92	34-23
WG1301CER17B	7321/9-1	20-30	139-93	35-23

3.2 Methodology

3.2.1 Biostratigraphy and detrital zircon U/Pb geochronology

Palynological analyses and detrital zircon U/Pb geochronology was carried out by the Geological Survey of Denmark and Greenland (GEUS) in Denmark. Palynological dating (for details, see Nøhr-Hansen et al., 2019) was carried out in order to establish age control and correlate key events (e.g. unconformity) through the five wells in the Fingerdjupet Subbasin (Fig. 3.1). For the palynological analysis, 30 dicth cutting samples were studied from well 7321/4-1, two in the Upper Jurassic and 28 in the Lower Cretaceous. The Lower Cretaceous interval was sampled from 29 ditch cutting samples in well 7321/7-1, 23 ditch cutting samples in 7321/8-1 and 38 ditch cutting samples in well 7321/9-1. Three sidewall cores and 34 ditch cutting samples were studied from well 7322/7-1.

The samples for the detrital zircon U-Pb geochronology were made from average samples in well 7321/4-1 and in well 7322/7-1 ( ). Four average samples from cuttings were made from the following four intervals in well 7321/4-1; (1) 1521 – 1524 m MD (Snadd Formation), (2) 1422 – 1428 m MD (Fruholmen Formation), (3) 1348 – 1354 m MD (Stø Formation) and (4) 1010 – 1020 m MD (SU2, Fig. 3.1). For well 7322/7-1, one average sample were made from cuttings and sidewall cores in the interval between 679 to 763 MD (Kolje FM, Fig. 3.1).

Table 3.5 Zircon U/Pb Samples

Well	Sample Interval [MD]	Unit
7322/7-1	679-763	Kolje FM (Lower Cretaceous)
7321/4-1	1010-1020	SU2 (Lower Cretaceous)
7321/4-1	1348-1354	Stø FM (Lower – Middle Jurassic)
7321/4-1	1422-1428	Fruholmen FM (Upper Triassic)
7321/4-1	1521-1524	Snadd FM (Middle – Upper Triassic)

The analysis of zircon for U/Pb isotopic dating were performed using laser ablation inductively coupled plasma mass spectrometry (LA-ICPMS). The equipment used included a NWR 213 laser ablation instrument from Elemental Scientific lasers (ESL) that was coupled to an Element2 magnetic sector-field ICPMS from Thermo-Fisher Scientific. The analyses was carried out on zircon grains mounted in epoxy pucks, polished, and imaged by SEM using either cathodeluminescence (CL) or back-scattered elecetrons (BSE) prior to the LA-ICPMS analyses.

For quality control of the geochronology analyses, the secondary standards, Plešovice and Harvard 91500 was measured during the zircon analyses, yielding an average accuracy and precision (2σ) on the dates within 3% deviation. Zircon U-Pb ages ($^{206}Pb/^{238}U$, $^{206}Pb/^{238}U$ and $^{207}Pb/^{206}P^{b}$) presented in this study have 2σ error and are constrained by a concordance-discordance criterion of 10% (see appendix).

The ISOPLOT program (Ludwig, 2008) was used to present the zircon U-Pb ages in histograms and probability density plots. These plots includes concordant $^{206}Pb/^{238}U$ < 1000 Ma and $^{207}Pb/^{206}P^{b}$ > 1000 Ma.

3.2.2 Well logs and Seismic interpretation

The seismic stratigraphic framework was interpreted using petrophysical logs, palynological analyses and seismic interpretation. Two seismic units (SU1 and SU2) bound by three key seismic surfaces (BSU1, TSU1 and TSU2, Fig. 3.1) were defined mainly based on seismic downlap terminations and seismically guided well correlations. This is due to poor identification of maximum flooding surfaces on the gamma ray logs and poor correlation of the NPD lithostratigraphic units. The interval of interest (between BSU1 and TSU2) is locally eroded by an unconformity in the top of the Barremian aged interval (TBU, Fig. 3.1) and by an unconformity in the top of Lower Cretaceous succession which is interpreted to represent Base Quaternary Unconformity (BQU). These reflectors were mapped but will not be described in any further detail.

The seismic units were correlated in the wells and the faults affecting the units were mapped throughout the seismic dataset. Fault interpretations and time thickness maps generated from the seismic interpretation were used to describe the main structures and to interpreted the infill of the basin. The seismic character of the seismic units is described based on main reflector characteristics including continuity, amplitude and geometry. Seismic sections parallel to the clinoform progradation direction are flattened along the clinoform downlap surface (BSU1), considered to be closest to paleo-horizontal datum in the studied interval, to describe the clinoform geometry and the tjacetrory of the rollover point (shelf-edge).

Identification of lithological trends and interpretation of the sandstone distribution were based on gamma ray logs, cuttings from well 7321/4-1 and sidewall cores from well 7321/7-1, 7321/8-1 and 7321/9-1.

3.2.3 Seismic-Well Tie

The integrated seismic well-tie suite in the Petrel Schlumberger software were used to perform the seismic-well tie. Checkshot data from the wells were used to establish a time-depth relationship, by calibrating (correct the sonic log to seismic times) the sonic log. In order to produce a synthetic seismogram, the density log and the sonic log were used to compute acoustic impedance and the reflection coefficient for normal incidence. Furthermore, the reflection coefficient was convolved with a zero phase wavelet to generate synthetic traces to match with the seismic traces. The Ricker wavelet were used to compare synthetic traces with the real seismic traces. The frequency of the Ricker wavelet was adjusted to obtain the best possible match with the frequency spectrum of the seismic traces. The BSU1 and TBU were used to tie the seismic data and the well data in the in the study area. The BSU1 is modelled as a positive reflector with high amplitude in the synthetic seismogram and correlates good with the seismic data (Fig. 3.3). A negative amplitude reflector were picked for the TBU which shows medium to high amplitude in the synthetic and high amplitude in the seismic, giving a moderate good correlation (Fig. 3.3).

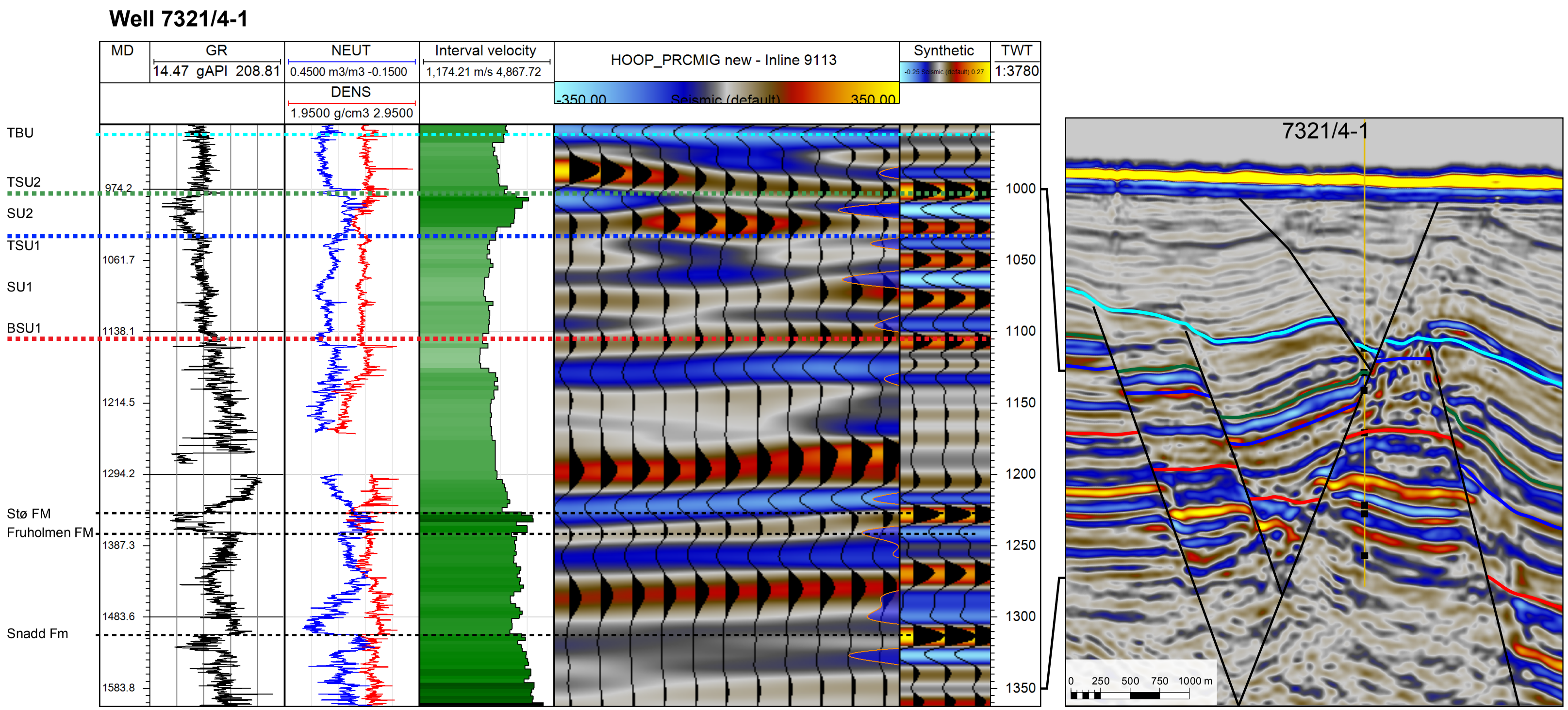

Fig. 3.3 Synthetic Seismogram *Well logs, seismic data and synthetic seismogram are shown to the left. An NW-SE arbitrary seismic line across well 7321/4-1 is shown to the right. MD = Measured Depth, GR = Gamma-ray log, NEUT = Neutron log, DENS = Density log, TWT = two-way-time, Unc. = Unconformity. The seismic data display an N-S inline across the well. A 25-30-35 Hz zero phase Ricker wavelet was used to compute the synthetic seismogram. A increase in acoustic impedance yields positive amplitude displayed as a red reflector. The picked horizons for the interval of interest is defined two positive reflectors named Base Seismic Unit 1 and Top Seismic Unit 2.*

4 RESULTS

4.1 Fault Families

The main faults affecting the seismic units in the study area are divided into four fault families (FF1-FF4) of similar trend and age (Fig. 4.1). Fault Family 1 (FF1) offset both of the seismic units and constitute normal fault striking NNW-SSE, N-S and NNE-SSW located in the north-western part of the study area (Fig. 4.1, Fig. 4.2,Fig. 4.3, Fig. 4.4). Well 7321/4-1 penetrates the fault plane of a NNE-SSW striking fault segment of FF1 at 1035 m MD, in this location the TSU1 is displaced out of the wellbore and the well penetrated the middle part SU1 (Fig. 4.3). Fault Family 2 (FF2) consist of south-dipping normal faults striking E-W between the individual segments of FF1 (Fig. 4.1). Most these fault offset both of the seismic unit in the north-western part of the study area. Fault family 3 (FF3) offset both of the seismic units and constitute normal faults striking N-S to NE-SW along the central part of the study area (Fig. 4.5 and Fig. 4.6). Fault Family 4 (FF4) is located in the south and northeast and consists of normal fault striking N-S to NE-SW and offset both of the seismic units (Fig. 4.1, Fig. 4.6).

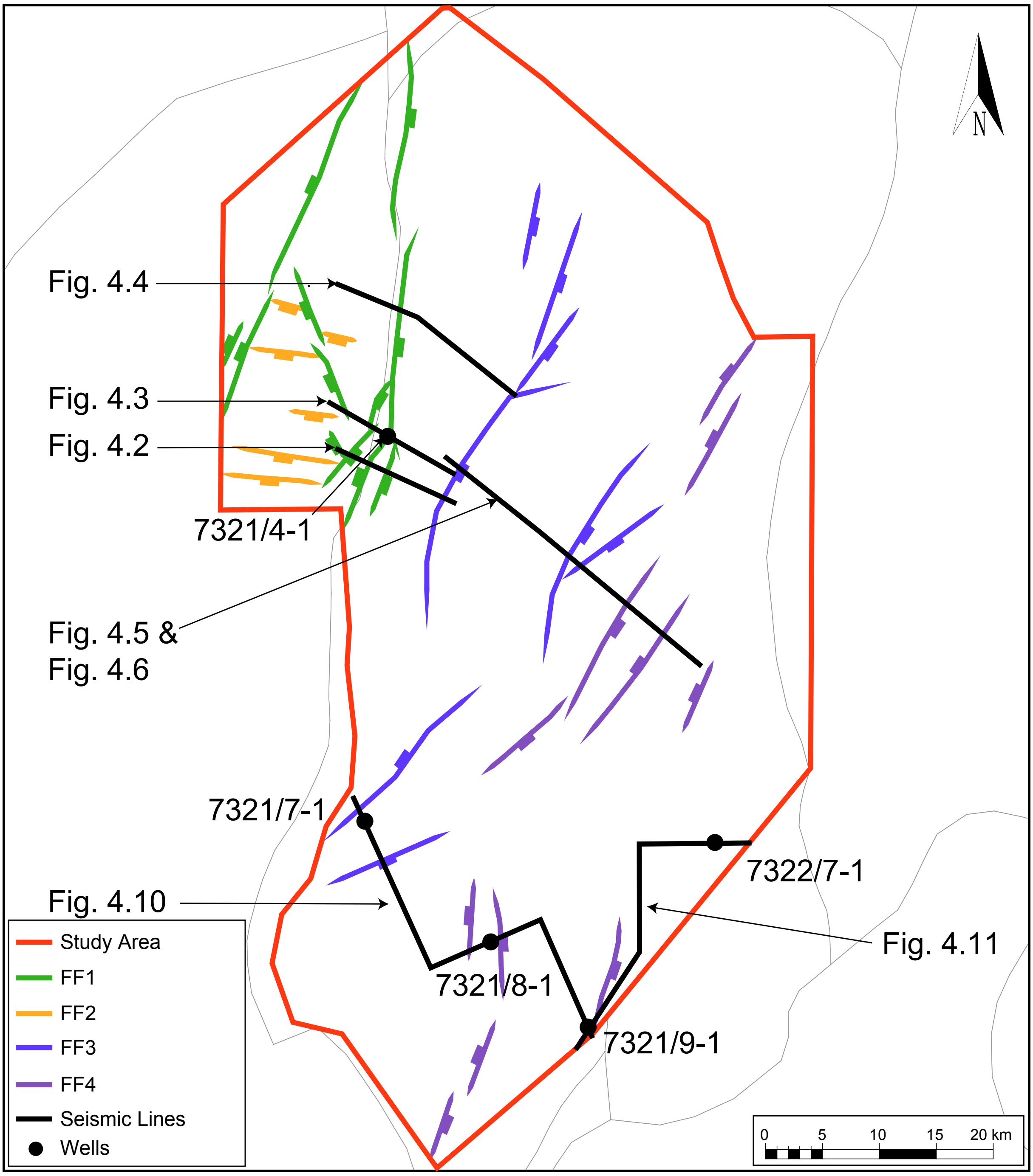

Fig. 4.1 Fault Families and Presented Seismic Lines *Map of the study area (outlined in red) including four fault families defined in this study, exploration wells and location of presented seismic lines.*

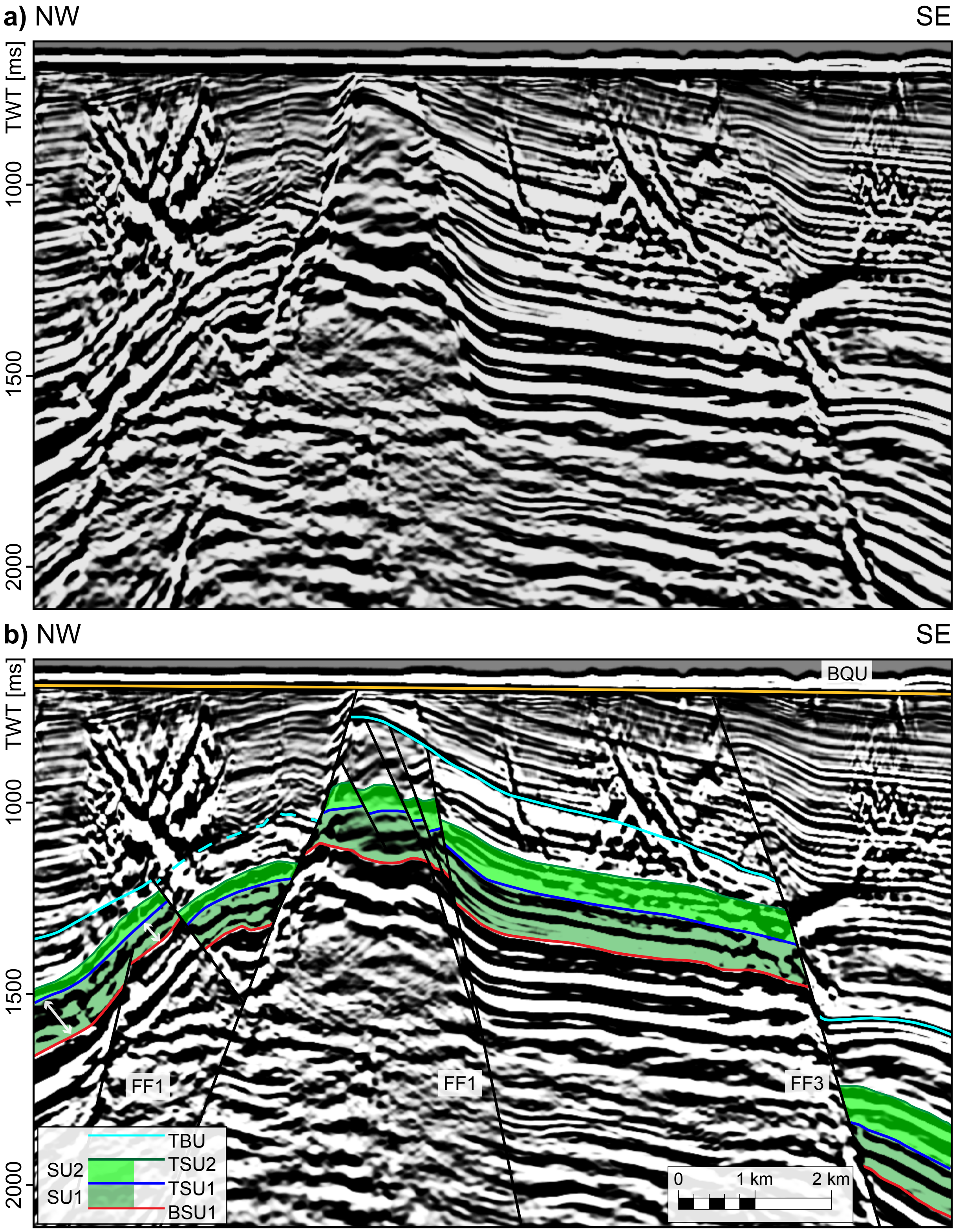

Fig. 4.2 Crossline 1 *Uninterpreted (a) and interpreted (b) northwest-southeast crossline (see Fig. 4.1 for orientation of the line). BQU = Base Quaternary Unconformity, TBU = Top Barremian Unconformity, TSU2 = Top Seismic Unit 2, SU2 = Seismic Unit 2, TSU1 = Top Seismic Unit 1, SU1 = Seismic Unit 1, BSU1= Base Seismic Unit 1, FF1 = Fault Family 1, FF3 = Fault Family 3. The SU1 show a thickness growth in the hanging wall of FF1. The SU2 display a thickness increase from the NW towards the SE.*

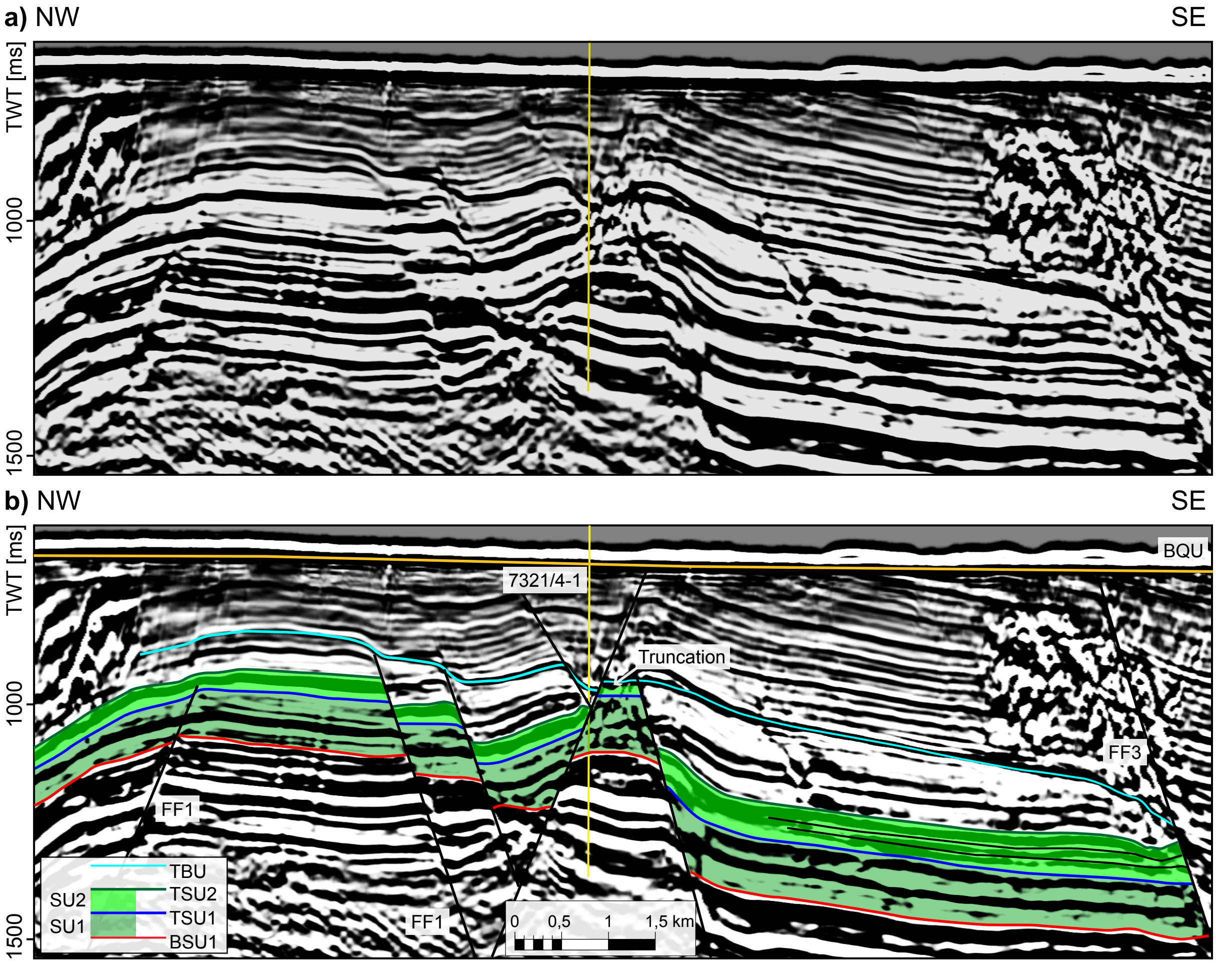

Fig. 4.3 Crossline 2 *Uninterpreted (a) and interpreted (b) northwest-southeast crossline (see Fig. 4.1 for orientation of the line). BQU = Base Quaternary Unconformity, TBU = Top Barremian Unconformity, TSU2 = Top Seismic Unit 2, SU2 = Seismic Unit 2, TSU1 = Top Seismic Unit 1, SU1 = Seismic Unit 1, BSU1= Base Seismic Unit 1, FF1 = Fault Family 1, FF3 = Fault Family 3. The TSU1 is not penetrated by well 7321/4-1 and the TSU2 is truncated by TBU.*

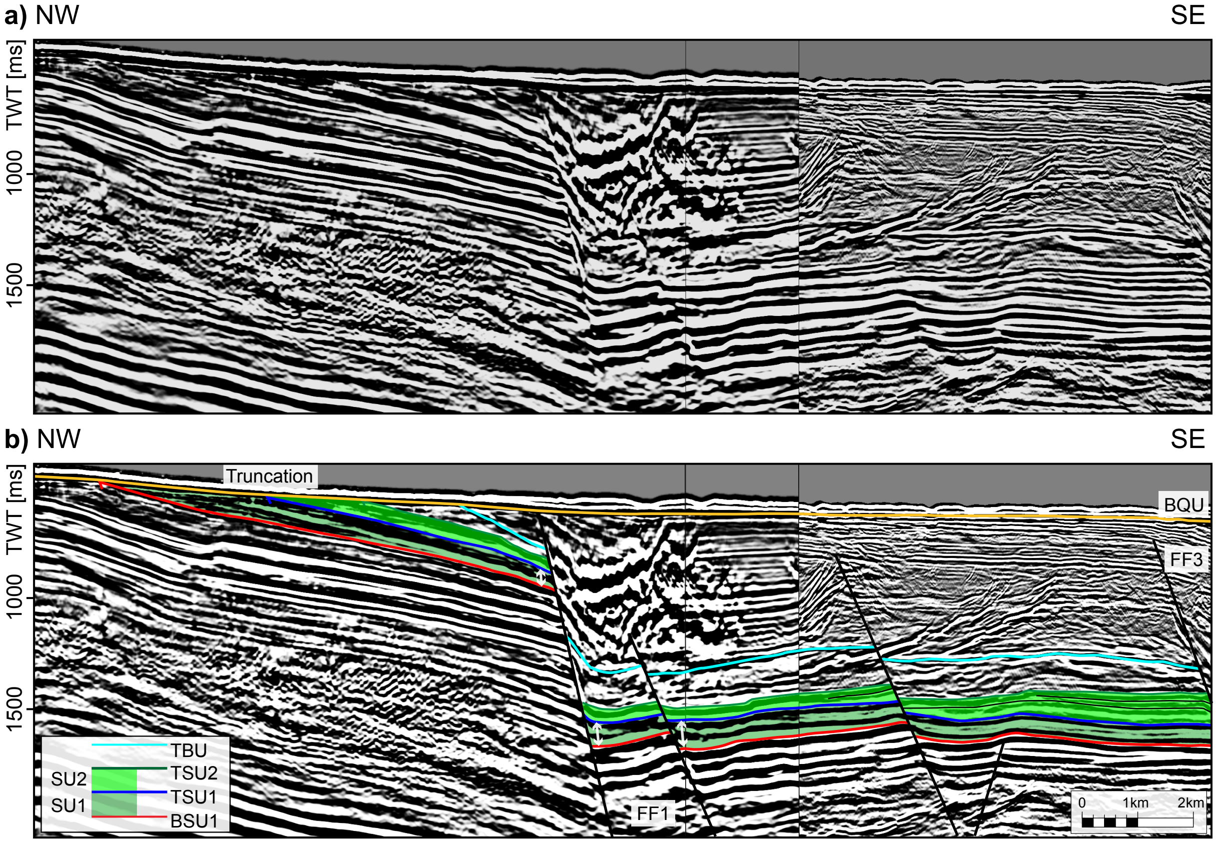

Fig. 4.4 Composite Line 1 *Uninterpreted (a) and interpreted (b) northwest-southeast composite line (see Fig. 4.1 for orientation of the line). BQU = Base Quaternary Unconformity, TBU = Top Barremian Unconformity, TSU2 = Top Seismic Unit 2, SU2 = Seismic Unit 2, TSU1 = Top Seismic Unit 1, SU1 = Seismic Unit 1, BSU1= Base Seismic Unit 1, FF1 = Fault Family 1, FF3 = Fault Family 3. Minor thickness differences in SU1 is observed between the footwall and hanging wall of FF1. The SU2 display a thickness increase from NW towards SE.*

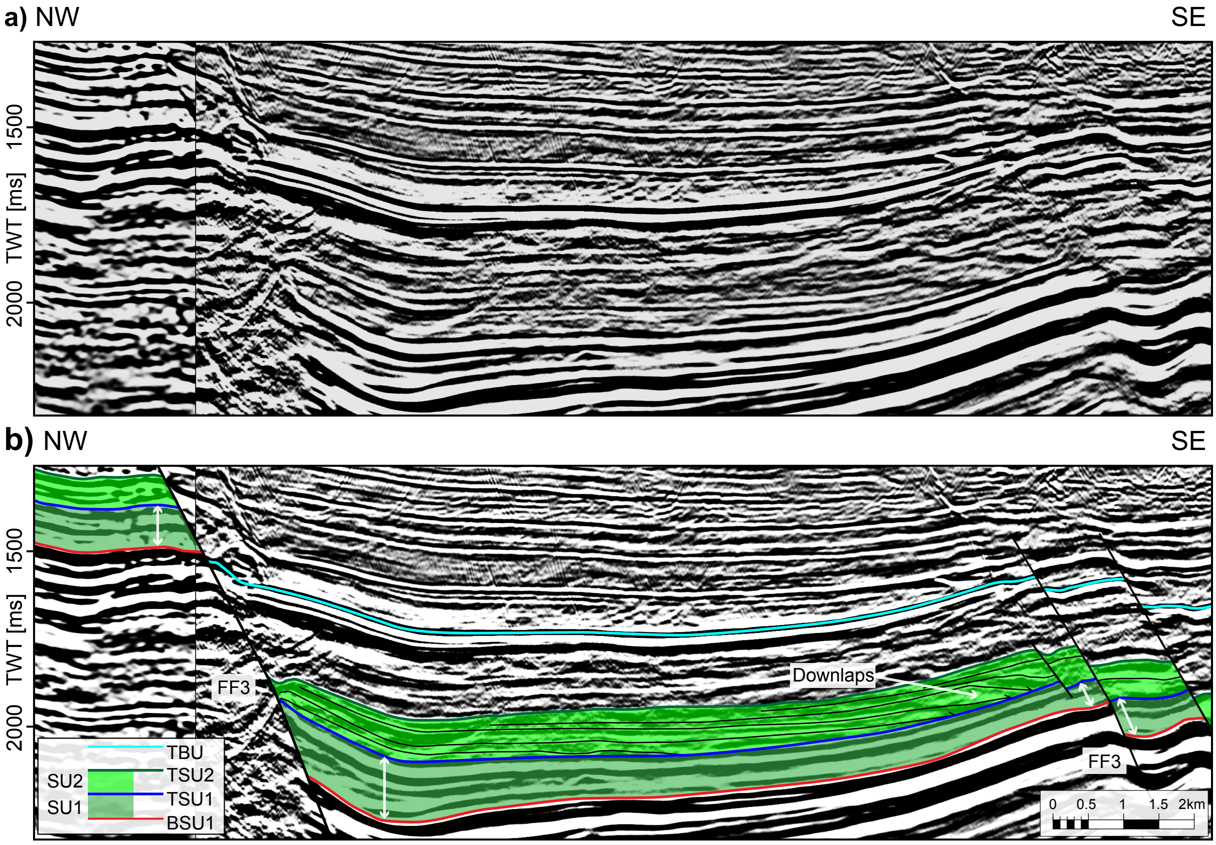

Fig. 4.5 Composite Line 2a *Uninterpreted (a) and interpreted (b) northwest-southeast composite line (see Fig. 4.1 for orientation of the line). TBU = Top Barremian Unconformity, TSU2 = Top Seismic Unit 2, SU2 = Seismic Unit 2, TSU1 = Top Seismic Unit 1, SU1 = Seismic Unit 1, BSU1= Base Seismic Unit 1, FF3 = Fault Family 3. The SU1 show thickness growth towards the fault plane of FF3 and internal reflectors in SU2 show a sigmoidal clinoform geometry.*

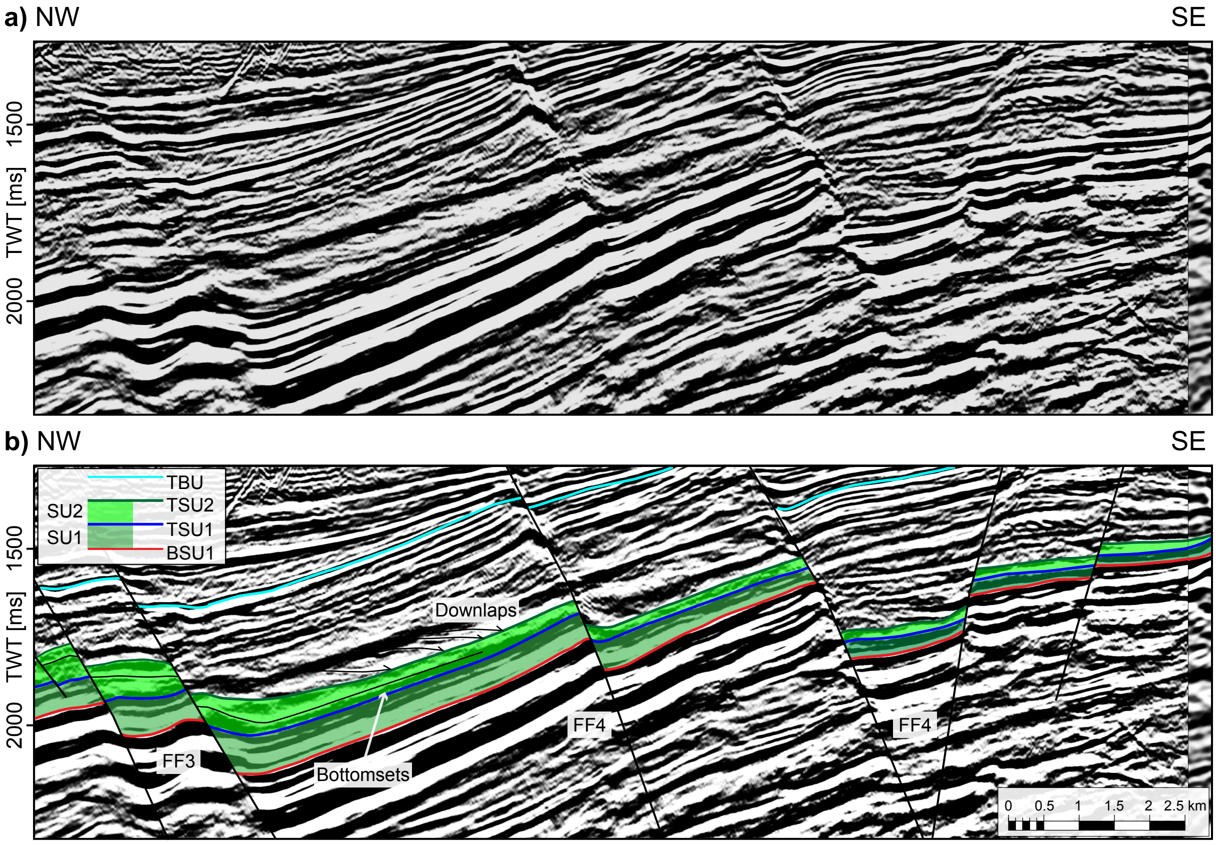

Fig. 4.6 Composite Line 2b *Uninterpreted (a) and interpreted (b) northwest-southeast composite line (see Fig. 4.1 for orientation of the line). TBU = Top Barremian Unconformity, TSU2 = Top Seismic Unit 2, SU2 = Seismic Unit 2, TSU1 = Top Seismic Unit 1, SU1 = Seismic Unit 1, BSU1= Base Seismic Unit 1, FF3 = Fault Family 3, FF4 = Fault Family 4. The SU1 thins towards the SE and reflectors above SU2 downlaps onto the the TSU2.*

4.2 Age Model and Seismic Unit Definition

The age of the Lower Cretaceous succession in Fingerdjupet Subbasin spans from ?Hauterivian to middle Albian (Fig. 4.7, Fig. 4.8, Fig. 4.9 and Fig. 3.1). The Jurassic-Cretaceous transition is only indicated in well 7321/4-1 at 1145 m (Fig. 4.7a and Fig. 3.1).) and has not been identified in the other wells (Fig. 4.7-Fig. 4.9 and Fig. 3.1). A unconformity is present in the base of the ?Hauterivian in well 7321/7-1 (Fig. 4.7a and Fig. 3.1) and the early Barremian in well 7321/4-1, 7321/8-1 and 7321/9-1 (Fig. 4.7a-Fig. 4.9 and Fig. 3.1). A second unconformity is present in the top of an interval dated ?Hauterivian–late Barremian which is penetrated by all of the wells (Fig. 4.7a-Fig. 4.9 and Fig. 3.1). The upper part, above the second unconformity, is dated early Aptian to middle Albian (Fig. 4.7a-Fig. 4.9 and Fig. 3.1).

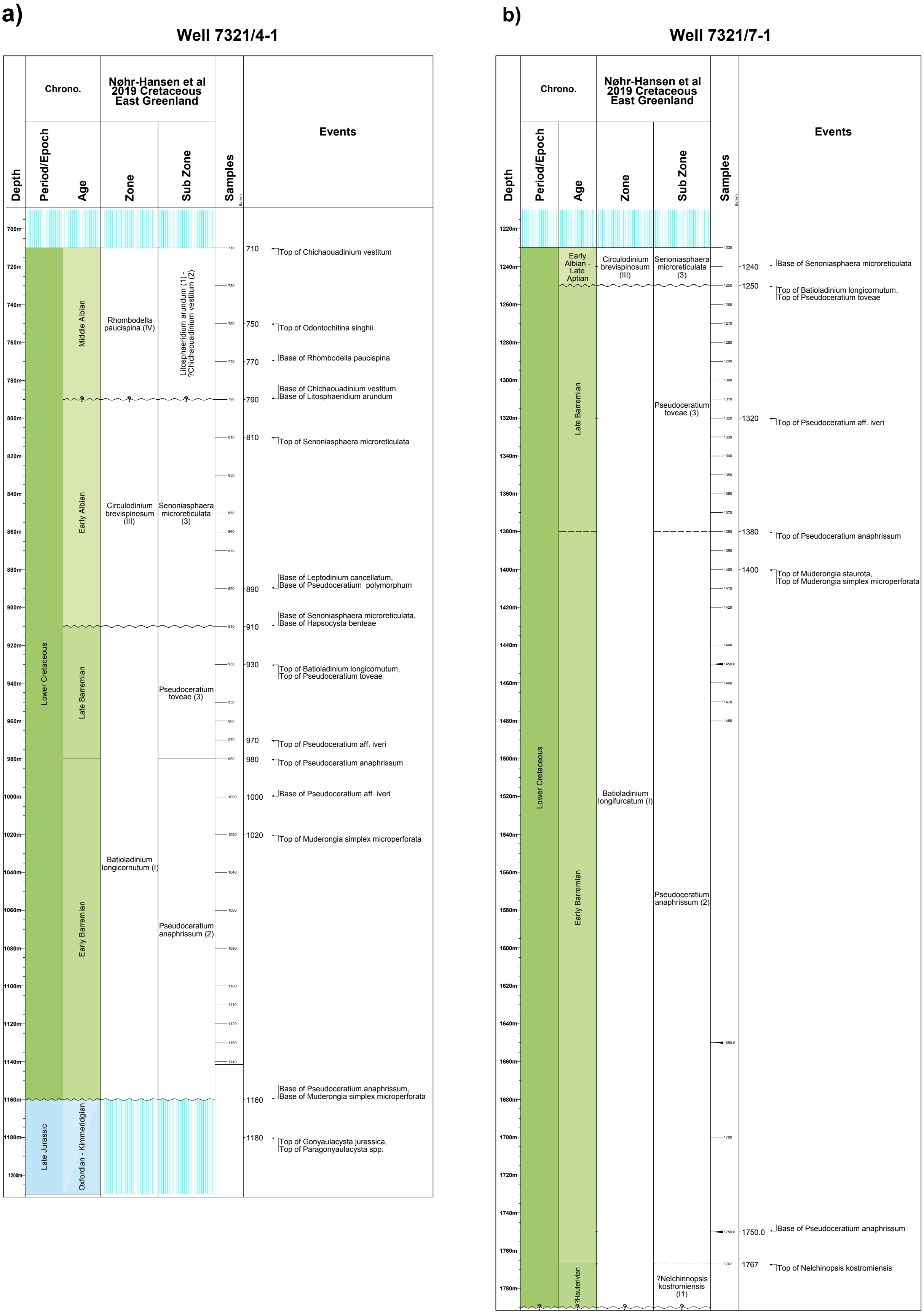

Fig. 4.7 Biostratigraphy for well 7321/4-1 and 7321/7-1

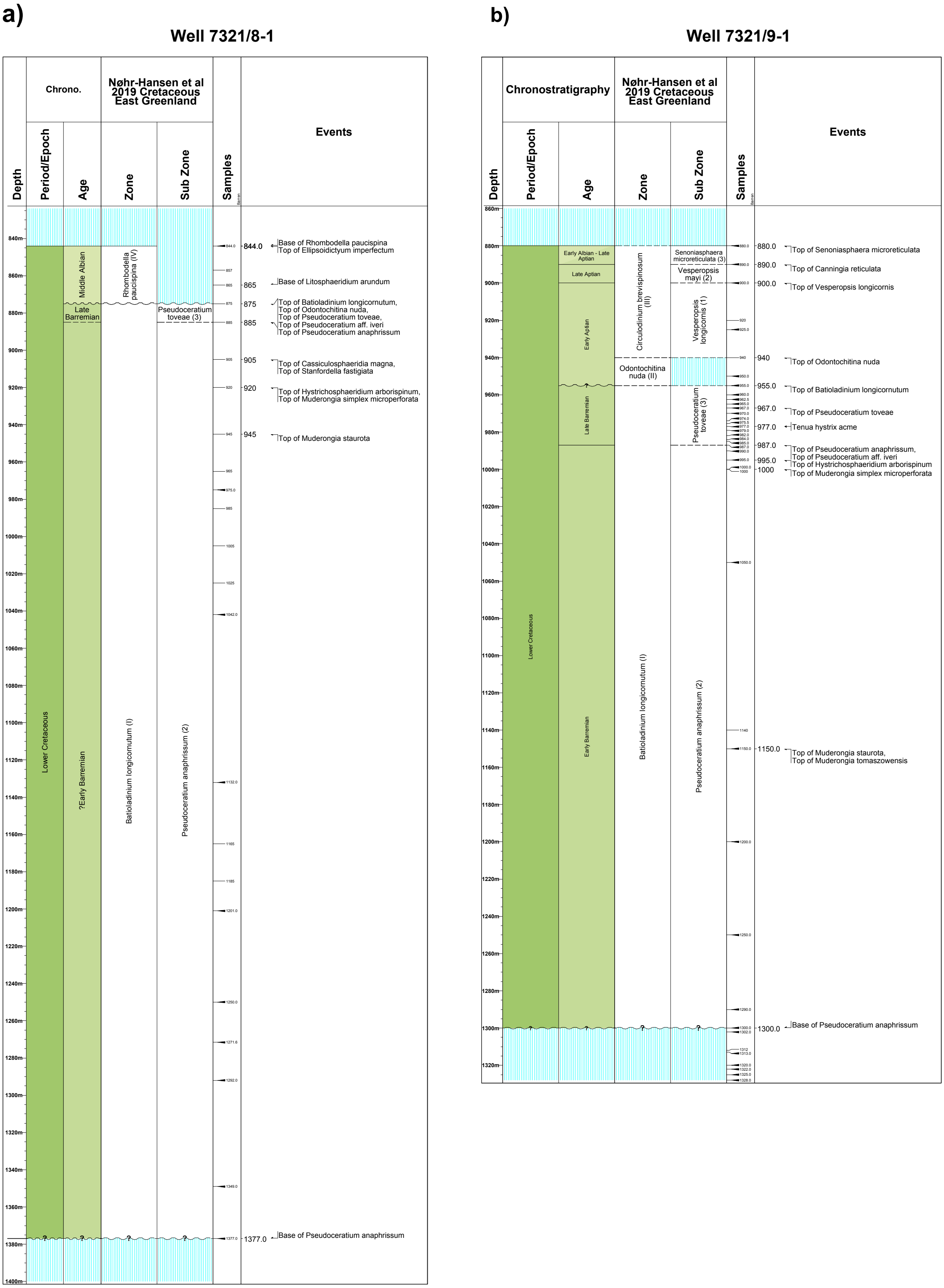

Fig. 4.8 Biostratigraphy for well 7321/8-1 and 7321/9-1

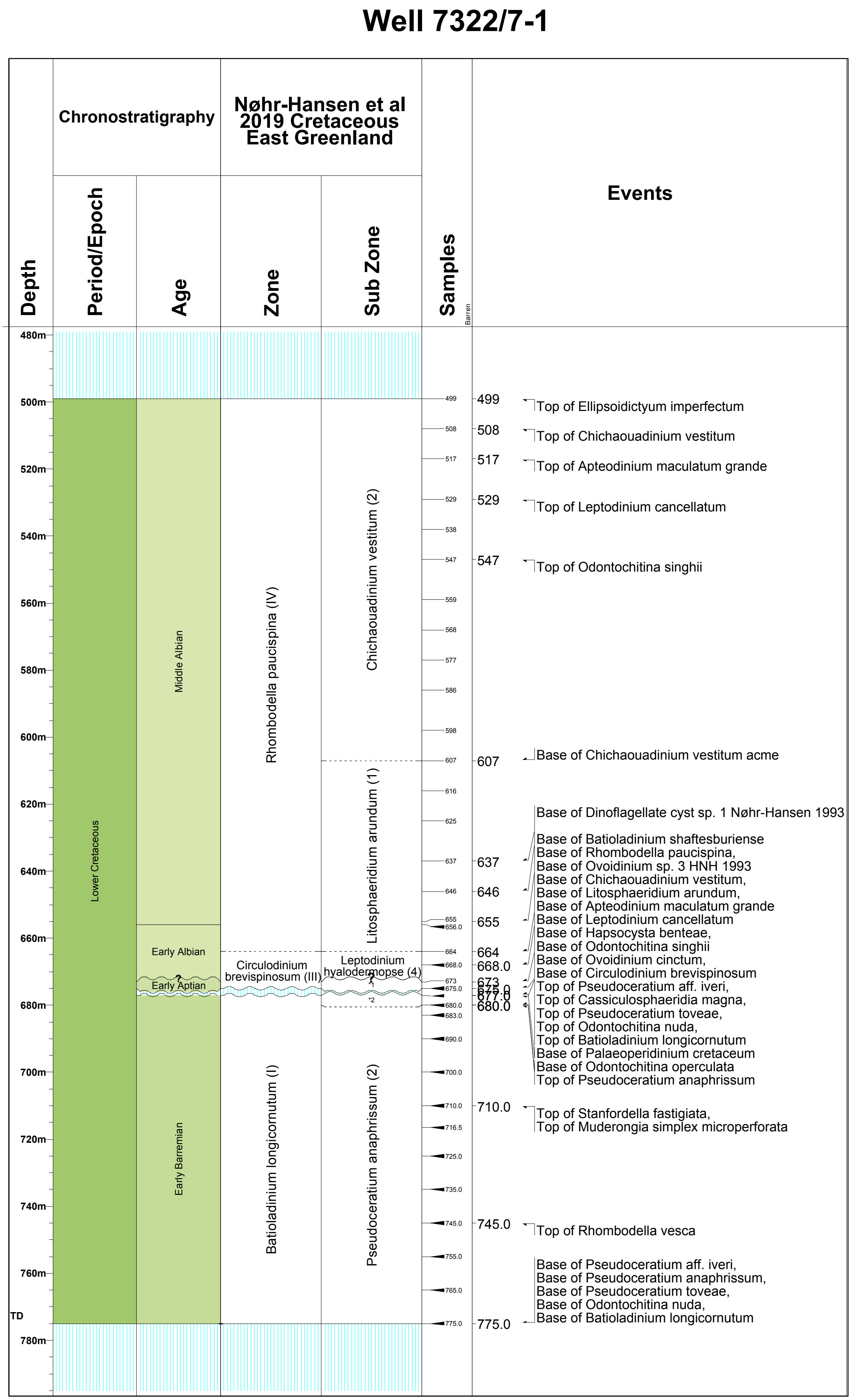

Fig. 4.9 Biostratigraphy for well 7322/7-1

The seismic units are penetrated by all of the wells except for well 7322/7-1 (Fig. 3.1, Fig. 4.3, Fig. 4.10 and Fig. 4.11). The seismic horizon defining the base of unit 1 (BSU1) is a seismic surface near the regional Base Cretaceous Unconformity characterized as a reflector with medium to high amplitude. For BSU1, the gamma ray log show high values with increasing and decreasing trends at the pick of this horizon (Fig. 3.1). The age of BSU1 is early Barremian in well 7322/4-1 and age control is missing for well 7322/7-1, 7321/8-1 and 7321/9-1 (Fig. 3.1). By comparing the BSU1 with official well tops from NPD, the BSU1 correlates to the Kolje Formation (Barremian to early Aptian) in well 7321/7-1 and Hekkingen Formation (late Oxfordian/early Kimmeridgian to Ryazanian) in well 7321/8-1 and 7321/9-1 (NPD, 2020), suggesting a Ryazanian to early Barremian age for BSU1 (Fig. 3.1). The top of Seismic Unit 1 (TSU1) is characterized as a reflector with medium to high amplitude and seismic reflectors downlaps onto the top of this surface (Fig. 4.5, Fig. 4.10). High gamma ray values with decreasing and increasing trends are observed for the TSU1 (Fig. 3.1). The age of TSU1 spans from ?Hauterivian to early Barremian, suggesting a Ryazanian to early Barremian for SU1 (Fig. 3.1).

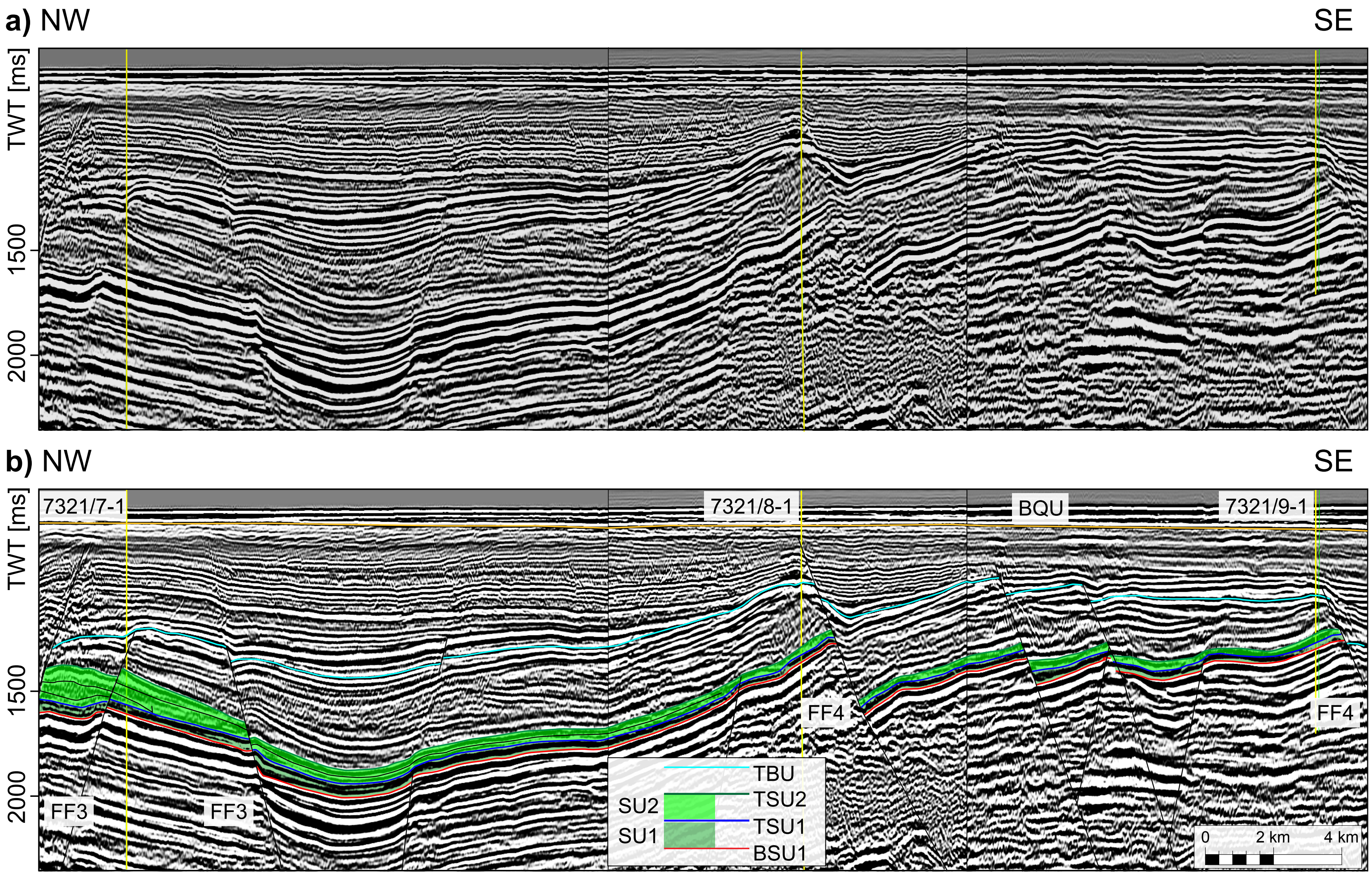

Fig. 4.10 Composite Line 3 *Uninterpreted (a) and interpreted (b) northwest-southeast composite line (see Fig. 4.1 for orientation of the line). TBU = Top Barremian Unconformity, TSU2 = Top Seismic Unit 2, SU2 = Seismic Unit 2, TSU1 = Top Seismic Unit 1, SU1 = Seismic Unit 1, BSU1= Base Seismic Unit 1, FF3 = Fault Family 3, FF4 = Fault Family 4. The thins in the footwall of FF3. Well 7321/7-1 penetrates the lower part of the foresets in SU2. Well 7321/8-1 and 7321/9-1 penetrates the bottomsets.*

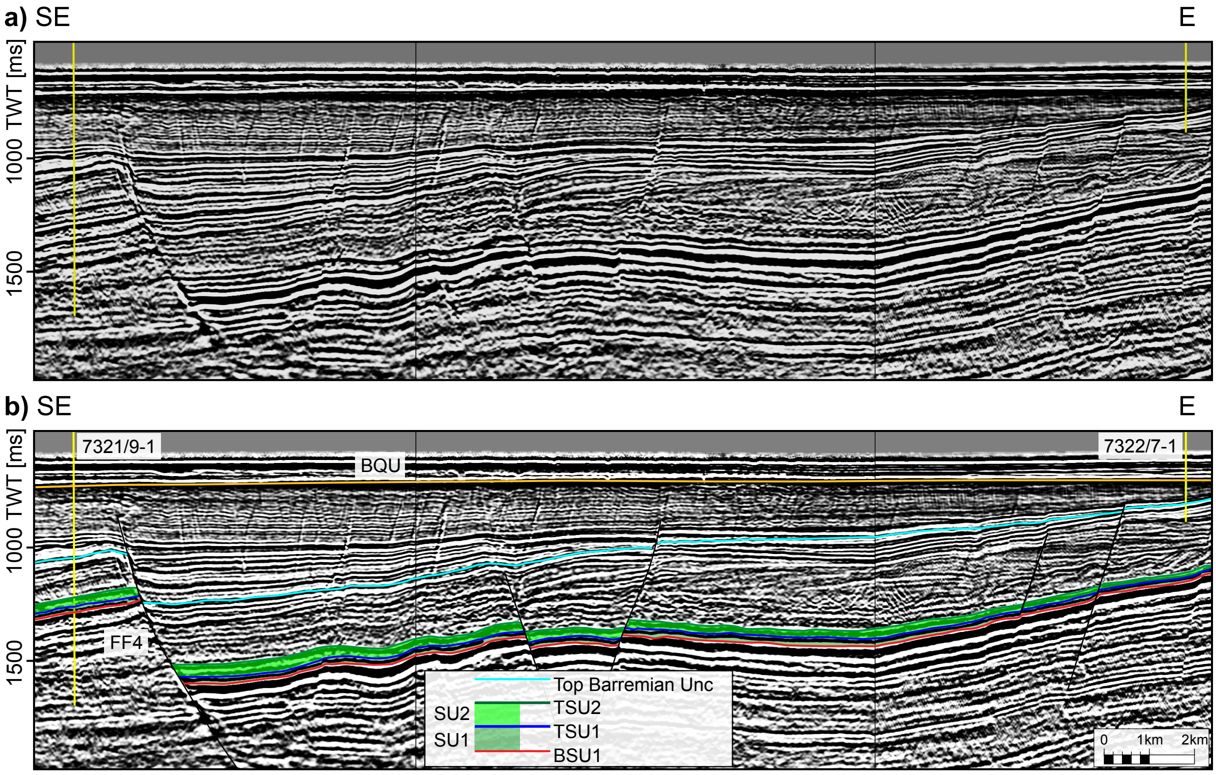

Fig. 4.11 Composite Line 4 *Uninterpreted (a) and interpreted (b) southeast-East composite line (see Fig. 4.1 for orientation of the line). TBU = Top Barremian Unconformity, TSU2 = Top Seismic Unit 2, SU2 = Seismic Unit 2, TSU1 = Top Seismic Unit 1, SU1 = Seismic Unit 1, BSU1= Base Seismic Unit 1, FF3 = Fault Family 3, FF4 = Fault Family 4. Well 7322/7-1 do not penetrate the units.*

The top of Seismic Unit 2 (TSU2) is characterized by a reflector with medium to high amplitude and seismic reflectors downlaps onto the top of this surface in the central (Fig. 4.6) and eastern part of the study area. The gamma ray character of the TSU2 varies from a peak of high gamma ray values in well 7321/4-1 to increasing and no change in the log response in the other wells (Fig. 3.1). The TSU2 is aged early Barremian to late Barremian, suggesting a ?Hauterivian to late Barremian age for SU2 (Fig. 3.1).

4.3 Seismic Unit 1

Observation

Well Character

The gamma ray pattern in well 7321/4-1 and 7321/7-1 show two intervals of coarsening to fining upward trends followed by a coarsening trend in the top (Fig. 3.1). Drill cuttings and SWC from these wells show sand, silt and caly in addition to dolomite, limestone and marl. Well 7321/8-1 and 7321/9-1 display overall higher reading with a signature characterized by low gamma ray values in the lower part followed by a fining to coarsening trend in the upper part. The SWC in these wells are dominated by fine-grained sediments.

Thickness Variations

Seismic unit 1 show a thickness decrease from the from 110 meter in well 7321/4-1 to 90 meter in well 7321/9-1 in the east (Fig. 3.1). The time thickness map indicates that the unit is thickest in the north-western part of the study area and thins towards the southeast (Fig. 4.12). A thickness increase is observed towards the fault plane of FF3 in the soutwest (Fig. 4.10) and in the center of the study area, where the thickness reaches around 200 ms (Fig. 4.5 and Fig. 4.12). The thicknes of the unit increase in the hanging wall of the southern segments of FF2 (Fig. 4.12) and locally in the hanging wall of FF1 (Fig. 4.2, Fig. 4.4 and Fig. 4.12). No thickness variations is obeserved in hangingwall of FF4 (Fig. 4.6, Fig. 4.10, Fig. 4.11 and Fig. 4.12).

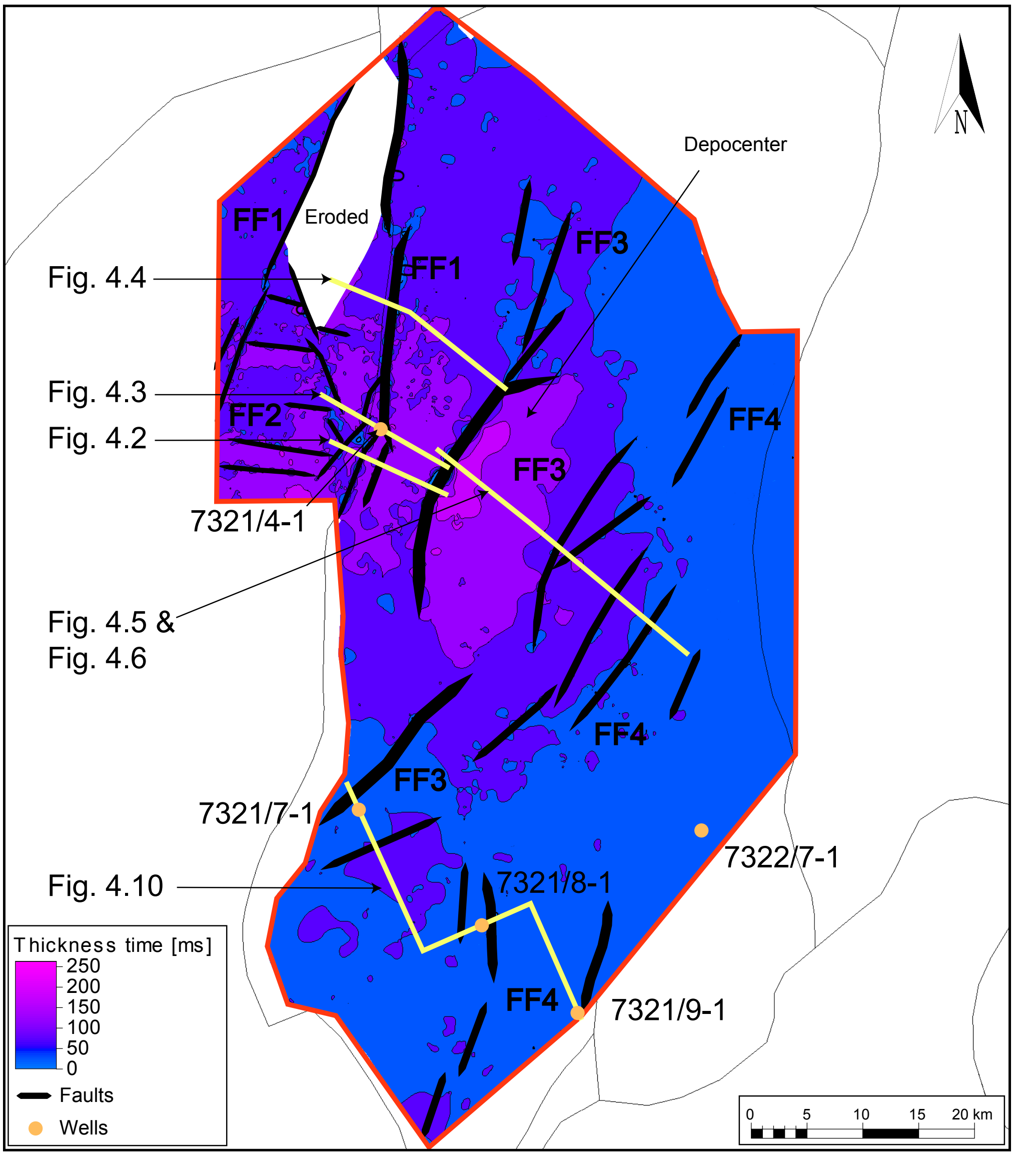

Fig. 4.12 Time Thickness Map of SU1 *Time thickness map of Seismic Unit 1 (SU1), fault families and location of seismic lines.*

Seismic Character

The SU1 is truncated by the BQU in footwall of FF1 in the northwest and is not present in the northeast trending horst structure defined by FF1 in north-western part of the study area (Fig. 4.12 and Fig. 4.4). The internal reflectors of SU1 vary from discontinous to continous reflectors with low to high amplitude (e.g. Fig. 4.2) and characterized by sub-parallel reflector patterns. Growth wedges related to FF3 occure in the central part (Fig. 4.5) and in the southwest (Fig. 4.10). Reflectors downlap onto the top of SU1 in the northeastern, central (Fig. 4.5) and southwestern part of the study area (Fig. 4.10).

Interpretation

The SU1 unit was deposited during active faulting controlled by FF2 and locally by FF1 in the north-western part of the study area. A depocenter developed in the central part of the basin and a syn-rift wedge developed along the fault plane of FF3. The constant thickness of the unit in the southeastern part indicates that FF4 was not active (Fig. 4.12). The discontinous to continous reflectors with sub-parallel geometry indicate stable and unstable low energy during deposition of SU2. The SU1 comprises dominantly fine-grained rocks with the occurrence of carbonates, which could indicate a shallow to deep marine environment. Sandstone is encountered by the wells in the west (7321/4-1 and 7321/7-1) which indicate a source of coarse-grained sediments existed for this unit. The source of these sediments was most likely in the west or north based on the southeastward thinning of the unit.

4.4 Seismic Unit 2

Observation

Well Log Character

Well 7321/4-1 display a coarsening to fining upward trend in the lower part (Fig. 3.1). The upper part is characterized by a coarsening upward trend followed by a serrated signature with intervals of low gamma ray and a fining upward trend reaching a peak of high values in the top of the SU2 (TSU2). Drill cuttings from the same interval includes clay, silt, sand and limestone. The lower part of well 7321/7-1 shows two intervals of coarsening to fining upward trends, followed by an interval with a serrated signature and two intervals of coarsening to fining upward trends in the upper part. The sidewall cores from well 7321/7-1 shows limestone in the lowermost part followed by alternating siltstone and claystone. The gamma ray pattern for well 7321/8-1 and 7321/9-1 is characterised by a coarsening upward trend followed by a serrated signature. The sidewall cores from these wells is dominated by shale and claystone.

Thickness Variations

The thickness increase from the northwest to a depocenter located in central axis of the basin and thins towards the southeast of the study area (Fig. 4.13). The same trend is observed in the wells, thickens from 56 meter thick in well 7321/4-1 to 261 meter in well 7321/7-1 and thins to 75 meter in well 7321/9-1 (Fig. 3.1). The SU2 show a gradual increasing to decreasing thickness trend.

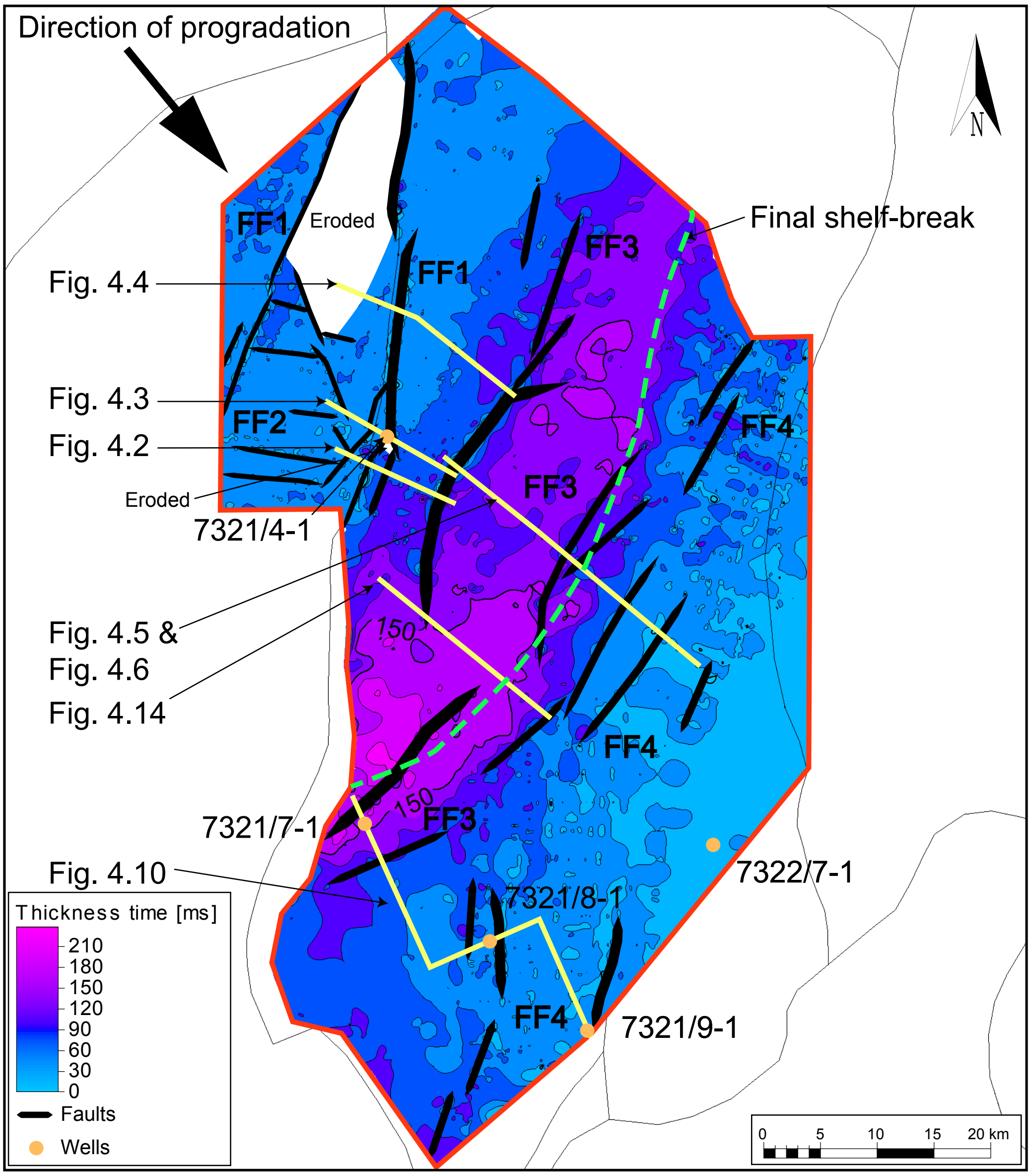

Fig. 4.13 Time Thickness Map of SU2 *Time thickness map of Seismic Unit 1 (SU2), fault families and location of seismic lines.*

Seismic Character

The TSU2 is truncated by the TBU in BQU in the footwall of FF1 in the northwest and is not present in the structural high defined by FF1 in the northwest (Fig. 4.4 and Fig. 4.13). The internal reflectors of SU2 consists of continuous reflectors with medium to high amplitude in the north-western part of the study area (Fig. 4.2-Fig. 4.4). Further southeast, subparallel to gently dipping continuous reflectors occur with low to medium amplitude (Fig. 4.5, Fig. 4.6, Fig. 4.10, Fig. 4.11). These reflectors displaying a sigmoidal clinoform geometry prograding towards the southeast. The upper boundary of the clinoforms is characterized by thin topsets with medium to high amplitude and low angle foresets which display a rising trajectory (Fig. 4.14). The clinoforms downlap onto the TSU1 in the central part of the study area and bottomsets are observed further southeast-east in the the study area (Fig. 4.5, Fig. 4.6, Fig. 4.10, Fig. 4.11).

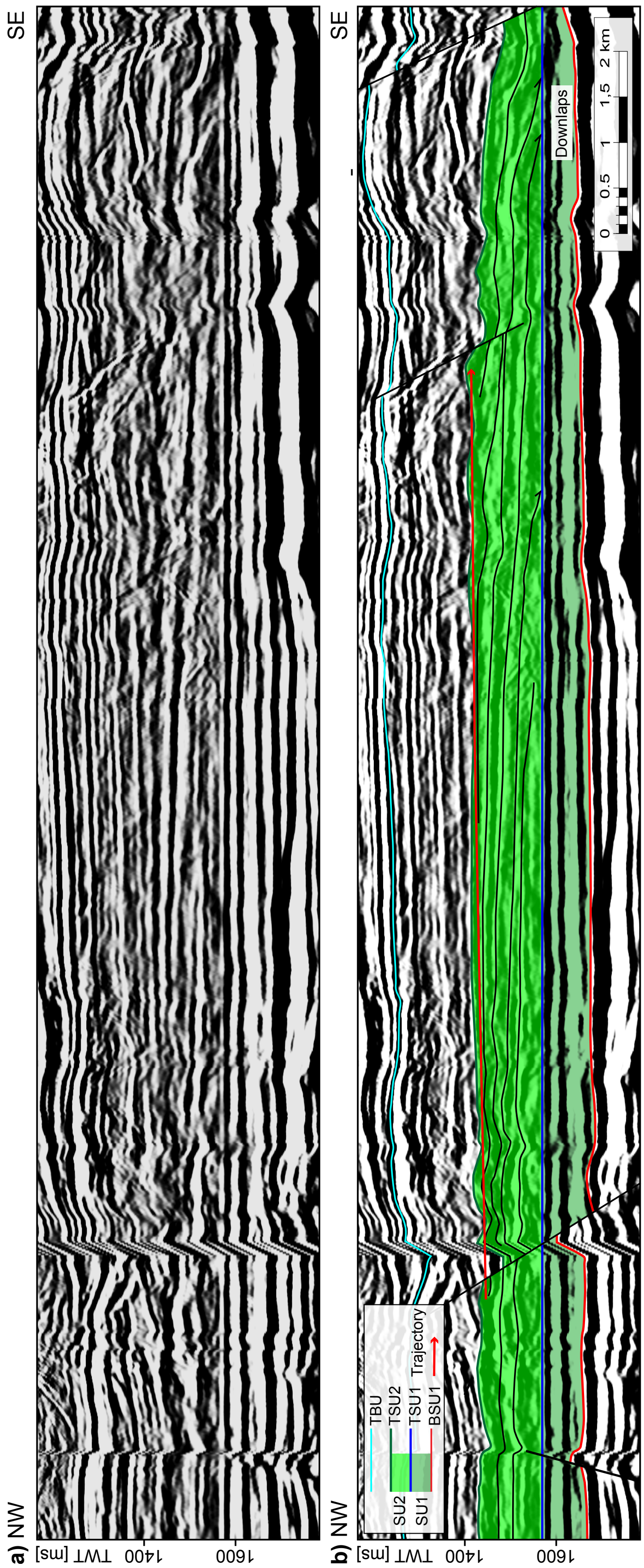

Fig. 4.14 Crossline 3 *Uninterpreted (a) and interpreted (b) northwest-southeast crossline line (see Fig. 4.13 for orientation of the line). TBU = Top Barremian Unconformity, TSU2 = Top Seismic Unit 2, SU2 = Seismic Unit 2, TSU1 = Top Seismic Unit 1, SU1 = Seismic Unit 1, BSU1= Base Seismic Unit 1, FF3 = Fault Family 3, FF4 = Fault Family 4. The crossline is flattened on TSU1. Internal reflectors in SU2 downlaps onto the TSU1.*

Interpretation

The sigmoidal clinoform geometries are interpreted to represent clinoforms prograding towards the southeast. Well 7321/4-1 is interpreted to penetrate clinoform topsets (Fig. 4.15) consisting of shales coarsening upwards into silty sandstones overlaid by shales and possibly carbonates. This stacking pattern reflects a prograding trend in the lower part followed by a middle aggrading trend and a upper retrograding trend. Well 7321/7-1 is interpreted to penetrate the middle slope wich consisting of alternating siltstone and claystone. The final shelf-break occure few km north of well Well 7321/7-1 (Fig. 4.13)The bottomsets is interpreted to be penetrated by well 7321/8-1 and 7321/9-1, fine-grained basin floor deposits. The southeast prograding direction of the clinoiforms indicate that the source of sediment was located in the northwest. Based on the gradual increasing to decreasing thickness trend of the unit, the faults in the study area was not active during deposition of SU2.

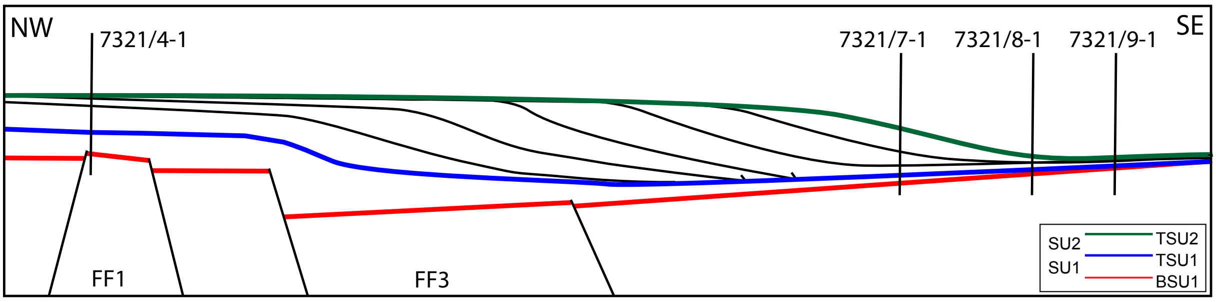

Fig. 4.15 Interpretation of SU2 *Conceptual sketch of a cross-section showing the SU1 and the SU2 just after deposition of S2. The wells has been projected to show where they are inferred to penetrate the clinoforms. Well 7321/4-1 is inferred to penetrated the topsets, Well 7321/7-1 penetrates the middle part of the foresets. Well 7321/8-1 and Well 7321/7-1 penetrates the bottomsets.*

4.5 Detrital Zircon Ages

Snadd FM (Middle – Upper Triassic)

The detrital zircon age spectra within the Snadd FM samples in well 7321/4-1 lacks grains with Archean ages and display two main younger age polulations (Fig. 4.16). A polulation from 2 to 1 Ga with similar frequencythe except for the populations from 1.1 to 1 Ga (Late Mesoproterozoic). The second population, between 0.6 – 0.24 Ga (Late proterozoic – Early Mesozoic), are all of similar frequency.

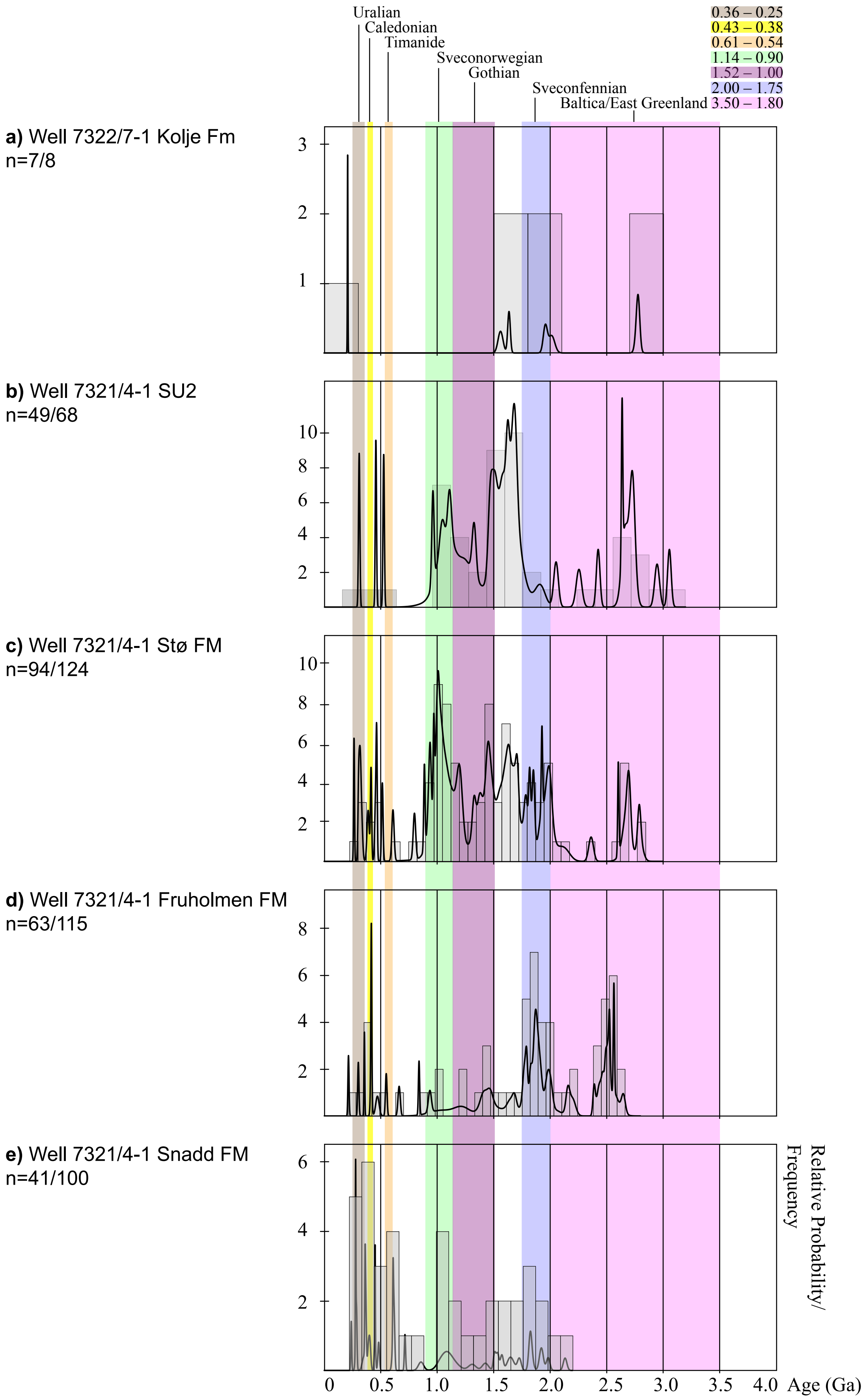

Fig. 4.16 Detrital Zircon Ages *Zircon data from well 7321/4-1 and 7322/7-1. Probability density plots and histograms. n = number of <10% discordant samples/total number of samples.*

Fruholmen FM (Upper Triassic)

The Fruholmen FM samples (well 7321/4-1) contain aboundant grains of Archean ages from 2.6 to 2.4 Ga (Fig. 4.16). The Proterozoic age distribution show a significant population betwenn 1.75 – 2.0 Ga (late Paleoproterozoic) and smaller amounts of 1 to 1.5 Ga (late Mesoproterozoic). Grains of 0.47 Ga to 0,4 Ga (mid-Ordovician to early Devonian) are abundant among the younger dated samples.

Stø FM (Lower – Middle Jurassic)

The Stø Formation (well 7321/4-1) consist of Archean dated grains in the interval between 2.8 – 2.6 Ga (Fig. 4.16). The Proterozoic age distribution is dominated by grains dated between 2.0 – 1.0 Ga characterized by two main age populations. The oldest population, between 2 – 1.3 Ga, show the highest frequency at c. 1.4 Ga (early Mesoproterozoic) and the younger population, between 1.2 – 0.9 Ga, display the highest frequency from 1.1 Ga to Ga (late Mesoproterozoic). The most significant population among the youngest dated grains are the intervals 0.46 – 0.4 Ga (mid-Ordovician – Early Devonian) and 0.4 – 3.0 Ga (Early Devonian – Late Carboniferous).

Seismic Unit 2 and Kolje FM (Lower Cretaceous)

The SU2 (well 7321/4-1) have highest frequency of Archean aged grains in the 2.6 – 2.75 Ga interval (Fig. 4.16). The dominant age populations in the Proterozoic ages range from 1.7 to 1.5 Ga (Paleo-Mesoproterozoic) and between 1.2 – 1 Ga (late Mesoproterozoic). Three younger dated grains are of 0.52 Ga (late Cambrian), 0.45 Ga (late Ordovician) and 0.30 Ga (late Carboniferous) age.

Kolje FM in well 7322/7-1 contains seven dated grains. The two oldest are dated Archean (c. 2.8 Ga), followed four Proterozoic aged grains (2, 1.9, 1.6, and 1.5 Ga) and the youngest sample is of Late Triassic age (0.21 Ga).

5 DISCUSSION

5.1 Provenance Evaluation and Implications for Reservoir Development

The northern part of Greenland and Canada (Laurentia) are potential source regions situated in the north-western corner of the Barents shelf during the Early Cretaceous. Because the clinoforms observed in the ?Hauterivian to late Barremian aged unit (SU2) in this study evolved from the northwest to the southeast in the Fingerdjupet Subbasin. The detrital zircon abundances of the studied SU2 unit (Well 7321/4-1) is similar to the zircon age signatures in Lower Cretaceous strata on Svalbard including Rurikfjellet Formation, Festningen Member and Helvetiafjellet Formation (Fig. 5.1 a,b and d). The main difference is the 1.8–1.9 Ga age population in the Svalbard samples appears to be different (Fig. 5.1). The Helvetiafjellet Formation on Svalbard, Lower Cretaceous sediments in Wandel Sea Basin (northern Greenland) and Sverdrup Basin (Arctic Canada) also shares similar detrital zircon abundances (Røhr et al., 2008, 2010; Røhr & Andersen 2009). Detrital zircon ages from Lower–Middle Triassic sediments on Svalbard also show similar age distribution as the Helvetiafjellet FM (Bue and andersen, 2013). In addition to older deposits, Cambrian aged sediments in Northwest Territories (northern Canada, Hadlari et al., 2012), Neoproterozoic to late Devonian aged sediments in Franklinian Basin (Arctic Canada, Anfinson et al. 2012) and Mesoproterozoic to early Cambrian sediments in Peary Land (North Greenland, Kirkland et al. 2009), display similar age distribution as the Helvetiafjellet FM and Lower–Middle Triassic sediments on Svalbard (Bue & andersen, 2013). The provenance of the Lower–Middle Triassic (Svalbard) and Lower Cretaceous (Svalbard, Wandel Sea Basin and Sverdrup Basin) detritus are interprted to be older deposits in the Franklinian Basin (Artic Canada) and the North Greenland (Fig. 5.2, Røhr et al., 2008, 2010; Røhr & Andersen 2009; Bue% Andersen, 2013). The similar detrital zircon abundances of the Barremian strata in the Fingerdjupet Subbasin (this study), the Lower Cretaceous succession in Svalbard, Wandel Sea Basin and Sverdrup Basin indicate that they originate from the same source area located in the northern Greenland and Franklinian Basin (Fig. 5.2) The reason why the dominant 1.8–1.9 Ga peak is not present in studiet unit could due to the distribution of the detritus characterized 1.8–1.9 Ga protosource could be limited to the north and did not reach the Barents shelf.

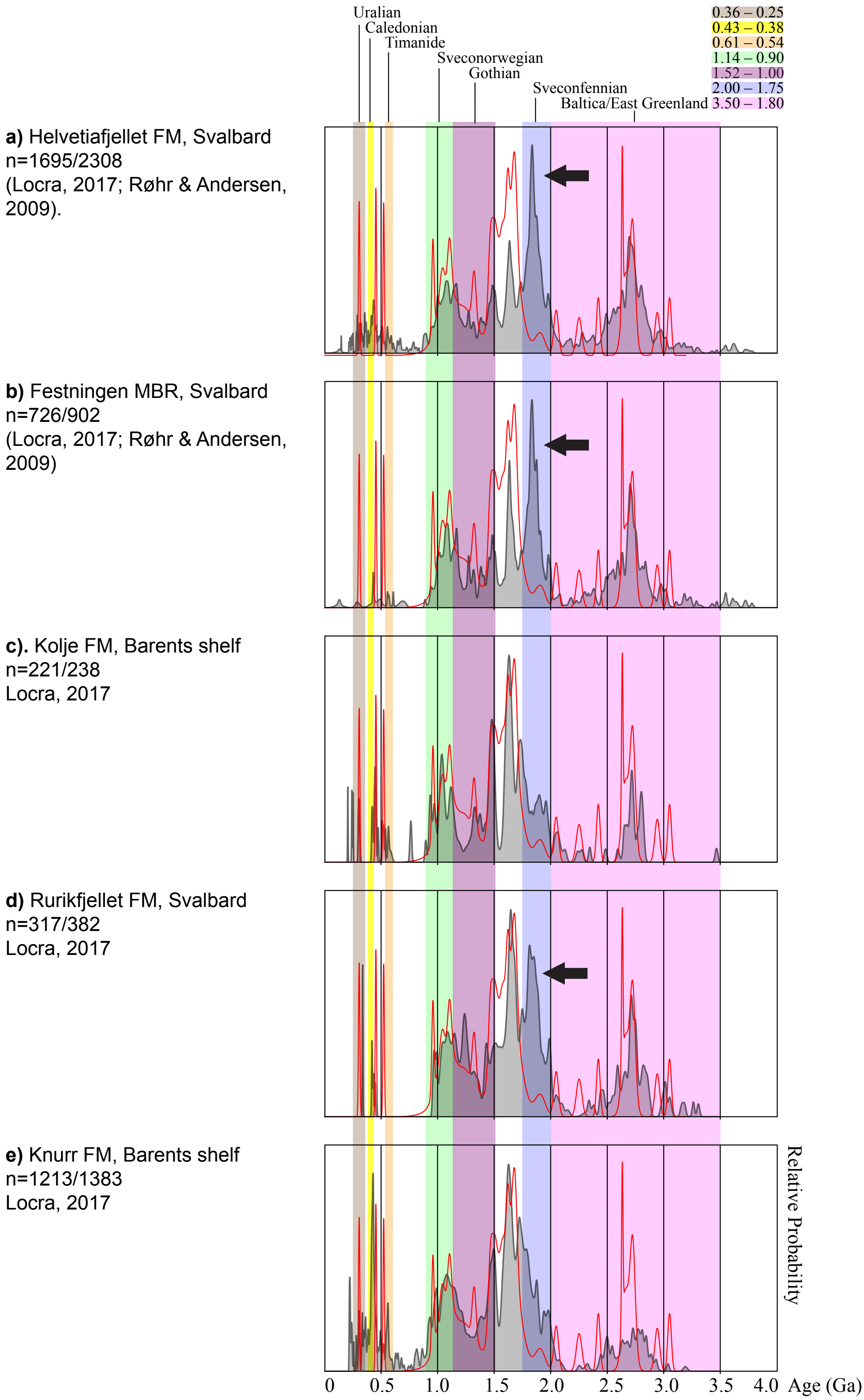

Fig. 5.1 Lower Cretaceous Comparison of Zircon Ages *The red curve represents the is the SU2 in well 7321/4-1.*

Probability density plots and histograms. n = number of <10% discordant samples/total number of samples.

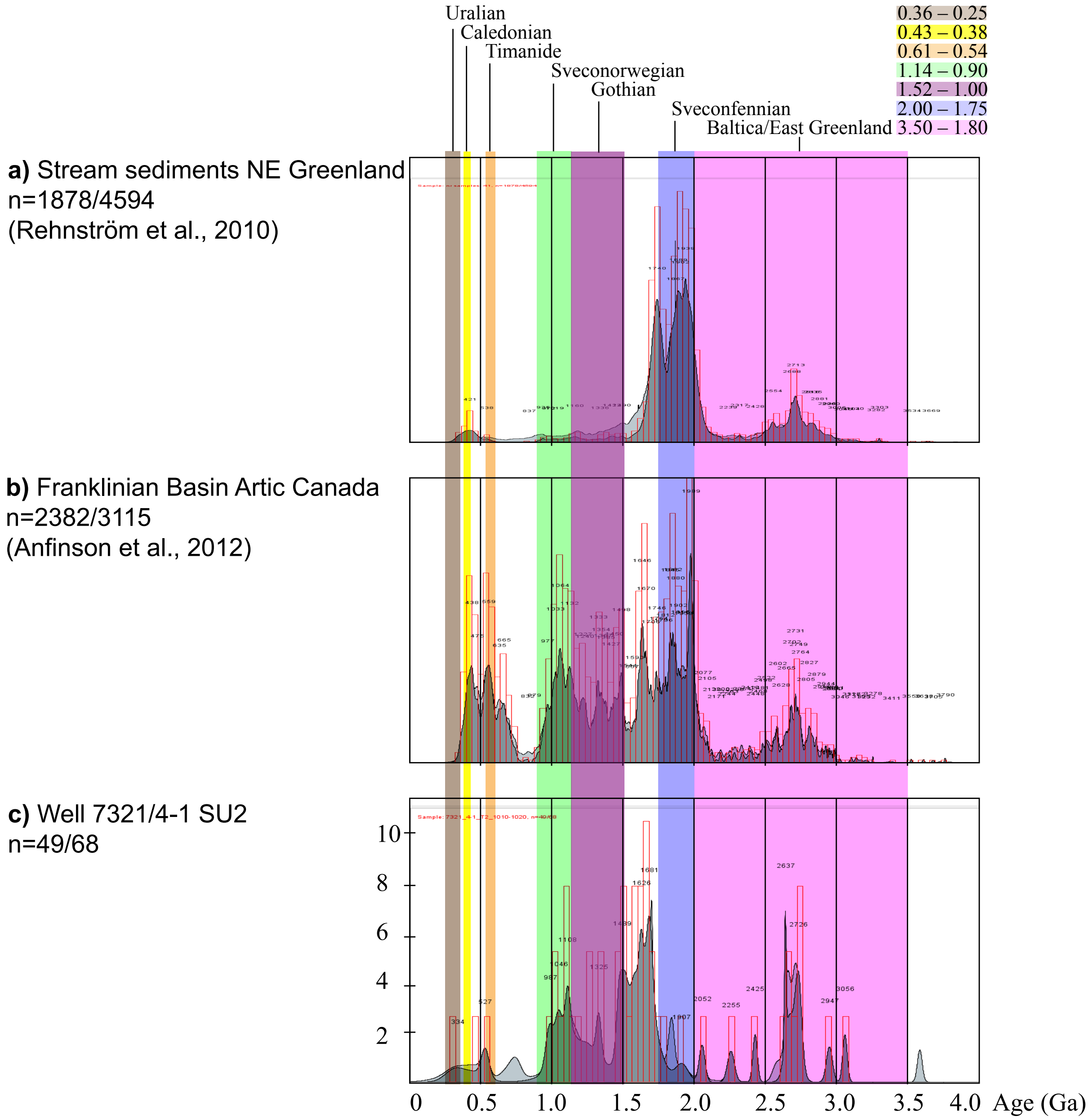

Fig. 5.2 NE Greenland and Franklinian Basin *a) Stream sediments in NE Greenland. b) Franklinian Basin. c) SU2*

The uplift and present day structuring of the Stappen high is suggested to occur during early Cenozoic (Faleide, 1993; Worsley et al., 2001, Blaich et al., 2017). However, the northern part of Stappen High (not open for petroleum exploration) is poorly constrained (e.g. Anell et al., 2016; Blaich et al., 2017) and could represent a potential source region. Permian to Middle Triassic rocks outcrops in the highest point of Stappen High (Bjørnøya, Vigran et al. 2014) and the Middle Jurassic Stø Formation is interpreted to be present in the southern margin of the Stappen High (Blaich et al., 2017). The detrital zircon abundances of the studied SU2 unit is similar to age signatures of the Stø Formation, in well 7321/4-1 (Fig. 4.16) and in the Barents shelf (Klausen et al., 2017), Knurr Formation and Kolje Formation (Fig. 5.1 c and e). Exposure and recycling of underlying Stø Formation on the northern Stappen High could explain the similar detrital zircon abundances observed in the studied SU2 unit (Well 7321/4-1) and in Knurr and Kolje formations. This may also explain why the dominant 1.8–1.9 Ga age population observed in the Lower Cretaceous succession on Svalbard is not present in the SU2 unit, Knurr and Kolje formations (Fig. 5.1). The inferred northern position of the northern Stappen High also supports the southeast prograding direction of the clinoforms in SU2. Although, petrographic and geochemical analysis preformed on the Knurr and Kolje formations in the Hammerfest and Tromsø basins do not indicate a complete recycling of younger or older strata (Locra, 2017). Locra (2017) suggest Baltica as the main provenance for the Lower Cretaceous succession in addition to a exotic source area located to the north of the Barents shelf. The exotic source is characterized by 0.4 – 0.225 Ga (Early Devonian – Late Triassic) aged sediments, intermediate to mafic detritus and strongly reworked material of Gothian and Neoarchean age (Locra, 2017).

The Loppa high is another potential source area situated in the southeastern margin of Fingerdjupet Subbasin (Fig. 1.1) The upflit the Loppa High is interpreted to reach a peak during Barremian (Indrevær et al., 2016) and may provide sediments influx from the southeastern margin of the Fingerdjupet Subbasin. However, based on the southeast prograding direction of the clinoforms in SU2, the Loppa High was unlikely the the source of SU2.

Implications for Reservoir Development

The clinoforms penetrated by well 7231/7-1 suggesting they are of shelf-edge delta scale (relief between 100 - 1000 m, e.g. Patruno et al., 2015) based on the thickness in well 7321/7-1 (261m) penetrating the middle part of the slope . The topset segment of shelf-edge delta clinoforms includes paralic to shallow marine facies which can be prolific reservoirs (Porebski and Steel 2003). Transport of sediment across the shelf is largely controlled by the successive migration of repeated regressive-transgressive delta scale clinoforms and draping clinoforms (compound clinoform systems, Patruno Helland-Hansen, Fig. 5.3) The interaction of mud-prone draping with mud-prone and sand-prone shoreline progradation gives a mixed facies relationship within shelf prism clinoforms (, Patruno & Helland-Hansen, 2018).

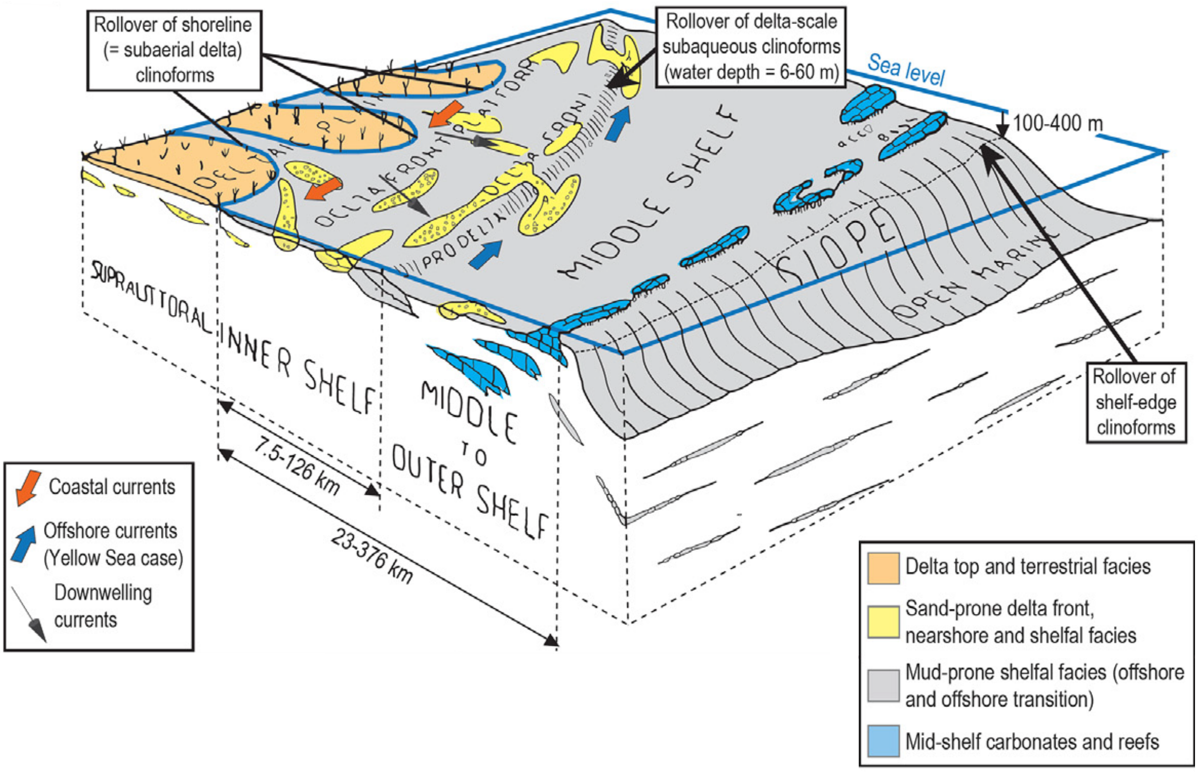

Fig. 5.3 Depositional Environment *3D cartoon illustrating facies related to a shoreline, subaqueous delta-scale and time equivalent shelf-edge clinoform system (figure modified from Patrunoa & Helland-Hansen, 2018).*

Well 7321/4-1 penetrates the topset segment of the clinoforms at a position which could represent inner to middle shelf environment. The overall coarsening to fining upward trend in SU2 can inicate a regressive lower part followed by a transgressive interval in the top. This trend may represent a shoreline system followed by transgressive shales in the top. Thus, be a system of a potentially laterally extensive shorelines systems. Example, the Battfjellet Formation (Eocene) on Svalbard consists of 20 sand-prone shelf-margin clinoforms. The topsets of these clinoforms consists of a regressive lower part of fluvial-wave dominated delta-front deposits overlain by tide-influenced estuarine deposits (Steel and Olsen, 2002). Thick sand wedges can develop at the shelf-edge consisting of upward coarsening delta-front, mouth bar and channel system. Sand sheets of turbidite deposits commonly form in the upper to middle slope and deep water fans sand may accumulate in both during rising and falling sea levels (porębski & Steel, 2003). Hence shelf-edge delta systems can form good reservoirs in the shelf, slope and in the basin floor.

The only indicator of sand in the SU2 clinoforms is in well 7321/4-1 which corresponds to the topset segment of the clinoforms. The middle part of the slope is penetrated by well 7321/7-1 which show dominant fine-grain rocks. Well 7321/8-1 and well 7321/9-1 penetrated the bottomsets which is also dominated by fine-grain rocks. There are no seismic evidence of delta scale clinoforms with steep foresets and base on dominant fine grain deposits in the slope and bottomsets penetrated by the other wells, sand is probably restricted to the topsets.

6 CONCLUSION

Well 7321/4-1 penetrates a unit with reltaive low gammar ray values compared to the other exploration wells in the Fingerdjupet Subbasin. Palynological analyses (carried out by GEUS) indicated a ?Hauterivian to late Barremian age for this interval and seismic interpretation shows that this interval corresponds to southeast prograding clinoforms.

Detrital zircon U/Pb geochronology (carried out by GEUS) from samples in well 7321/4-1 and from in well 7322/7-1 was preformed to interpret the source of these sediments. The samples from well 7321/4-1 are dominated by three age polulations: (1) 2.6 – 2.75 Ga, (2) 1.7 to 1.5 Ga and (3) 1.2 – 1 Ga. While the samples from well 7322/7-1 contain only seven dated grains, thus making it difficult to intepret the origin of these siltsontes. The dominant age polulations observed SU2 turns out to be quite similar to the age distribution that dominates several chronostratigraphic units in the northern Greenland, the Arctic Canada and on Svalbard. Based on the similar age signatures of SU2 with these and southeast prograding direction of the cinoforms in SU2, the source of sediments to the Fingerdjupet is suggested to be North Greenland and/or Arctic Canada.

The sandstones in well 7321/4-1 is interpreted to be the topsets of shelf-edge delta scale clinoforms that prograded from the Ringsel Ridge in the northwest and into the Fingerdjupet Subbasin. The gamma ray signature of the topsets indiacates a coarsening to fining upwards stacking pattern which can potentially form good shallow marin sandstones. The lack of coarse clastics in wells penetrating the slope and basin floor segment of the system constrains the lateral distribution of sandstones in the study area.

7 APPENDIX

Fig. 7.1

Well	Sample Interval [MD]	Unit
7322/7-1	679-763	Kolje FM (Lower Cretaceous)
7321/4-1	1010-1020	SU2 (Lower Cretaceous)
7321/4-1	1348-1354	Stø FM (Lower – Middle Jurassic)
7321/4-1	1422-1428	Fruholmen FM (Upper Triassic)
7321/4-1	1521-1524	Snadd FM (Middle – Upper Triassic)

Kolje FM		CONCENTRATIONS[a]						RATIOS								AGES						Con-cordance
Sample	Analysis	U [ppm]	2 σ	Th [ppm]	2 σ	Pb [ppm]	2 σ	U/Th[a]	$^{207}Pb/^{235}U$[b]	2 σ[d]	$^{206}Pb/^{238}U$[b]	2 σ[d]	rho[c]	$^{207}Pb/^{206}Pb$[e]	2 σ[d]	$^{207}Pb/^{235}U$[b]	2 σ[d]	$^{206}Pb/^{238}U$[b]	2 σ[d]	$^{207}Pb/^{206}Pb$[e]	2 σ[d]	
7322/7-1__679-763	Zircon_sample-007.FIN2	429	45	151	25	141	22	2,91	0,267	0,018	0,037	0,001	0,459	0,0526	0,0038	240	15	233	7,5	300	160	77,8
7322/7-1__679-763	Zircon_sample-008.FIN2	646	56	168	26	145	35	3,88	0,231	0,030	0,033	0,001	0,889	0,0501	0,0055	211	25	209	4,8	200	240	104,4
7322/7-1__679-763	Zircon_sample-009.FIN2	337	99	49	14	365	91	7,60	5,863	0,091	0,332	0,018	0,848	0,1239	0,0038	1956	13	1850	87	2013	55	91,9
7322/7-1__679-763	Zircon_sample-010.FIN2	886	61	299	39	1920	170	3,04	3,840	0,140	0,271	0,008	0,929	0,1006	0,0013	1600	29	1546	40	1636	23	94,5
7322/7-1__679-763	Zircon_sample-012.FIN2	215	27	64	3	504	33	3,38	5,780	0,340	0,337	0,026	0,895	0,1201	0,0024	1942	50	1870	130	1957	36	95,6
7322/7-1__679-763	Zircon_sample-013.FIN2	400	100	61	16	670	180	6,48	13,690	0,430	0,500	0,012	0,660	0,1936	0,0044	2727	30	2636	63	2772	37	95,1
7322/7-1__679-763	Zircon_sample-014.FIN2	310	120	52	12	488	99	5,90	14,100	1,200	0,521	0,039	0,990	0,1944	0,0033	2754	77	2700	160	2779	28	97,2
Common-Pb corrected[f]																						
7322/7-1__679-763	Zircon_sample-011.FIN2	546	71	132	32	870	140	4,94	3,860	0,180	0,284	0,015	0,906	0,0968	0,0023	1604	35	1613	75	1561	44	103,3

SU2		CONCENTRATIONS[a]						RATIOS								AGES						Con-cordance
Sample	Analysis	U [ppm]	2 σ	Th [ppm]	2 σ	Pb [ppm]	2 σ	U/Th[a]	$^{207}Pb/^{235}U$[b]	2 σ[d]	$^{206}Pb/^{238}U$[b]	2 σ[d]	rho[c]	$^{207}Pb/^{206}Pb$[e]	2 σ[d]	$^{207}Pb/^{235}U$[b]	2 σ[d]	$^{206}Pb/^{238}U$[b]	2 σ[d]	$^{207}Pb/^{206}Pb$[e]	2 σ[d]	
7321-4 1T2__1010-1020	Zircon_sample-007.FIN2	175	24	99	10	187	18	1,82	0,569	0,043	0,073	0,002	0,000	0,0563	0,0041	456	28	455	11	450	160	101,1
7321-4 1T2__1010-1020	Zircon_sample-008.FIN2	182	6	72	2	673	48	2,62	8,550	0,420	0,438	0,014	0,776	0,1422	0,0040	2290	45	2341	63	2254	49	103,9
7321-4 1T2__1010-1020	Zircon_sample-009.FIN2	472	70	30	3	116	11	16,60	1,661	0,069	0,168	0,008	0,856	0,0717	0,0017	993	26	1003	43	977	48	102,7
7321-4 1T2__1010-1020	Zircon_sample-013.FIN2	380	110	148	48	199	55	2,73	0,411	0,035	0,057	0,002	-0,486	0,0522	0,0057	349	25	360	12	280	240	128,6
7321-4 1T2__1010-1020	Zircon_sample--025.FIN2	266	56	22	6	239	48	13,30	15,180	0,990	0,595	0,038	0,940	0,1852	0,0041	2824	62	3010	150	2699	37	111,5
7321-4 1T2__1010-1020	Zircon_sample--028.FIN2	1260	330	7	3	100	28	200,00	0,625	0,019	0,071	0,003	0,926	0,0641	0,0022	493	12	443	19	745	71	59,5
7321-4 1T2__1010-1020	Zircon_sample-036.FIN2	52	3	47	4	548	60	1,13	18,900	0,940	0,596	0,042	0,981	0,2305	0,0046	3036	48	3010	170	3055	32	98,5
7321-4 1T2__1010-1020	Zircon_sample-041.FIN2	195	30	41	9	267	68	4,82	4,179	0,087	0,294	0,009	0,498	0,1035	0,0030	1670	17	1663	42	1687	53	98,6
7321-4 1T2__1010-1020	Zircon_sample-050.FIN2	249	16	56	3	408	61	4,45	4,258	0,095	0,307	0,008	0,551	0,1000	0,0016	1685	18	1725	38	1623	29	106,3
7321-4 1T2__1010-1020	Zircon_sample--052.FIN2	301	16	128	9	203	21	2,34	0,633	0,096	0,067	0,003	0,096	0,0690	0,0100	496	61	416	16	860	340	48,4
7321-4 1T2__1010-1020	Zircon_sample-053.FIN2	132	9	96	4	1040	100	1,37	13,240	0,740	0,533	0,018	0,976	0,1801	0,0052	2696	54	2754	76	2653	48	103,8
7321-4 1T2__1010-1020	Zircon_sample-056.FIN2	480	100	42	7	262	49	11,60	3,830	0,130	0,268	0,010	0,867	0,1034	0,0021	1599	27	1532	50	1686	37	90,9
7321-4 1T2__1010-1020	Zircon_sample-064.FIN2	864	53	302	28	1760	130	2,84	3,370	0,140	0,266	0,011	0,907	0,0920	0,0017	1497	34	1518	57	1467	35	103,5
7321-4 1T2__1010-1020	Zircon_sample-066.FIN2	346	46	60	8	680	120	5,69	10,770	0,690	0,498	0,026	0,986	0,1570	0,0030	2502	60	2600	110	2424	32	107,3
7321-4 1T2__1010-1020	Zircon_sample-070.FIN2	530	190	56	10	239	51	8,80	1,733	0,071	0,173	0,007	0,815	0,0741	0,0017	1020	26	1029	40	1043	47	98,7
7321-4 1T2__1010-1020	Zircon_sample-082.FIN2	207	18	70	12	430	35	2,95	3,890	0,340	0,279	0,011	0,016	0,1009	0,0087	1609	69	1587	55	1630	160	97,4
7321-4 1T2__1010-1020	Zircon_sample-083.FIN2	111	24	38	5	397	30	2,96	13,580	0,730	0,546	0,009	0,874	0,1806	0,0079	2720	51	2808	36	2657	72	105,7
7321-4 1T2__1010-1020	Zircon_sample-084.FIN2	151	32	89	26	600	150	1,84	3,720	0,120	0,278	0,012	0,558	0,0979	0,0053	1576	26	1579	61	1580	100	99,9
7321-4 1T2__1010-1020	Zircon_sample-093.FIN2	114	7	110	9	464	38	1,03	2,010	0,150	0,190	0,005	-0,690	0,0773	0,0076	1118	52	1120	27	1120	200	100
7321-4 1T2__1010-1020	Zircon_sample-098.FIN2	388	99	75	19	306	53	5,15	1,889	0,093	0,172	0,004	0,166	0,0780	0,0031	1076	33	1025	24	1145	79	89,5
7321-4 1T2__1010-1020	Zircon_sample-108.FIN2	123	26	44	5	625	81	2,74	26,140	0,690	0,587	0,027	0,854	0,3224	0,0071	3351	26	2980	110	3581	34	83,2
7321-4 1T2__1010-1020	Zircon_sample-109.FIN2	508	39	73	21	530	140	8,00	4,120	0,220	0,292	0,011	0,612	0,1027	0,0044	1658	43	1652	53	1671	78	98,9
7321-4 1T2__1010-1020	Zircon_sample-112.FIN2	320	110	137	44	1010	200	2,29	4,060	0,160	0,299	0,013	0,546	0,0976	0,0027	1646	31	1684	65	1576	52	106,9
7321-4 1T2__1010-1020	Zircon_sample-120.FIN2	103	13	29	5	147	27	3,52	2,150	0,250	0,190	0,002	0,131	0,0820	0,0100	1162	81	1121	11	1240	250	90,4
7321-4 1T2__1010-1020	Zircon_sample-123.FIN2	127	6	60	3	541	33	2,01	6,050	0,260	0,376	0,013	0,623	0,1172	0,0056	1982	37	2056	59	1911	87	107,6
7321-4 1T2__1010-1020	Zircon_sample-125.FIN2	91	7	31	4	237	26	2,91	4,450	0,240	0,305	0,015	0,674	0,1063	0,0047	1719	45	1713	72	1733	80	98,8
7321-4 1T2__1010-1020	Zircon_sample-135.FIN2	820	120	180	45	1110	210	4,66	3,540	0,140	0,274	0,010	0,827	0,0940	0,0023	1536	33	1559	50	1507	47	103,5
7321-4 1T2__1010-1020	Zircon_sample-136.FIN2	560	160	85	19	414	83	6,28	2,228	0,091	0,208	0,006	0,647	0,0765	0,0013	1189	29	1216	31	1107	35	109,8
7321-4 1T2__1010-1020	Zircon_sample-138.FIN2	272	58	141	50	312	75	2,07	0,790	0,048	0,094	0,002	-0,222	0,0626	0,0031	590	27	576	13	690	100	83,5
7321-4 1T2__1010-1020	Zircon_sample-139.FIN2	233	22	43	5	554	53	5,38	15,860	0,610	0,534	0,012	0,804	0,2154	0,0057	2868	37	2759	52	2946	43	93,7
7321-4 1T2__1010-1020	Zircon_sample-149.FIN2	205	32	65	20	399	89	3,37	3,620	0,350	0,282	0,010	0,019	0,0928	0,0089	1551	78	1600	48	1470	190	108,8
7321-4 1T2__1010-1020	Zircon_sample-153.FIN2	91	16	20	3	78	6	4,63	2,230	0,120	0,197	0,005	0,406	0,0824	0,0039	1188	38	1157	26	1252	92	92,4
7321-4 1T2__1010-1020	Zircon_sample-154.FIN2	341	20	10	5	58	24	42,00	2,020	0,120	0,186	0,003	0,961	0,0792	0,0042	1123	41	1102	17	1180	100	93,4
7321-4 1T2__1010-1020	Zircon_sample-163.FIN2	227	10	45	3	526	25	5,11	14,510	0,110	0,569	0,015	0,810	0,1881	0,0047	2784	7,4	2903	61	2725	41	106,5
7321-4 1T2__1010-1020	Zircon_sample-165.FIN2	121	35	24	16	108	74	6,80	1,630	0,180	0,161	0,004	-0,175	0,0736	0,0091	978	68	960	20	1020	250	94,1
7321-4 1T2__1010-1020	Zircon_sample-176.FIN2	233	37	98	10	1121	62	2,37	13,500	1,200	0,533	0,047	0,953	0,1845	0,0061	2710	88	2750	200	2692	53	102,2
7321-4 1T2__1010-1020	Zircon_sample-177.FIN2	189	11	53	4	374	23	3,59	4,110	0,220	0,293	0,006	-0,390	0,1019	0,0066	1653	44	1656	29	1650	120	100,4
7321-4 1T2__1010-1020	Zircon_sample-180.FIN2	184	13	89	5	530	14	2,06	2,910	0,130	0,247	0,011	0,766	0,0859	0,0051	1384	34	1422	59	1330	120	106,9
7321-4 1T2__1010-1020	Zircon_sample-181.FIN2	642	20	171	5	1850	110	3,74	11,160	0,420	0,462	0,010	0,640	0,1782	0,0012	2536	35	2448	46	2636	12	92,9
7321-4 1T2__1010-1020	Zircon_sample-190.FIN2	380	77	102	19	680	110	3,65	3,630	0,190	0,279	0,008	0,678	0,0949	0,0040	1555	43	1585	40	1523	80	104,1
7321-4 1T2__1010-1020	Zircon_sample-191.FIN2	392	41	8	3	53	16	59,00	1,714	0,076	0,171	0,005	0,085	0,0728	0,0038	1013	29	1018	28	1010	100	100,8
7321-4 1T2__1010-1020	Zircon_sample-195.FIN2	328	19	34	3	220	29	9,41	3,760	0,180	0,278	0,011	0,671	0,0981	0,0037	1583	39	1583	53	1584	71	99,9
7321-4 1T2__1010-1020	Zircon_sample-204.FIN2	1405	61	726	32	1470	100	1,92	0,676	0,010	0,085	0,002	0,076	0,0580	0,0014	525	6,1	524	12	528	54	99,2
7321-4 1T2__1010-1020	Zircon_sample-205.FIN2	377	19	111	10	950	110	3,23	7,110	0,260	0,400	0,017	0,884	0,1266	0,0029	2125	34	2169	81	2051	41	105,8
7321-4 1T2__1010-1020	Zircon_sample-207.FIN2	249	26	45	5	347	68	5,43	4,030	0,330	0,292	0,014	0,862	0,1004	0,0052	1638	67	1651	71	1629	96	101,4
7321-4 1T2__1010-1020	Zircon_sample-208.FIN2	386	27	64	2	368	49	5,94	2,970	0,120	0,252	0,010	0,906	0,0855	0,0016	1400	31	1448	49	1325	35	109,3
7321-4 1T2__1010-1020	Zircon_sample-220.FIN2	204	21	48	6	218	27	4,32	1,900	0,100	0,177	0,010	0,612	0,0768	0,0031	1080	35	1048	55	1113	79	94,2
7321-4 1T2__1010-1020	Zircon_sample-224.FIN2	780	70	186	17	1100	160	4,19	3,360	0,210	0,260	0,013	0,632	0,0935	0,0041	1494	50	1491	68	1495	81	99,7
7321-4 1T2__1010-1020	Zircon_sample-232.FIN2	365	28	78	6	499	39	4,72	3,300	0,180	0,256	0,006	0,741	0,0934	0,0033	1479	42	1469	29	1493	67	98,4
7321-4 1T2__1010-1020	Zircon_sample-233.FIN2	397	22	131	8	940	110	3,08	4,550	0,110	0,327	0,006	0,495	0,1023	0,0028	1740	20	1825	28	1664	51	109,7
7321-4 1T2__1010-1020	Zircon_sample-236.FIN2	805	77	191	31	189	41	4,26	0,315	0,021	0,041	0,001	0,844	0,0564	0,0040	278	16	257	8	460	150	55,8
7321-4 1T2__1010-1020	Zircon_sample-247.FIN2	324	37	59	8	430	400	5,53	1,690	0,170	0,156	0,004	0,786	0,0787	0,0058	1005	64	935	23	1160	150	80,6
7321-4 1T2__1010-1020	Zircon_sample-248.FIN2	540	180	172	80	1410	550	3,50	4,700	0,360	0,316	0,005	0,552	0,1084	0,0078	1766	64	1769	22	1770	130	99,9
7321-4 1T2__1010-1020	Zircon_sample-250.FIN2	523	73	54	10	337	60	10,40	4,310	0,230	0,308	0,008	0,492	0,1017	0,0049	1694	45	1730	37	1652	92	104,7
7321-4 1T2__1010-1020	Zircon_sample-251.FIN2	146	7	95	9	1210	160	1,48	14,540	0,720	0,558	0,025	0,880	0,1891	0,0049	2783	48	2850	110	2733	42	104,3
7321-4 1T2__1010-1020	Zircon_sample-252.FIN2	339	65	52	12	570	130	6,56	13,530	0,310	0,518	0,021	0,234	0,1892	0,0068	2717	21	2690	89	2734	59	98,4
Common-Pb corrected[f]																						
7321-4 1T2__1010-1020	Zircon_sample--026.FIN2	980	110	525	69	930	100	1,92	2,930	0,270	0,124	0,012	0,993	0,1720	0,0061	1389	70	752	66	2577	59	29,2
7321-4 1T2__1010-1020	Zircon_sample-065.FIN2	274	14	153	28	1152	96	1,81	9,940	0,280	0,402	0,018	0,979	0,1802	0,0030	2429	26	2176	81	2655	28	82
7321-4 1T2__1010-1020	Zircon_sample-068.FIN2	350	190	67	53	1050	660	7,70	4,050	0,880	0,242	0,029	0,655	0,1230	0,0270	1620	180	1400	150	1940	360	72,2
7321-4 1T2__1010-1020	Zircon_sample-121.FIN2	2050	290	460	150	4700	1100	4,90	9,130	0,850	0,357	0,028	0,929	0,1856	0,0051	2348	87	1970	130	2703	46	72,9
7321-4 1T2__1010-1020	Zircon_sample-134.FIN2	1260	160	108	3	428	36	11,50	2,810	0,023	0,197	0,002	0,997	0,1040	0,0008	1358	6,2	1159	11	1697	14	68,3
7321-4 1T2__1010-1020	Zircon_sample-164.FIN2	489	45	201	37	2080	360	2,46	10,220	0,420	0,413	0,011	0,949	0,1796	0,0056	2455	37	2228	50	2649	52	84,1
7321-4 1T2__1010-1020	Zircon_sample-168.FIN2	378	22	291	19	1450	170	1,30	4,220	0,220	0,273	0,012	0,864	0,1118	0,0029	1678	44	1558	62	1828	46	85,2
7321-4 1T2__1010-1020	Zircon_sample-178.FIN2	889	97	235	9	573	83	3,78	2,580	0,120	0,197	0,010	0,903	0,0953	0,0052	1295	33	1161	52	1530	100	75,9
7321-4 1T2__1010-1020	Zircon_sample-194.FIN2	2286	87	739	84	1080	140	2,99	0,349	0,030	0,049	0,002	0,679	0,0519	0,0032	303	22	307	12	310	130	99
7321-4 1T2__1010-1020	Zircon_sample-206.FIN2	1604	84	374	20	1830	120	4,23	2,610	0,120	0,196	0,007	0,730	0,0967	0,0033	1302	33	1152	39	1559	63	73,9
7321-4 1T2__1010-1020	Zircon_sample-209.FIN2	1258	81	385	45	1830	170	3,23	3,770	0,100	0,244	0,008	0,943	0,1125	0,0021	1586	22	1405	41	1840	34	76,4
7321-4 1T2__1010-1020	Zircon_sample-234.FIN2	619	43	367	44	1640	230	1,71	1,880	0,140	0,180	0,004	0,766	0,0759	0,0052	1072	47	1068	23	1080	140	98,9

Fig. 7.1 Appendix1

Fig. 7.2

Stø FM		CONCENTRATIONS[a]						RATIOS								AGES						Con-cordance
Sample	Analysis	U [ppm]	2 σ	Th [ppm]	2 σ	Pb [ppm]	2 σ	U/Th[a]	$^{207}Pb/^{235}U$[b]	2 σ[d]	$^{206}Pb/^{238}U$[b]	2 σ[d]	rho[c]	$^{207}Pb/^{206}Pb$[e]	2 σ[d]	$^{207}Pb/^{235}U$[b]	2 σ[d]	$^{206}Pb/^{238}U$[b]	2 σ[d]	$^{207}Pb/^{206}Pb$[e]	2 σ[d]	
7321-4 1T2__1348-1354	Zircon_sample-290.FIN2	252	20	108	7	49	7	2,37	1,591	0,094	0,162	0,002	0,521	0,0717	0,0041	966	37	970	12	970	120	100,0
7321-4 1T2__1348-1354	Zircon_sample-292.FIN2	439	24	172	17	94	4	2,61	2,299	0,061	0,212	0,006	0,835	0,0797	0,0020	1212	19	1237	34	1190	49	103,9
7321-4 1T2__1348-1354	Zircon_sample-294.FIN2	215	46	84	18	74	16	2,60	5,190	0,210	0,320	0,011	0,438	0,1178	0,0036	1850	34	1789	56	1923	55	93,0
7321-4 1T2__1348-1354	Zircon_sample-302.FIN2	292	26	184	32	42	18	1,63	0,720	0,320	0,072	0,002	0,493	0,0720	0,0320	540	180	447	14	880	830	50,8
7321-4 1T2__1348-1354	Zircon_sample-303.FIN2	228	39	103	11	41	5	2,33	1,680	0,120	0,170	0,007	0,714	0,0718	0,0031	999	45	1013	40	976	85	103,8
7321-4 1T2__1348-1354	Zircon_sample-304.FIN2	177	16	101	15	18	4	1,83	0,537	0,074	0,067	0,003	0,595	0,0541	0,0018	435	48	417	16	490	240	85,1
7321-4 1T2__1348-1354	Zircon_sample-305.FIN2	119	11	92	16	14	4	1,34	0,480	0,150	0,051	0,003	0,263	0,0680	0,0210	394	97	320	20	760	540	42,1
7321-4 1T2__1348-1354	Zircon_sample-308.FIN2	96	14	63	10	29	7	1,54	1,940	0,250	0,188	0,006	0,947	0,0750	0,0066	1093	87	1108	32	1060	180	104,5
7321-4 1T2__1348-1354	Zircon_sample-316.FIN2	169	10	41	4	20	2	4,21	1,687	0,055	0,170	0,007	0,517	0,0726	0,0038	1003	21	1009	36	1000	110	100,9
7321-4 1T2__1348-1354	Zircon_sample-317.FIN2	71	9	32	4	17	2	2,27	2,960	0,110	0,236	0,012	0,744	0,0914	0,0049	1398	28	1364	64	1450	100	94,1
7321-4 1T2__1348-1354	Zircon_sample-318.FIN2	168	56	61	13	26	6	2,71	1,860	0,230	0,173	0,011	0,814	0,0780	0,0061	1066	78	1030	58	1140	150	90,4
7321-4 1T2__1348-1354	Zircon_sample-319.FIN2	218	30	118	20	22	4	1,89	0,573	0,060	0,075	0,002	0,459	0,0562	0,0066	460	38	465	10	450	250	103,3
7321-4 1T2__1348-1354	Zircon_sample-320.FIN2	197	18	153	22	116	18	1,30	3,900	0,200	0,283	0,006	0,860	0,1003	0,0049	1612	42	1606	29	1627	87	98,7
7321-4 1T2__1348-1354	Zircon_sample-321.FIN2	150	19	109	14	50	5	1,39	1,700	0,100	0,169	0,009	0,719	0,0716	0,0012	1008	39	1004	50	974	35	103,1
7321-4 1T2__1348-1354	Zircon_sample-322.FIN2	83	3	42	2	28	3	2,06	2,892	0,092	0,242	0,006	0,263	0,0862	0,0032	1379	24	1395	29	1339	72	104,2
7321-4 1T2__1348-1354	Zircon_sample-330.FIN2	97	7	66	10	33	7	1,49	1,717	0,088	0,174	0,005	0,900	0,0723	0,0026	1014	33	1033	25	992	74	104,1
7321-4 1T2__1348-1354	Zircon_sample-331.FIN2	169	11	120	12	57	8	1,43	1,770	0,110	0,172	0,003	0,683	0,0752	0,0036	1033	40	1020	19	1069	97	95,4
7321-4 1T2__1348-1354	Zircon_sample-332.FIN2	323	25	558	36	401	22	0,58	3,770	0,190	0,278	0,009	0,709	0,0987	0,0030	1586	42	1579	45	1598	56	98,8
7321-4 1T2__1348-1354	Zircon_sample-333.FIN2	448	41	162	11	84	6	2,82	1,881	0,048	0,184	0,003	0,022	0,0745	0,0021	1074	17	1087	17	1054	55	103,1
7321-4 1T2__1348-1354	Zircon_sample-334.FIN2	142	8	65	5	60	5	2,23	6,050	0,110	0,358	0,008	0,582	0,1217	0,0030	1983	15	1973	40	1980	44	99,6
7321-4 1T2__1348-1354	Zircon_sample-336.FIN2	310	32	244	32	26	3	1,35	0,299	0,025	0,042	0,001	0,370	0,0520	0,0041	265	20	265	8,2	270	180	98,0
7321-4 1T2__1348-1354	Zircon_sample-344.FIN2	196	19	299	34	54	8	0,67	0,481	0,041	0,065	0,002	0,655	0,0535	0,0034	398	28	408	13	350	140	116,6
7321-4 1T2__1348-1354	Zircon_sample-345.FIN2	829	42	159	12	78	7	5,11	1,799	0,093	0,179	0,006	0,747	0,0734	0,0015	1044	33	1059	35	1024	41	103,4
7321-4 1T2__1348-1354	Zircon_sample-346.FIN2	340	120	117	30	116	21	2,97	12,290	0,440	0,481	0,018	-0,434	0,1850	0,0034	2627	34	2530	80	2698	30	93,8
7321-4 1T2__1348-1354	Zircon_sample-347.FIN2	172	2	68	2	37	4	2,56	1,900	0,100	0,180	0,003	0,310	0,0779	0,0039	1082	37	1068	15	1140	100	93,7
7321-4 1T2__1348-1354	Zircon_sample-349.FIN2	42	2	44	5	8	1	1,04	0,380	0,038	0,052	0,003	-0,125	0,0538	0,0080	326	28	329	20	330	320	99,7
7321-4 1T2__1348-1354	Zircon_sample-350.FIN2	188	35	84	13	73	13	2,10	4,302	0,066	0,297	0,004	0,811	0,1047	0,0014	1694	13	1676	20	1709	25	98,1
7321-4 1T2__1348-1354	Zircon_sample-358.FIN2	161	19	54	7	41	4	3,07	4,430	0,260	0,310	0,010	0,731	0,1038	0,0024	1718	49	1742	48	1692	44	103,0
7321-4 1T2__1348-1354	Zircon_sample-360.FIN2	445	23	138	5	92	6	3,31	3,120	0,170	0,247	0,005	0,736	0,0920	0,0024	1437	42	1423	24	1466	50	97,1
7321-4 1T2__1348-1354	Zircon_sample-361.FIN2	65	11	47	5	38	6	1,45	4,590	0,150	0,310	0,011	-0,363	0,1077	0,0045	1746	28	1742	52	1757	77	99,1
7321-4 1T2__1348-1354	Zircon_sample-362.FIN2	293	40	106	15	62	7	2,83	2,650	0,130	0,225	0,009	0,620	0,0855	0,0013	1314	37	1309	45	1326	30	98,7
7321-4 1T2__1348-1354	Zircon_sample-363.FIN2	387	29	146	12	71	7	2,73	1,831	0,080	0,176	0,005	0,253	0,0759	0,0030	1056	29	1045	26	1089	81	96,0
7321-4 1T2__1348-1354	Zircon_sample-364.FIN2	158	32	96	23	11	2	1,83	0,318	0,022	0,046	0,001	0,044	0,0502	0,0036	280	17	291	8,8	200	150	145,3
7321-4 1T2__1348-1354	Zircon_sample-372.FIN2	221	5	300	11	366	25	0,76	12,850	0,300	0,509	0,013	0,686	0,1844	0,0044	2668	22	2653	55	2692	40	98,6
7321-4 1T2__1348-1354	Zircon_sample-373.FIN2	352	83	210	90	43	13	1,96	0,569	0,022	0,065	0,002	0,486	0,0624	0,0030	457	14	407	12	750	170	54,3
7321-4 1T2__1348-1354	Zircon_sample-374.FIN2	314	72	181	47	28	6	1,79	0,376	0,052	0,051	0,002	0,718	0,0540	0,0062	323	38	318	14	350	240	90,9
7321-4 1T2__1348-1354	Zircon_sample-375.FIN2	215	46	21	11	26	14	13,10	13,850	0,500	0,530	0,017	0,814	0,1933	0,0038	2739	34	2742	73	2795	56	98,1
7321-4 1T2__1348-1354	Zircon_sample-376.FIN2	301	36	29	9	13	5	11,10	1,790	0,150	0,173	0,005	0,744	0,0741	0,0061	1041	55	1030	26	1040	170	99,0
7321-4 1T2__1348-1354	Zircon_sample-377.FIN2	140	32	62	14	33	11	2,28	2,970	0,220	0,243	0,007	-0,374	0,0877	0,0018	1400	57	1403	37	1376	40	102,0
7321-4 1T2__1348-1354	Zircon_sample-378.FIN2	79	2	38	2	37	2	2,12	5,640	0,170	0,349	0,008	0,565	0,1177	0,0030	1921	27	1929	36	1921	47	100,4
7321-4 1T2__1348-1354	Zircon_sample-386.FIN2	205	10	149	6	134	3	1,38	5,920	0,200	0,355	0,008	0,707	0,1229	0,0025	1963	29	1959	37	1998	36	98,0
7321-4 1T2__1348-1354	Zircon_sample-387.FIN2	435	43	176	23	20	3	2,49	0,307	0,036	0,040	0,001	-0,350	0,0553	0,0056	272	28	254	3,5	410	240	61,9
7321-4 1T2__1348-1354	Zircon_sample-388.FIN2	370	110	800	1300	87	9	1,26	1,440	0,160	0,155	0,005	0,514	0,0683	0,0063	906	66	928	25	870	190	106,7
7321-4 1T2__1348-1354	Zircon_sample-389.FIN2	86	11	59	12	31	4	1,50	1,770	0,097	0,168	0,004	0,480	0,0770	0,0037	1034	35	999	24	1118	93	89,4
7321-4 1T2__1348-1354	Zircon_sample-391.FIN2	64	6	37	6	18	5	1,75	1,720	0,100	0,170	0,009	0,426	0,0779	0,0089	1015	38	1014	51	1120	220	90,5
7321-4 1T2__1348-1354	Zircon_sample-392.FIN2	222	52	114	23	25	2	1,93	0,549	0,025	0,073	0,003	0,461	0,0562	0,0034	444	16	456	16	450	140	101,3
7321-4 1T2__1348-1354	Zircon_sample-400.FIN2	200	16	181	12	143	10	1,06	4,150	0,110	0,293	0,013	0,901	0,1018	0,0016	1665	23	1656	64	1671	38	99,1
7321-4 1T2__1348-1354	Zircon_sample-402.FIN2	61	5	35	4	38	4	1,79	8,890	0,250	0,427	0,009	0,861	0,1515	0,0037	2326	25	2293	43	2362	42	97,1
7321-4 1T2__1348-1354	Zircon_sample-403.FIN2	142	31	42	10	21	1	3,34	2,120	0,130	0,202	0,008	0,465	0,0758	0,0059	1155	43	1188	43	1090	160	109,0
7321-4 1T2__1348-1354	Zircon_sample-404.FIN2	132	14	57	3	38	4	2,29	3,210	0,110	0,253	0,008	0,735	0,0930	0,0029	1459	26	1453	41	1488	58	97,6
7321-4 1T2__1348-1354	Zircon_sample-405.FIN2	504	35	338	45	83	10	1,49	0,651	0,049	0,083	0,002	0,825	0,0569	0,0028	508	30	515	13	480	110	107,3
7321-4 1T2__1348-1354	Zircon_sample-406.FIN2	105	29	81	14	58	8	1,37	3,180	0,150	0,257	0,007	0,193	0,0923	0,0054	1468	48	1473	36	1470	110	100,2
7321-4 1T2__1348-1354	Zircon_sample-414.FIN2	400	130	232	80	200	60	1,71	5,540	0,180	0,326	0,014	0,722	0,1239	0,0034	1907	28	1819	68	2013	50	90,4
7321-4 1T2__1348-1354	Zircon_sample-416.FIN2	280	100	137	44	103	32	1,96	3,505	0,067	0,258	0,005	0,402	0,0989	0,0021	1528	15	1478	27	1603	40	92,2
7321-4 1T2__1348-1354	Zircon_sample-417.FIN2	244	11	10	2	13	3	24,90	11,760	0,150	0,490	0,006	0,635	0,1747	0,0011	2585	12	2572	24	2603	11	98,8
7321-4 1T2__1348-1354	Zircon_sample-418.FIN2	151	9	149	10	26	2	1,02	0,519	0,041	0,064	0,001	0,794	0,0583	0,0033	424	27	400	8,7	530	130	75,4
7321-4 1T2__1348-1354	Zircon_sample-419.FIN2	339	33	194	34	38	4	1,73	0,567	0,042	0,071	0,003	0,741	0,0583	0,0027	456	27	440	15	540	100	81,5
7321-4 1T2__1348-1354	Zircon_sample-420.FIN2	405	70	233	53	34	8	1,74	0,356	0,023	0,049	0,002	0,284	0,0536	0,0038	309	17	306	13	340	160	90,0
7321-4 1T2__1348-1354	Zircon_sample-428.FIN2	305	37	34	6	16	2	9,10	1,477	0,082	0,157	0,003	0,593	0,0679	0,0034	920	34	939	18	860	110	109,2
7321-4 1T2__1348-1354	Zircon_sample-429.FIN2	113	23	62	17	43	8	1,81	3,250	0,300	0,264	0,007	0,489	0,0894	0,0063	1467	72	1509	36	1410	140	107,0
7321-4 1T2__1348-1354	Zircon_sample-430.FIN2	320	5	203	12	167	9	1,54	4,010	0,120	0,283	0,005	0,665	0,1035	0,0031	1635	24	1607	24	1686	55	95,3
7321-4 1T2__1348-1354	Zircon_sample-431.FIN2	95	11	68	9	60	4	1,37	4,730	0,250	0,311	0,009	0,101	0,1110	0,0074	1771	44	1747	46	1810	120	96,5
7321-4 1T2__1348-1354	Zircon_sample-432.FIN2	98	7	58	8	55	13	1,70	6,390	0,320	0,367	0,011	0,330	0,1267	0,0073	2030	44	2014	53	2051	99	98,2
7321-4 1T2__1348-1354	Zircon_sample-433.FIN2	165	25	68	10	36	7	2,41	2,295	0,076	0,198	0,003	0,018	0,0845	0,0031	1211	23	1164	14	1302	72	89,4
7321-4 1T2__1348-1354	Zircon_sample-434.FIN2	180	34	91	18	55	9	1,98	3,030	0,150	0,243	0,005	0,033	0,0902	0,0045	1415	37	1401	28	1425	95	98,3
7321-4 1T2__1348-1354	Zircon_sample-442.FIN2	173	3	123	3	111	4	1,40	4,180	0,100	0,302	0,005	0,673	0,1007	0,0021	1671	20	1701	23	1635	39	104,0
7321-4 1T2__1348-1354	Zircon_sample-443.FIN2	157	17	94	7	38	6	1,66	1,403	0,064	0,148	0,002	0,652	0,0701	0,0023	890	28	887	12	928	68	95,6
7321-4 1T2__1348-1354	Zircon_sample-444.FIN2	296	9	137	5	129	7	2,19	5,390	0,130	0,343	0,006	0,159	0,1133	0,0012	1882	21	1900	31	1853	20	102,5
7321-4 1T2__1348-1354	Zircon_sample-445.FIN2	272	93	330	180	50	23	1,07	0,431	0,022	0,055	0,002	0,638	0,0586	0,0014	364	16	343	11	552	54	62,1
7321-4 1T2__1348-1354	Zircon_sample-446.FIN2	87	13	41	8	35	9	2,14	3,880	0,160	0,270	0,008	0,871	0,1049	0,0044	1608	33	1541	39	1710	77	90,1
7321-4 1T2__1348-1354	Zircon_sample-447.FIN2	144	17	111	16	149	13	1,30	11,990	0,350	0,480	0,019	0,881	0,1815	0,0066	2603	27	2529	83	2666	61	94,9
7321-4 1T2__1348-1354	Zircon_sample-448.FIN2	211	23	121	18	105	15	1,76	4,500	0,150	0,303	0,008	0,642	0,1092	0,0017	1730	28	1704	38	1785	29	95,5
7321-4 1T2__1348-1354	Zircon_sample-456.FIN2	510	43	99	11	67	8	5,23	2,680	0,280	0,222	0,010	0,670	0,0877	0,0065	1321	77	1291	50	1370	140	94,2
7321-4 1T2__1348-1354	Zircon_sample-457.FIN2	182	24	64	14	32	2	2,93	2,030	0,110	0,194	0,006	0,959	0,0742	0,0041	1124	36	1145	33	1040	110	110,1
7321-4 1T2__1348-1354	Zircon_sample-458.FIN2	270	46	193	49	43	9	1,43	0,558	0,019	0,070	0,001	0,069	0,0571	0,0016	450	13	438	5,2	494	59	88,6
7321-4 1T2__1348-1354	Zircon_sample-459.FIN2	167	46	128	39	22	7	1,32	0,474	0,041	0,061	0,002	0,206	0,0560	0,0058	394	28	380	10	440	230	86,4
7321-4 1T2__1348-1354	Zircon_sample-460.FIN2	562	29	637	32	539	43	0,88	4,990	0,150	0,327	0,005	0,806	0,1111	0,0010	1817	26	1825	22	1818	17	100,4
7321-4 1T2__1348-1354	Zircon_sample-461.FIN2	216	37	62	19	36	11	3,70	1,960	0,056	0,189	0,003	0,352	0,0749	0,0021	1101	19	1115	17	1064	57	104,8
7321-4 1T2__1348-1354	Zircon_sample-470.FIN2	314	87	59	11	53	9	4,97	5,290	0,170	0,340	0,010	0,789	0,1129	0,0022	1866	27	1888	50	1845	35	102,3
7321-4 1T2__1348-1354	Zircon_sample-471.FIN2	83	16	51	14	65	13	1,65	13,190	0,370	0,530	0,013	-0,379	0,1826	0,0078	2693	26	2741	53	2675	69	102,5
7321-4 1T2__1348-1354	Zircon_sample-472.FIN2	101	4	84	2	42	8	1,21	1,780	0,150	0,171	0,003	0,880	0,0765	0,0054	1038	56	1018	14	1100	150	92,5
7321-4 1T2__1348-1354	Zircon_sample-473.FIN2	236	5	194	19	164	7	1,22	5,143	0,060	0,320	0,004	0,879	0,1181	0,0008	1843	9,9	1791	18	1927	12	92,9
7321-4 1T2__1348-1354	Zircon_sample-474.FIN2	439	18	342	34	70	6	1,30	0,550	0,016	0,070	0,002	0,152	0,0572	0,0025	445	11	437	14	495	97	88,3
7321-4 1T2__1348-1354	Zircon_sample-475.FIN2	235	38	132	24	171	31	1,79	14,530	0,290	0,541	0,012	0,637	0,1954	0,0032	2785	19	2787	51	2788	27	100,0
7321-4 1T2__1348-1354	Zircon_sample-484.FIN2	100	14	36	5	29	4	2,78	3,770	0,120	0,289	0,007	0,639	0,0966	0,0025	1586	25	1634	32	1558	49	104,9
7321-4 1T2__1348-1354	Zircon_sample-485.FIN2	117	3	79	4	73	4	1,51	5,970	0,180	0,359	0,010	0,707	0,1207	0,0029	1970	26	1978	46	1965	42	100,7
7321-4 1T2__1348-1354	Zircon_sample-486.FIN2	218	45	109	30	77	22	2,02	3,462	0,080	0,264	0,009	0,613	0,0958	0,0028	1518	18	1511	45	1543	55	97,9
7321-4 1T2__1348-1354	Zircon_sample-487.FIN2	84	12	76	16	59	8	1,10	4,070	0,270	0,295	0,004	-0,700	0,1007	0,0074	1647	54	1665	18	1630	140	102,1
7321-4 1T2__1348-1354	Zircon_sample-489.FIN2	184	14	54	3	43	5	3,37	3,890	0,160	0,284	0,013	0,558	0,0998	0,0038	1610	33	1613	64	1617	70	99,8
7321-4 1T2__1348-1354	Zircon_sample-490.FIN2	311	85	143	50	83	27	2,30	2,120	0,120	0,198	0,004	0,308	0,0782	0,0032	1154	38	1162	22	1148	79	101,2
7321-4 1T2__1348-1354	Zircon_sample-498.FIN2	163	21	84	10	29	4	1,93	1,196	0,049	0,132	0,004	0,578	0,0663	0,0026	799	23	799	22	813	82	98,3
7321-4 1T2__1348-1354	Zircon_sample-499.FIN2	96	10	47	8	40	6	2,01	4,150	0,370	0,288	0,010	0,403	0,1007	0,0019	1660	70	1629	51	1636	35	99,6
7321-4 1T2__1348-1354	Zircon_sample-500.FIN2	89	4	63	2	44	3	1,36	3,238	0,094	0,256	0,005	0,795	0,0911	0,0016	1466	23	1470	25	1448	33	101,5
7321-4 1T2__1348-1354	Zircon_sample-501.FIN2	105	9	116	10	114	7	0,89	6,740	0,310	0,371	0,016	0,416	0,1328	0,0073	2077	40	2034	77	2131	95	95,4
7321-4 1T2__1348-1354	Zircon_sample-502.FIN2	786	73	259	28	115	14	2,98	1,764	0,091	0,175	0,005	0,768	0,0735	0,0014	1032	33	1039	29	1026	39	101,3
7321-4 1T2__1348-1354	Zircon_sample-503.FIN2	490	120	184	28	103	9	2,58	2,900	0,130	0,232	0,013	0,715	0,0913	0,0038	1381	34	1344	68	1451	79	92,6
7321-4 1T2__1348-1354	Zircon_sample-504.FIN2	219	40	97	32	81	25	2,37	4,810	0,150	0,320	0,017	0,539	0,1101	0,0054	1787	26	1789	83	1797	94	99,6
7321-4 1T2__1348-1354	Zircon_sample-512.FIN2	276	47	210	92	57	24	1,32	0,818	0,044	0,099	0,004	0,332	0,0603	0,0029	606	24	609	20	610	110	99,8
7321-4 1T2__1348-1354	Zircon_sample-513.FIN2	737	38	371	39	75	8	1,99	0,497	0,029	0,067	0,002	0,892	0,0545	0,0028	409	20	415	11	390	120	106,4
7321-4 1T2__1348-1354	Zircon_sample-514.FIN2	162	17	70	7	65	5	2,29	5,710	0,140	0,343	0,008	-0,141	0,1217	0,0038	1933	21	1899	39	1980	56	95,9
7321-4 1T2__1348-1354	Zircon_sample-516.FIN2	114	3	86	5	64	4	1,34	3,560	0,180	0,268	0,006	0,546	0,0971	0,0046	1538	41	1528	28	1565	92	97,6
7321-4 1T2__1348-1354	Zircon_sample-517.FIN2	720	27	335	23	66	4	2,20	0,506	0,016	0,070	0,002	0,437	0,0533	0,0018	416	11	434	8,8	339	78	128,0
7321-4 1T2__1348-1354	Zircon_sample-518.FIN2	294	35	177	9	113	3	1,59	2,354	0,055	0,215	0,003	0,735	0,0800	0,0017	1229	16	1253	18	1197	42	104,7
7321-4 1T2__1348-1354	Zircon_sample-526.FIN2	154	21	68	10	45	6	2,29	2,940	0,150	0,236	0,008	0,501	0,0911	0,0043	1391	38	1363	43	1446	88	94,3
7321-4 1T2__1348-1354	Zircon_sample-527.FIN2	231	27	79	7	47	7	3,00	2,920	0,150	0,225	0,005	0,335	0,0953	0,0042	1386	40	1306	26	1532	86	85,2
7321-4 1T2__1348-1354	Zircon_sample-528.FIN2	261	8	126	10	15	1	2,12	0,248	0,023	0,037	0,001	0,395	0,0483	0,0039	225	19	234	5,7	110	180	213,1
7321-4 1T2__1348-1354	Zircon_sample-529.FIN2	440	56	3	1	0	0	160,00	1,667	0,099	0,167	0,006	0,648	0,0725	0,0033	996	37	996	31	998	91	99,8
7321-4 1T2__1348-1354	Zircon_sample-530.FIN2	339	12	157	8	93	8	2,21	2,233	0,088	0,202	0,003	0,683	0,0807	0,0019	1191	27	1188	16	1213	46	97,9
7321-4 1T2__1348-1354	Zircon_sample-531.FIN2	70	24	38	24	49	27	2,30	11,770	0,620	0,467	0,034	0,297	0,1830	0,0120	2585	48	2470	150	2680	110	92,2
7321-4 1T2__1348-1354	Zircon_sample-532.FIN2	266	18	122	5	59	4	2,35	1,692	0,071	0,169	0,004	0,316	0,0727	0,0026	1005	27	1007	22	1002	72	100,5
Common-Pb corrected[f]																						
7321-4 1T2__1348-1354	Zircon_sample-288.FIN2	480	420	120	100	53	44	4,32	3,010	0,260	0,215	0,028	0,957	0,1015	0,0059	1409	66	1250	150	1650	110	75,8
7321-4 1T2__1348-1354	Zircon_sample-289.FIN2	616	56	379	94	193	50	1,68	1,800	0,150	0,148	0,005	0,847	0,0887	0,0033	1045	53	892	29	1397	72	63,9
7321-4 1T2__1348-1354	Zircon_sample-291.FIN2	124	14	84	18	49	10	1,52	2,340	0,400	0,208	0,011	0,931	0,0820	0,0110	1220	120	1220	61	1220	260	100,0
7321-4 1T2__1348-1354	Zircon_sample-306.FIN2	48	19	39	14	16	6	1,21	1,240	0,590	0,164	0,018	0,314	0,0560	0,0280	780	260	976	97	1420	160	68,7
7321-4 1T2__1348-1354	Zircon_sample-335.FIN2	125	82	99	64	42	27	1,27	1,320	0,510	0,155	0,012	0,633	0,0630	0,0270	830	230	927	69	1190	570	77,9
7321-4 1T2__1348-1354	Zircon_sample-348.FIN2	184	40	108	33	20	4	1,82	0,170	0,240	0,062	0,003	0,525	0,0180	0,0300	130	230	389	20	380	380	102,4
7321-4 1T2__1348-1354	Zircon_sample-359.FIN2	568	39	143	8	100	7	4,09	3,420	0,160	0,243	0,003	0,900	0,1030	0,0042	1508	36	1401	18	1678	73	83,5
7321-4 1T2__1348-1354	Zircon_sample-390.FIN2	1280	350	1370	600	152	64	1,12	0,246	0,022	0,035	0,003	0,789	0,0511	0,0049	223	18	222	19	404	85	55,0
7321-4 1T2__1348-1354	Zircon_sample-401.FIN2	210	130	21	11	27	23	9,40	1,610	0,370	0,156	0,014	0,032	0,0740	0,0170	970	140	935	77	1010	440	92,6
7321-4 1T2__1348-1354	Zircon_sample-415.FIN2	154	36	132	15	81	15	1,14	7,930	0,410	0,319	0,013	0,866	0,1819	0,0041	2222	46	1786	64	2670	38	66,9
7321-4 1T2__1348-1354	Zircon_sample-462.FIN2	82	68	31	27	27	21	3,01	1,500	1,300	0,169	0,010	0,551	0,0590	0,0540	1020	380	1008	55	1460	450	69,0
7321-4 1T2__1348-1354	Zircon_sample-476.FIN2	286	65	206	57	117	26	1,41	2,720	0,220	0,170	0,015	0,992	0,1173	0,0038	1332	60	1009	85	1915	58	52,7
7321-4 1T2__1348-1354	Zircon_sample-488.FIN2	103	22	100	4	17	3	0,91	0,330	0,140	0,049	0,003	0,563	0,0470	0,0190	280	110	310	17	850	210	36,5
7321-4 1T2__1348-1354	Zircon_sample-515.FIN2	630	68	460	47	294	9	1,36	5,900	1,100	0,282	0,047	0,918	0,1519	0,0026	1950	170	1600	240	2368	30	67,6

Fig. 7.2 Appendix2

Fig. 7.3

Fruholmen FM		CONCENTRATIONS[a]						RATIOS								AGES						Con-cordance
Sample	Analysis	U [ppm]	2 σ	Th [ppm]	2 σ	Pb [ppm]	2 σ	U/Th[a]	$^{207}Pb/^{235}U$[b]	2 σ[d]	$^{206}Pb/^{238}U$[b]	2 σ[d]	rho[c]	$^{207}Pb/^{206}Pb$[e]	2 σ[d]	$^{207}Pb/^{235}U$[b]	2 σ[d]	$^{206}Pb/^{238}U$[b]	2 σ[d]	$^{207}Pb/^{206}Pb$[e]	2 σ[d]	
7321-4 1T2__1422-1428	Zircon_sample-023.FIN2	1287	81	237	97	330	150	5,90	0,517	0,021	0,067	0,002	0,304	0,0545	0,0027	423	14	417	14	390	110	106,9
7321-4 1T2__1422-1428	Zircon_sample--026.FIN2	1530	850	119	62	480	270	11,70	4,860	0,590	0,306	0,040	0,991	0,1143	0,0016	1790	110	1720	200	1868	25	92,1
7321-4 1T2__1422-1428	Zircon_sample--028.FIN2	334	63	146	22	138	29	2,15	0,290	0,030	0,039	0,002	0,031	0,0546	0,0069	258	24	244	12	370	280	65,9
7321-4 1T2__1422-1428	Zircon_sample-036.FIN2	345	61	110	14	714	83	3,18	4,720	0,220	0,307	0,010	0,906	0,1095	0,0036	1770	40	1727	47	1790	60	96,5
7321-4 1T2__1422-1428	Zircon_sample-040.FIN2	405	87	138	35	670	120	3,00	2,922	0,091	0,218	0,003	0,598	0,0977	0,0019	1388	24	1268	17	1581	37	80,2
7321-4 1T2__1422-1428	Zircon_sample-041.FIN2	350	120	106	33	126	38	3,37	0,452	0,070	0,046	0,002	0,049	0,0711	0,0091	377	50	290	13	930	270	31,2
7321-4 1T2__1422-1428	Zircon_sample-042.FIN2	72	3	39	3	230	19	1,87	4,873	0,096	0,302	0,006	0,504	0,1150	0,0033	1797	17	1699	28	1879	52	90,4
7321-4 1T2__1422-1428	Zircon_sample-050.FIN2	730	480	126	67	1700	1100	5,50	11,100	0,410	0,458	0,016	-0,607	0,1740	0,0110	2531	34	2428	69	2590	100	93,7
7321-4 1T2__1422-1428	Zircon_sample--051.FIN2	472	74	93	25	118	45	5,24	0,566	0,089	0,068	0,003	0,842	0,0601	0,0077	455	57	426	18	600	270	71,0
7321-4 1T2__1422-1428	Zircon_sample-053.FIN2	361	37	96	17	176	23	3,86	0,587	0,021	0,072	0,001	0,163	0,0596	0,0022	469	13	447	7,3	586	83	76,3
7321-4 1T2__1422-1428	Zircon_sample-055.FIN2	610	140	217	45	1073	91	2,84	5,030	0,100	0,299	0,010	0,006	0,1201	0,0042	1824	17	1684	49	1958	61	86,0
7321-4 1T2__1422-1428	Zircon_sample-056.FIN2	240	120	88	21	410	130	2,71	3,480	0,650	0,240	0,010	0,743	0,1040	0,0180	1520	140	1386	53	1670	310	83,0
7321-4 1T2__1422-1428	Zircon_sample-064.FIN2	630	140	259	28	242	34	2,45	0,309	0,019	0,042	0,001	0,355	0,0529	0,0029	274	15	266	6,6	320	120	83,0
7321-4 1T2__1422-1428	Zircon_sample-067.FIN2	292	32	85	6	765	20	3,48	10,140	0,290	0,452	0,017	0,975	0,1634	0,0016	2447	26	2405	76	2491	17	96,5
7321-4 1T2__1422-1428	Zircon_sample-068.FIN2	800	210	127	17	740	300	6,40	4,950	0,300	0,294	0,017	0,968	0,1233	0,0009	1811	51	1660	85	2004	13	82,8
7321-4 1T2__1422-1428	Zircon_sample-069.FIN2	387	34	77	4	102	15	5,16	0,427	0,033	0,057	0,001	0,246	0,0549	0,0044	361	23	357	7	390	170	91,4
7321-4 1T2__1422-1428	Zircon_sample-070.FIN2	447	20	166	7	137	35	2,75	0,322	0,009	0,037	0,002	0,123	0,0700	0,0140	284	7	233	13	870	350	26,8
7321-4 1T2__1422-1428	Zircon_sample-078.FIN2	460	110	157	77	153	72	3,32	0,341	0,020	0,042	0,002	-0,642	0,0589	0,0051	297	15	266	10	550	190	48,4
7321-4 1T2__1422-1428	Zircon_sample-079.FIN2	918	80	287	25	334	38	3,25	0,350	0,023	0,048	0,002	0,273	0,0523	0,0031	305	17	303	11	290	130	104,5
7321-4 1T2__1422-1428	Zircon_sample-081.FIN2	510	240	250	130	190	100	2,07	0,236	0,019	0,034	0,002	-0,592	0,0503	0,0056	215	15	216	9,8	200	230	108,0
7321-4 1T2__1422-1428	Zircon_sample-082.FIN2	610	100	67	23	480	140	9,00	5,080	0,210	0,325	0,015	0,909	0,1142	0,0017	1833	34	1811	71	1866	27	97,1
7321-4 1T2__1422-1428	Zircon_sample-092.FIN2	325	64	27	2	263	20	14,60	11,330	0,430	0,475	0,018	0,872	0,1704	0,0010	2550	36	2506	78	2561,4	9,3	97,8
7321-4 1T2__1422-1428	Zircon_sample-094.FIN2	190	6	94	5	192	15	1,99	0,980	0,068	0,107	0,004	0,907	0,0668	0,0069	693	35	655	23	820	220	79,9
7321-4 1T2__1422-1428	Zircon_sample-095.FIN2	1155	94	447	44	1860	130	2,55	1,824	0,099	0,146	0,000	0,473	0,0884	0,0030	1054	35	881	2,3	1390	64	63,4
7321-4 1T2__1422-1428	Zircon_sample-096.FIN2	516	76	116	10	137	20	4,41	0,358	0,028	0,050	0,002	0,659	0,0520	0,0024	310	21	313	11	280	110	111,8
7321-4 1T2__1422-1428	Zircon_sample-097.FIN2	147	32	42	9	189	44	3,45	2,230	0,150	0,199	0,004	0,553	0,0817	0,0062	1190	46	1167	21	1240	150	94,1
7321-4 1T2__1422-1428	Zircon_sample-107.FIN2	213	14	56	4	314	32	3,74	2,806	0,080	0,229	0,007	0,381	0,0889	0,0038	1357	21	1328	35	1397	81	95,1
7321-4 1T2__1422-1428	Zircon_sample-108.FIN2	852	66	37	8	321	95	23,60	5,250	0,160	0,325	0,006	0,960	0,1174	0,0019	1860	26	1812	27	1917	28	94,5
7321-4 1T2__1422-1428	Zircon_sample-109.FIN2	1700	100	45	23	206	99	42,00	2,163	0,091	0,180	0,002	0,975	0,0871	0,0036	1169	29	1069	9,6	1362	80	78,5
7321-4 1T2__1422-1428	Zircon_sample-110.FIN2	2050	430	138	73	1050	610	19,20	5,480	0,470	0,318	0,017	0,922	0,1236	0,0037	1895	73	1777	82	2008	54	88,5
7321-4 1T2__1422-1428	Zircon_sample-111.FIN2	616	59	216	43	2370	220	2,76	11,180	0,310	0,476	0,014	0,949	0,1709	0,0009	2537	25	2510	62	2566,4	9,2	97,8
7321-4 1T2__1422-1428	Zircon_sample-112.FIN2	830	130	330	100	3040	780	2,64	10,180	0,400	0,441	0,020	0,811	0,1665	0,0025	2451	36	2357	88	2523	25	93,4
7321-4 1T2__1422-1428	Zircon_sample-121.FIN2	680	20	132	15	757	58	5,18	3,780	0,130	0,273	0,004	-0,264	0,0983	0,0049	1588	28	1554	18	1591	94	97,7
7321-4 1T2__1422-1428	Zircon_sample-122.FIN2	1390	250	240	130	1740	800	13,00	5,690	0,390	0,341	0,015	0,763	0,1207	0,0041	1927	58	1890	70	1964	61	96,2
7321-4 1T2__1422-1428	Zircon_sample-123.FIN2	1170	74	408	43	660	83	2,90	0,523	0,014	0,067	0,001	0,871	0,0564	0,0017	427	9,6	419	7,7	465	65	90,0
7321-4 1T2__1422-1428	Zircon_smple-124.FIN2	618	82	293	45	2670	270	2,06	10,130	0,420	0,440	0,018	0,773	0,1656	0,0032	2446	38	2350	80	2513	32	93,5
7321-4 1T2__1422-1428	Zircon_sample-125.FIN2	381	31	82	6	564	22	4,67	4,945	0,035	0,310	0,005	0,847	0,1158	0,0020	1810	5,9	1742	25	1892	31	92,1
7321-4 1T2__1422-1428	Zircon_sample-134.FIN2	257	67	50	17	99	22	5,23	0,709	0,038	0,079	0,004	0,292	0,0661	0,0060	544	23	488	27	790	180	61,8
7321-4 1T2__1422-1428	Zircon_sample-135.FIN2	746	72	312	33	324	57	2,36	0,315	0,031	0,040	0,001	0,004	0,0575	0,0056	278	24	252	7,9	490	230	51,4
7321-4 1T2__1422-1428	Zircon_sample-136.FIN2	588	54	195	20	170	19	2,97	0,279	0,024	0,036	0,001	0,650	0,0559	0,0038	250	19	228	7,5	440	150	51,8
7321-4 1T2__1422-1428	Zircon_sample-137.FIN2	574	59	183	16	1670	110	3,12	10,480	0,690	0,454	0,028	0,970	0,1650	0,0020	2476	61	2410	120	2508	20	96,1
7321-4 1T2__1422-1428	Zircon_sample-138.FIN2	584	52	222	40	1600	280	2,64	5,810	0,210	0,338	0,008	0,819	0,1236	0,0024	1947	31	1878	38	2009	33	93,5
7321-4 1T2__1422-1428	Zircon_sample-139.FIN2	1580	360	64	12	420	41	25,40	4,590	0,410	0,299	0,026	0,967	0,1116	0,0014	1745	73	1680	130	1826	23	92,0
7321-4 1T2__1422-1428	Zircon_sample-149.FIN2	795	59	289	34	60	7	2,65	0,514	0,033	0,067	0,001	0,525	0,0552	0,0025	421	22	418	7,7	420	100	99,4
7321-4 1T2__1422-1428	Zircon_sample-150.FIN2	694	44	398	31	66	7	1,70	0,442	0,026	0,056	0,002	0,291	0,0572	0,0033	371	18	353	9	490	130	72,1
7321-4 1T2__1422-1428	Zircon_sample-151.FIN2	300	150	270	170	64	27	1,18	0,655	0,063	0,080	0,005	0,462	0,0600	0,0050	510	39	493	32	590	180	83,6
7321-4 1T2__1422-1428	Zircon_sample-152.FIN2	1148	57	607	57	83	5	1,90	0,358	0,023	0,045	0,002	0,223	0,0578	0,0025	311	17	284	12	517	96	54,9
7321-4 1T2__1422-1428	Zircon_sample-153.FIN2	325	42	98	5	70	8	3,30	2,940	0,038	0,237	0,005	0,537	0,0893	0,0025	1392	9,9	1373	28	1409	54	97,4
7321-4 1T2__1422-1428	Zircon_sample-164.FIN2	216	21	272	37	148	19	0,80	2,390	0,230	0,214	0,007	0,515	0,0808	0,0052	1237	69	1251	36	1210	130	103,4
7321-4 1T2__1422-1428	Zircon_sample-165.FIN2	256	46	287	88	45	9	0,91	0,437	0,008	0,056	0,002	0,191	0,0563	0,0019	368	5,7	350	11	461	73	75,9
7321-4 1T2__1422-1428	Zircon_sample-166.FIN2	372	82	136	20	150	20	2,63	10,120	0,190	0,469	0,015	0,597	0,1538	0,0019	2446	18	2479	65	2389	21	103,8
7321-4 1T2__1422-1428	Zircon_sample-167.FIN2	95	7	80	7	100	4	1,19	10,580	0,710	0,434	0,008	-0,221	0,1770	0,0110	2485	62	2323	36	2620	100	88,7
7321-4 1T2__1422-1428	Zircon_sample-168.FIN2	137	11	156	15	200	21	0,88	12,140	0,410	0,492	0,013	0,826	0,1796	0,0037	2614	32	2578	56	2648	34	97,4
7321-4 1T2__1422-1428	Zircon_sample-176.FIN2	912	63	330	46	153	16	2,81	1,274	0,047	0,139	0,002	0,930	0,0664	0,0030	834	21	840	11	818	94	102,7
7321-4 1T2__1422-1428	Zircon_sample-177.FIN2	111	47	73	25	125	51	1,25	10,750	0,460	0,460	0,023	0,799	0,1706	0,0056	2500	40	2440	100	2562	55	95,2
7321-4 1T2__1422-1428	Zircon_sample-179.FIN2	1080	180	710	110	533	63	1,55	5,650	0,120	0,310	0,007	0,972	0,1322	0,0034	1923	18	1742	33	2127	45	81,9
7321-4 1T2__1422-1428	Zircon_sample-181.FIN2	116	9	60	3	31	3	1,97	1,720	0,150	0,169	0,006	-0,676	0,0741	0,0072	1013	58	1005	32	1030	190	97,6
7321-4 1T2__1422-1428	Zircon_sample-190.FIN2	326	53	135	23	165	26	2,64	9,940	0,390	0,442	0,009	0,678	0,1605	0,0020	2427	36	2360	41	2469	25	95,6
7321-4 1T2__1422-1428	Zircon_sample-191.FIN2	200	120	30	4	29	5	7,70	5,470	0,210	0,343	0,014	0,913	0,1158	0,0023	1895	34	1898	65	1892	36	100,3
7321-4 1T2__1422-1428	Zircon_sample-193.FIN2	198	9	91	8	85	9	2,24	6,050	0,110	0,357	0,007	0,489	0,1219	0,0023	1983	16	1970	35	1983	33	99,3
7321-4 1T2__1422-1428	Zircon_sample-194.FIN2	137	30	140	49	31	9	1,04	0,590	0,096	0,072	0,002	0,522	0,0594	0,0084	469	62	445	14	550	320	80,9
7321-4 1T2__1422-1428	Zircon_sample-195.FIN2	310	42	122	15	94	8	2,60	3,450	0,150	0,276	0,008	0,454	0,0911	0,0034	1514	34	1571	40	1445	71	108,7
7321-4 1T2__1422-1428	Zircon_sample-204.FIN2	1060	200	298	42	66	23	3,57	0,523	0,051	0,065	0,001	0,744	0,0594	0,0056	427	34	403	3,3	570	200	70,7
7321-4 1T2__1422-1428	Zircon_sample-205.FIN2	234	19	141	9	134	12	1,69	7,260	0,430	0,386	0,026	0,884	0,1357	0,0047	2143	53	2100	120	2172	60	96,7
7321-4 1T2__1422-1428	Zircon_sample-206.FIN2	247	20	165	19	29	6	1,52	0,466	0,080	0,059	0,003	0,344	0,0578	0,0082	388	55	368	20	510	300	72,2
7321-4 1T2__1422-1428	Zircon_sample-208.FIN2	333	23	145	19	138	11	2,41	5,680	0,140	0,342	0,008	0,579	0,1211	0,0033	1928	22	1897	38	1971	49	96,2
7321-4 1T2__1422-1428	Zircon_sample-209.FIN2	129	11	81	10	64	7	1,62	4,690	0,170	0,315	0,006	0,552	0,1085	0,0015	1765	31	1766	28	1773	26	99,6
7321-4 1T2__1422-1428	Zircon_sample-210.FIN2	1052	86	376	82	343	57	2,90	5,180	0,270	0,327	0,014	0,887	0,1141	0,0035	1848	45	1823	70	1865	55	97,7
7321-4 1T2__1422-1428	Zircon_sample-218.FIN2	286	9	143	48	114	28	2,13	4,427	0,042	0,299	0,013	0,047	0,1071	0,0060	1717	7,9	1688	67	1750	100	96,5
7321-4 1T2__1422-1428	Zircon_sample-220.FIN2	729	54	214	27	199	18	3,47	5,030	0,120	0,325	0,008	0,742	0,1128	0,0021	1823	20	1816	38	1844	33	98,5
7321-4 1T2__1422-1428	Zircon_sample-221.FIN2	212	12	149	13	48	8	1,44	0,931	0,034	0,109	0,003	0,472	0,0623	0,0036	668	18	664	20	680	120	97,6
7321-4 1T2__1422-1428	Zircon_sample-223.FIN2	318	40	272	67	253	54	1,26	7,500	0,340	0,405	0,016	0,913	0,1344	0,0024	2171	41	2192	74	2156	31	101,7
7321-4 1T2__1422-1428	Zircon_sample-232.FIN2	660	130	500	130	103	24	1,36	0,589	0,041	0,076	0,005	0,757	0,0576	0,0017	470	26	472	30	512	68	92,2
7321-4 1T2__1422-1428	Zircon_sample-233.FIN2	529	72	70	6	49	3	7,60	3,120	0,180	0,247	0,012	0,964	0,0921	0,0023	1437	43	1424	62	1468	48	97,0
7321-4 1T2__1422-1428	Zircon_sample-234.FIN2	259	33	186	20	133	10	1,39	3,270	0,180	0,256	0,010	0,953	0,0938	0,0039	1474	43	1467	53	1502	76	97,7
7321-4 1T2__1422-1428	Zircon_sample-236.FIN2	119	4	114	12	133	15	1,06	10,140	0,200	0,456	0,007	0,528	0,1586	0,0039	2448	18	2419	29	2439	42	99,2
7321-4 1T2__1422-1428	Zircon_sample-237.FIN2	408	46	680	160	68	13	0,62	0,248	0,019	0,034	0,001	0,654	0,0530	0,0039	225	16	215	9	320	170	67,2
7321-4 1T2__1422-1428	Zircon_sample-246.FIN2	740	120	700	160	93	20	1,06	0,382	0,023	0,047	0,002	0,450	0,0598	0,0021	328	17	293	10	595	74	49,2
7321-4 1T2__1422-1428	Zircon_sample-247.FIN2	535	98	321	75	36	10	1,57	0,280	0,010	0,037	0,002	0,097	0,0536	0,0032	250	8,1	237	9,4	340	130	69,6
7321-4 1T2__1422-1428	Zircon_sample-248.FIN2	357	41	98	18	80	12	3,71	5,190	0,190	0,323	0,006	0,824	0,1151	0,0022	1850	31	1802	28	1880	34	95,9
7321-4 1T2__1422-1428	Zircon_sample-260.FIN2	376	64	276	64	67	14	1,40	0,735	0,030	0,089	0,002	0,811	0,0601	0,0017	559	18	550	14	604	62	91,1
7321-4 1T2__1422-1428	Zircon_sample-262.FIN2	490	130	350	120	67	16	1,41	0,604	0,024	0,075	0,001	0,927	0,0586	0,0029	480	15	465	4,1	550	110	84,6
7321-4 1T2__1422-1428	Zircon_sample-263.FIN2	239	28	82	3	103	7	3,01	7,610	0,240	0,401	0,006	0,553	0,1383	0,0041	2186	29	2171	27	2204	52	98,5
7321-4 1T2__1422-1428	Zircon_sample-264.FIN2	122	4	56	2	48	3	2,17	4,310	0,130	0,309	0,006	0,436	0,1013	0,0029	1695	24	1735	31	1646	52	105,4
7321-4 1T2__1422-1428	Zircon_sample-266.FIN2	204	25	127	22	112	16	1,62	4,750	0,170	0,319	0,011	0,810	0,1086	0,0024	1775	30	1787	55	1775	41	100,7
7321-4 1T2__1422-1428	Zircon_sample-274.FIN2	271	24	209	26	24	3	1,31	0,308	0,020	0,042	0,001	0,779	0,0531	0,0041	272	16	267	4,9	320	170	83,6
7321-4 1T2__1422-1428	Zircon_sample-275.FIN2	139	41	107	59	136	60	1,22	11,050	0,660	0,468	0,010	0,512	0,1720	0,0092	2526	55	2476	45	2574	88	96,2
7321-4 1T2__1422-1428	Zircon_sample-277.FIN2	396	18	213	55	257	50	2,02	10,310	0,500	0,476	0,009	0,646	0,1577	0,0041	2462	45	2511	37	2430	45	103,3
7321-4 1T2__1422-1428	Zircon_sample-279.FIN2	506	37	44	12	68	21	13,70	5,160	0,160	0,342	0,009	0,670	0,1096	0,0010	1845	26	1893	41	1792	17	105,6
7321-4 1T2__1422-1428	Zircon_sample-280.FIN2	52	4	38	3	17	2	1,34	1,760	0,130	0,171	0,010	-0,901	0,0753	0,0098	1028	48	1017	52	1040	240	97,8
Common-Pb corrected[f]																						
7321-4 1T2__1422-1428	Zircon_sample-024.FIN2	2820	540	290	130	143	61	10,60	0,258	0,015	0,034	0,002	0,811	0,0541	0,0011	233	12	214	9,7	373	48	57,3
7321-4 1T2__1422-1428	Zircon_sample--025.FIN2	790	400	330	110	3100	1000	2,19	10,430	0,820	0,443	0,028	0,987	0,1667	0,0012	2470	73	2360	130	2525	12	93,5
7321-4 1T2__1422-1428	Zircon_sample--027.FIN2	2850	680	151	24	925	76	19,50	5,050	0,160	0,243	0,009	0,963	0,1484	0,0032	1827	26	1404	47	2327	37	60,3
7321-4 1T2__1422-1428	Zircon_sample-037.FIN2	1290	230	480	140	2900	830	3,00	4,120	0,110	0,267	0,003	0,982	0,1124	0,0019	1658	21	1523	17	1839	31	82,8
7321-4 1T2__1422-1428	Zircon_sample-038.FIN2	1210	310	98	30	610	100	12,80	8,330	0,250	0,377	0,010	0,990	0,1595	0,0016	2267	28	2061	49	2450	17	84,1
7321-4 1T2__1422-1428	Zircon_sample-054.FIN2	700	140	244	63	810	160	3,00	2,005	0,099	0,176	0,006	0,595	0,0821	0,0024	1117	34	1045	34	1247	57	83,8
7321-4 1T2__1422-1428	Zircon_sample-083.FIN2	860	110	76	27	240	100	15,80	1,519	0,032	0,156	0,005	0,257	0,0707	0,0019	938	13	936	27	947	54	98,8
7321-4 1T2__1422-1428	Zircon_sample-162.FIN2	150	21	66	7	52	7	2,27	3,590	0,240	0,256	0,008	0,814	0,1009	0,0042	1547	53	1467	38	1639	78	89,5
7321-4 1T2__1422-1428	Zircon_sample-163.FIN2	66	20	45	21	25	11	1,61	1,830	0,660	0,164	0,008	0,705	0,0800	0,0280	1030	270	980	46	1480	260	66,2
7321-4 1T2__1422-1428	Zircon_sample-178.FIN2	820	170	410	100	297	95	2,05	2,800	0,240	0,237	0,009	0,613	0,0863	0,0047	1353	65	1369	46	1340	100	102,2
7321-4 1T2__1422-1428	Zircon_sample-180.FIN2	189	72	67	17	8	3	2,79	0,180	0,180	0,043	0,003	-0,247	0,0310	0,0300	160	160	272	18	420	150	64,8
7321-4 1T2__1422-1428	Zircon_sample-192.FIN2	266	69	105	59	15	9	3,00	0,329	0,062	0,043	0,002	0,187	0,0556	0,0085	288	47	272	15	570	230	47,7
7321-4 1T2__1422-1428	Zircon_sample-196.FIN2	530	240	169	44	162	61	3,12	5,700	0,640	0,331	0,024	0,939	0,1262	0,0072	1928	97	1840	120	2040	100	90,2
7321-4 1T2__1422-1428	Zircon_sample-207.FIN2	499	52	336	47	34	4	1,52	0,194	0,063	0,033	0,002	0,666	0,0400	0,0110	176	54	207	12	420	210	49,3
7321-4 1T2__1422-1428	Zircon_sample-219.FIN2	190	18	187	19	121	11	1,02	2,370	0,280	0,221	0,020	0,733	0,0780	0,0073	1225	86	1280	110	1120	190	114,3
7321-4 1T2__1422-1428	Zircon_sample-222.FIN2	1150	320	231	49	151	32	4,96	4,270	0,270	0,270	0,019	0,914	0,1163	0,0049	1687	52	1538	97	1899	75	81,0
7321-4 1T2__1422-1428	Zircon_sample-224.FIN2	947	63	600	89	464	51	1,54	3,910	0,170	0,271	0,007	0,628	0,1034	0,0022	1615	35	1546	34	1685	38	91,8
7321-4 1T2__1422-1428	Zircon_sample-235.FIN2	315	26	400	130	165	44	0,84	1,256	0,037	0,143	0,010	0,631	0,0639	0,0055	826	17	861	54	730	190	117,9
7321-4 1T2__1422-1428	Zircon_sample-238.FIN2	350	160	75	9	66	8	3,90	5,590	0,370	0,370	0,022	0,934	0,1092	0,0023	1913	56	2030	100	1785	38	113,7
7321-4 1T2__1422-1428	Zircon_sample-249.FIN2	171	35	88	13	128	15	1,92	10,700	2,000	0,474	0,073	0,995	0,1613	0,0055	2480	180	2500	330	2468	57	101,3
7321-4 1T2__1422-1428	Zircon_sample-250.FIN2	760	330	440	220	370	150	1,76	7,410	0,960	0,361	0,045	0,990	0,1488	0,0035	2150	110	1980	210	2331	41	84,9
7321-4 1T2__1422-1428	Zircon_sample-261.FIN2	650	340	940	630	75	47	0,74	0,189	0,052	0,032	0,002	-0,969	0,0420	0,0130	176	45	205	11	148	18	138,5
7321-4 1T2__1422-1428	Zircon_sample-265.FIN2	731	44	620	120	113	53	1,21	2,520	0,290	0,151	0,006	0,645	0,1220	0,0120	1275	83	904	32	1970	180	45,9
7321-4 1T2__1422-1428	Zircon_sample-276.FIN2	376	66	327	68	129	38	1,15	2,780	0,430	0,194	0,015	0,885	0,1033	0,0097	1340	110	1145	81	1680	170	68,2
7321-4 1T2__1422-1428	Zircon_sample-278.FIN2	890	110	330	72	277	57	2,80	5,040	0,320	0,316	0,020	0,784	0,1169	0,0056	1824	53	1769	97	1906	87	92,8

Fig. 7.3 Appendix 3

Fig. 7.4

Snadd FM		CONCENTRATIONS[a]						RATIOS								AGES						Con-cordance
Sample	Analysis	U [ppm]	2 σ	Th [ppm]	2 σ	Pb [ppm]	2 σ	U/Th[a]	$^{207}Pb/^{235}U$ [b]	2 σ[d]	$^{206}Pb/^{238}U$ [b]	2 σ[d]	rho[c]	$^{207}Pb/^{206}Pb$ [e]	2 σ[d]	$^{207}Pb/^{235}U$ [b]	2 σ[d]	$^{206}Pb/^{238}U$ [b]	2 σ[d]	$^{207}Pb/^{206}Pb$ [e]	2 σ[d]	
7321-4 1T2__1521-1524	Zircon_sample-260.FIN2	690	290	163	66	280	130	3,50	0,391	0,024	0,056	0,005	0,814	0,0533	0,0033	349	30	351	29	340	140	103,2
7321-4 1T2__1521-1524	Zircon_sample-261.FIN2	242	7	42	2	376	35	5,76	6,980	0,440	0,383	0,019	0,568	0,1326	0,0024	2108	56	2091	90	2133	32	98,0
7321-4 1T2__1521-1524	Zircon_sample-265.FIN2	216	44	64	18	105	27	3,39	0,650	0,150	0,075	0,005	0,975	0,0625	0,0092	507	89	463	32	680	310	68,1
7321-4 1T2__1521-1524	Zircon_sample-266.FIN2	409	53	34	6	307	43	13,10	5,360	0,200	0,348	0,013	0,777	0,1109	0,0021	1878	32	1923	61	1828	24	105,2
7321-4 1T2__1521-1524	Zircon_sample-276.FIN2	336	59	199	55	221	44	1,78	0,480	0,100	0,055	0,005	0,701	0,0640	0,0120	397	68	347	32	660	410	52,6
7321-4 1T2__1521-1524	Zircon_sample-289.FIN2	450	61	149	20	376	87	2,98	0,964	0,068	0,105	0,002	0,221	0,0665	0,0042	685	35	643	12	820	130	78,4
7321-4 1T2__1521-1524	Zircon_sample-290.FIN2	200	18	39	6	97	23	5,15	0,777	0,067	0,091	0,001	-0,360	0,0623	0,0055	583	38	561	4,6	670	200	83,7
7321-4 1T2__1521-1524	Zircon_sample-291.FIN2	759	64	249	30	323	42	3,02	0,394	0,036	0,050	0,001	0,392	0,0573	0,0048	337	27	315	6,2	490	190	64,2
7321-4 1T2__1521-1524	Zircon_sample-293.FIN2	640	110	154	39	358	94	4,22	0,869	0,022	0,101	0,002	0,624	0,0624	0,0013	635	12	621	12	688	45	90,3
7321-4 1T2__1521-1524	Zircon_sample-294.FIN2	383	60	172	22	250	48	2,17	0,400	0,030	0,052	0,002	-0,625	0,0558	0,0039	342	22	325	13	440	160	73,9
7321-4 1T2__1521-1524	Zircon_sample-302.FIN2	1690	220	185	31	1440	220	9,16	5,500	0,180	0,345	0,010	0,938	0,1180	0,0022	1900	29	1909	50	1926	34	99,1
7321-4 1T2__1521-1524	Zircon_sample-303.FIN2	1150	190	137	42	180	50	8,60	0,429	0,042	0,058	0,001	-0,231	0,0540	0,0056	362	30	362	5,9	360	240	100,6
7321-4 1T2__1521-1524	Zircon_sample-304.FIN2	230	78	52	35	81	46	5,00	0,470	0,028	0,064	0,002	0,704	0,0533	0,0022	391	19	400	13	340	91	117,6
7321-4 1T2__1521-1524	Zircon_sample-305.FIN2	221	40	103	31	213	35	2,25	0,596	0,093	0,068	0,004	0,619	0,0637	0,0076	471	57	421	23	700	250	60,1
7321-4 1T2__1521-1524	Zircon_sample-308.FIN2	449	45	167	20	277	35	2,64	0,492	0,028	0,065	0,003	0,889	0,0552	0,0027	406	19	405	16	420	110	96,4
7321-4 1T2__1521-1524	Zircon_sample-316.FIN2	640	150	147	49	219	41	4,48	0,455	0,047	0,057	0,002	0,824	0,0580	0,0046	380	33	357	12	520	170	68,7
7321-4 1T2__1521-1524	Zircon_sample-317.FIN2	197	22	70	22	400	100	3,10	2,150	0,150	0,202	0,002	0,159	0,0769	0,0060	1163	50	1187	9,4	1110	160	106,9
7321-4 1T2__1521-1524	Zircon_sample-318.FIN2	118	29	28	11	33	9	4,72	0,454	0,057	0,058	0,002	0,381	0,0552	0,0060	379	39	365	11	400	240	91,3
7321-4 1T2__1521-1524	Zircon_sample-319.FIN2	180	13	53	6	82	14	3,48	0,492	0,057	0,063	0,003	0,563	0,0563	0,0055	405	39	392	17	430	220	91,2
7321-4 1T2__1521-1524	Zircon_sample-321.FIN2	392	19	170	0	202	26	2,29	0,309	0,018	0,044	0,000	0,846	0,0511	0,0029	273	14	275	1,5	240	130	114,8
7321-4 1T2__1521-1524	Zircon_sample-322.FIN2	169	13	47	3	83	14	3,56	0,612	0,067	0,071	0,002	0,254	0,0622	0,0068	483	42	445	13	640	240	69,5
7321-4 1T2__1521-1524	Zircon_sample-332.FIN2	274	72	172	59	360	120	1,62	0,740	0,210	0,081	0,002	-0,725	0,0660	0,0190	560	120	504	11	770	550	65,5
7321-4 1T2__1521-1524	Zircon_sample-333.FIN2	286	62	73	26	440	120	5,30	3,650	0,280	0,262	0,014	0,972	0,1010	0,0029	1557	62	1497	72	1641	54	91,2
7321-4 1T2__1521-1524	Zircon_sample-334.FIN2	510	120	102	30	570	160	5,08	3,187	0,073	0,256	0,004	0,253	0,0901	0,0026	1454	18	1471	21	1427	55	103,1
7321-4 1T2__1521-1524	Zircon_sample-335.FIN2	313	36	85	10	218	37	3,72	0,953	0,081	0,104	0,001	0,213	0,0658	0,0055	678	42	640	7,7	780	190	82,0
7321-4 1T2__1521-1524	Zircon_sample-336.FIN2	425	42	130	14	160	15	3,31	0,445	0,043	0,049	0,001	0,769	0,0664	0,0061	374	31	306	3,7	810	190	37,7
7321-4 1T2__1521-1524	Zircon_sample-344.FIN2	1080	210	550	130	930	170	2,00	0,455	0,018	0,062	0,001	0,132	0,0531	0,0023	381	13	390	7,2	329	99	118,6
7321-4 1T2__1521-1524	Zircon_sample-345.FIN2	191	16	66	8	174	32	3,06	0,834	0,072	0,100	0,002	0,100	0,0607	0,0052	614	39	614	11	610	180	100,7
7321-4 1T2__1521-1524	Zircon_sample-349.FIN2	1510	230	274	46	270	74	5,59	0,341	0,031	0,045	0,000	0,106	0,0550	0,0045	298	23	282	2	410	180	68,7
7321-4 1T2__1521-1524	Zircon_sample-358.FIN2	390	49	241	70	550	110	1,73	0,846	0,054	0,096	0,004	0,570	0,0643	0,0053	622	30	591	21	740	180	79,9
7321-4 1T2__1521-1524	Zircon_sample-360.FIN2	145	21	80	11	220	34	1,85	0,840	0,300	0,077	0,001	0,376	0,0800	0,0270	610	170	475	5,1	1110	760	42,8
7321-4 1T2__1521-1524	Zircon_sample-361.FIN2	1030	140	340	110	309	72	3,24	0,268	0,015	0,037	0,000	-0,190	0,0529	0,0024	241	12	233	2,7	320	100	72,7
7321-4 1T2__1521-1524	Zircon_sample-362.FIN2	333	50	79	26	342	97	5,20	1,918	0,062	0,184	0,004	0,315	0,0757	0,0026	1087	22	1088	24	1082	71	100,6
7321-4 1T2__1521-1524	Zircon_sample-363.FIN2	241	21	114	6	690	110	2,14	2,920	0,130	0,249	0,006	0,924	0,0848	0,0029	1387	34	1435	30	1311	66	109,5
7321-4 1T2__1521-1524	Zircon_sample-364.FIN2	1870	160	300	9	930	110	6,31	1,185	0,046	0,121	0,003	0,803	0,0707	0,0021	793	21	738	15	948	60	77,8
7321-4 1T2__1521-1524	Zircon_sample-372.FIN2	880	240	429	27	680	160	2,47	0,590	0,032	0,069	0,002	0,291	0,0625	0,0047	470	20	429	14	680	160	63,1
7321-4 1T2__1521-1524	Zircon_sample-373.FIN2	1260	120	426	79	500	100	3,19	0,316	0,010	0,044	0,001	0,676	0,0521	0,0014	279	7,7	279	4,1	288	60	96,8
7321-4 1T2__1521-1524	Zircon_sample-375.FIN2	159	18	34	4	219	33	4,71	3,600	0,110	0,280	0,005	0,886	0,0941	0,0011	1559	31	1592	27	1509	23	105,5
7321-4 1T2__1521-1524	Zircon_sample-376.FIN2	668	41	72	29	440	140	12,20	3,732	0,097	0,282	0,009	0,923	0,0954	0,0012	1578	21	1601	45	1536	24	104,2
7321-4 1T2__1521-1524	Zircon_sample-377.FIN2	224	44	165	50	205	47	1,41	0,398	0,031	0,049	0,002	0,387	0,0589	0,0061	340	23	311	15	550	230	56,5
7321-4 1T2__1521-1524	Zircon_sample-378.FIN2	388	48	79	10	103	12	5,00	0,383	0,039	0,053	0,002	0,524	0,0556	0,0064	343	38	331	14	400	240	82,8
7321-4 1T2__1521-1524	Zircon_sample-386.FIN2	169	17	61	6	150	10	2,81	0,840	0,036	0,096	0,004	0,022	0,0631	0,0032	619	20	591	21	700	110	84,4
7321-4 1T2__1521-1524	Zircon_sample-387.FIN2	442	57	188	42	1330	320	2,67	4,499	0,066	0,309	0,005	0,290	0,1058	0,0019	1731	12	1738	23	1728	33	100,6
7321-4 1T2__1521-1524	Zircon_sample-390.FIN2	282	28	70	7	110	8	4,12	0,544	0,065	0,065	0,004	0,778	0,0609	0,0057	440	44	404	24	620	210	65,2
7321-4 1T2__1521-1524	Zircon_sample-391.FIN2	248	40	139	32	348	72	1,87	0,823	0,049	0,099	0,003	0,261	0,0607	0,0052	609	27	608	18	610	190	99,7
7321-4 1T2__1521-1524	Zircon_sample-402.FIN2	236	11	55	6	75	7	4,44	0,369	0,054	0,053	0,002	0,162	0,0503	0,0076	318	40	335	13	190	320	176,3
7321-4 1T2__1521-1524	Zircon_sample-406.FIN2	188	7	67	6	290	62	2,89	1,510	0,140	0,138	0,005	0,828	0,0792	0,0049	933	58	835	28	1170	120	71,4
7321-4 1T2__1521-1524	Zircon_sample-414.FIN2	900	140	178	24	352	44	5,30	0,612	0,030	0,075	0,002	0,694	0,0593	0,0021	491	15	465	11	572	80	81,3
7321-4 1T2__1521-1524	Zircon_sample-415.FIN2	335	18	88	10	439	54	3,84	2,240	0,190	0,212	0,002	0,656	0,0766	0,0064	1193	59	1242	8,1	1110	160	111,9
7321-4 1T2__1521-1524	Zircon_sample-416.FIN2	616	64	27	6	111	28	24,70	0,974	0,044	0,117	0,002	0,624	0,0619	0,0030	700	28	715	11	660	100	108,3
7321-4 1T2__1521-1524	Zircon_sample-417.FIN2	1713	76	103	4	939	49	16,73	5,350	0,071	0,344	0,004	0,710	0,1123	0,0021	1877	11	1904	17	1837	34	103,6
7321-4 1T2__1521-1524	Zircon_sample-418.FIN2	694	26	425	43	465	26	1,62	0,311	0,015	0,044	0,001	0,937	0,0517	0,0021	275	12	277	4	266	96	104,1
7321-4 1T2__1521-1524	Zircon_sample-419.FIN2	1710	120	502	54	458	53	3,46	0,291	0,021	0,036	0,001	-0,579	0,0592	0,0053	259	17	227	5,1	560	190	40,5
7321-4 1T2__1521-1524	Zircon_sample-420.FIN2	345	24	83	12	419	55	4,21	2,966	0,053	0,219	0,005	0,972	0,0985	0,0020	1399	14	1274	25	1595	39	79,9
7321-4 1T2__1521-1524	Zircon_sample-430.FIN2	597	41	422	60	448	80	1,36	0,311	0,047	0,037	0,001	0,850	0,0607	0,0098	274	36	235	6,4	580	320	40,6
7321-4 1T2__1521-1524	Zircon_sample-431.FIN2	1280	170	370	340	730	440	4,70	0,578	0,043	0,072	0,000	0,834	0,0584	0,0045	463	28	448	0,45	540	170	82,9
7321-4 1T2__1521-1524	Zircon_sample-442.FIN2	210	13	30	2	148	15	7,03	2,047	0,095	0,188	0,001	0,322	0,0782	0,0040	1131	32	1110	5,7	1150	100	96,5
7321-4 1T2__1521-1524	Zircon_sample-443.FIN2	322	8	101	7	852	88	3,22	5,800	0,400	0,359	0,020	0,943	0,1176	0,0023	1945	59	1976	96	1920	35	102,9
7321-4 1T2__1521-1524	Zircon_sample-446.FIN2	609	23	139	8	934	66	4,45	3,830	0,120	0,272	0,006	0,771	0,1021	0,0032	1598	26	1552	28	1661	58	93,4
7321-4 1T2__1521-1524	Zircon_sample-447.FIN2	241	8	48	1	226	20	5,04	1,896	0,089	0,181	0,003	0,231	0,0761	0,0037	1079	31	1070	16	1091	98	98,1
7321-4 1T2__1521-1524	Zircon_sample-456.FIN2	279	20	197	14	466	43	1,42	0,771	0,041	0,098	0,003	0,073	0,0588	0,0047	590	29	601	18	540	180	111,3
7321-4 1T2__1521-1524	Zircon_sample-457.FIN2	104	11	56	12	413	89	1,92	4,078	0,082	0,305	0,010	0,185	0,0973	0,0014	1650	16	1715	52	1573	26	109,0
7321-4 1T2__1521-1524	Zircon_sample-458.FIN2	411	56	137	31	127	37	3,07	0,325	0,038	0,045	0,002	0,513	0,0522	0,0063	285	29	286	9,2	280	270	102,0
7321-4 1T2__1521-1524	Zircon_sample-459.FIN2	161	6	24	1	145	16	6,78	3,040	0,150	0,272	0,006	0,871	0,0812	0,0037	1416	37	1551	30	1224	90	126,7
7321-4 1T2__1521-1524	Zircon_sample-460.FIN2	584	82	273	52	1250	190	2,24	1,925	0,053	0,190	0,002	0,733	0,0735	0,0025	1090	18	1122	10	1027	69	109,3
7321-4 1T2__1521-1524	Zircon_sample-461.FIN2	478	12	156	7	762	55	3,13	2,035	0,095	0,192	0,003	0,371	0,0763	0,0037	1126	32	1133	16	1096	98	103,4
7321-4 1T2__1521-1524	Zircon_sample-462.FIN2	202	2	48	2	453	28	4,29	5,840	0,160	0,349	0,008	0,889	0,1219	0,0022	1953	24	1929	37	1983	31	97,3
7321-4 1T2__1521-1524	Zircon_sample-474.FIN2	676	82	179	35	321	56	3,84	0,523	0,036	0,066	0,001	0,326	0,0570	0,0044	427	24	414	6	480	180	86,2
7321-4 1T2__1521-1524	Zircon_sample-475.FIN2	214	13	54	3	70	11	3,88	0,356	0,035	0,048	0,002	0,036	0,0544	0,0061	308	27	300	13	360	240	83,3
7321-4 1T2__1521-1524	Zircon_sample-476.FIN2	722	64	173	17	175	32	4,18	0,290	0,030	0,043	0,002	0,665	0,0490	0,0036	258	24	271	11	150	160	180,7
7321-4 1T2__1521-1524	Zircon_sample-484.FIN2	246	23	96	22	106	24	2,75	0,313	0,020	0,045	0,002	0,758	0,0522	0,0028	276	15	281	14	280	120	100,4
7321-4 1T2__1521-1524	Zircon_sample-485.FIN2	148	6	33	2	73	21	4,57	0,640	0,080	0,082	0,003	0,779	0,0564	0,0057	501	51	509	17	450	240	113,1
7321-4 1T2__1521-1524	Zircon_sample-488.FIN2	176	8	44	3	66	38	4,03	0,540	0,420	0,052	0,002	0,245	0,0750	0,0550	410	240	327	15	600	1100	54,5
7321-4 1T2__1521-1524	Zircon_sample-489.FIN2	336	52	161	39	410	110	2,16	0,877	0,065	0,101	0,002	0,654	0,0642	0,0037	638	35	622	13	740	120	84,1
7321-4 1T2__1521-1524	Zircon_sample-498.FIN2	510	37	195	16	467	44	2,61	0,801	0,012	0,099	0,001	0,936	0,0588	0,0006	598	6,8	609	6,7	559	22	109,0
7321-4 1T2__1521-1524	Zircon_sample-499.FIN2	170	16	69	9	74	16	2,46	0,274	0,051	0,044	0,001	0,476	0,0450	0,0075	245	40	279	6,9	-10	320	-2788,0
7321-4 1T2__1521-1524	Zircon_sample-502.FIN2	296	50	100	27	102	29	3,07	0,328	0,029	0,044	0,002	0,621	0,0538	0,0039	288	23	278	13	350	160	79,4
7321-4 1T2__1521-1524	Zircon_sample-503.FIN2	731	93	284	63	386	58	2,69	0,367	0,019	0,052	0,001	0,307	0,0511	0,0023	317	14	327	6,1	240	110	136,1
7321-4 1T2__1521-1524	Zircon_sample-504.FIN2	1500	410	119	45	301	80	12,80	0,698	0,074	0,079	0,003	0,600	0,0642	0,0072	537	44	492	20	740	230	66,5
7321-4 1T2__1521-1524	Zircon_sample-512.FIN2	910	170	356	75	690	140	2,55	0,558	0,017	0,072	0,001	0,862	0,0561	0,0015	451	11	451	4,1	454	59	99,3
7321-4 1T2__1521-1524	Zircon_sample-515.FIN2	157	30	76	16	274	43	2,06	1,400	0,120	0,141	0,002	0,812	0,0724	0,0056	888	50	850	12	990	150	85,9
7321-4 1T2__1521-1524	Zircon_sample-526.FIN2	608	90	303	63	310	70	2,05	0,282	0,017	0,040	0,001	-0,295	0,0497	0,0030	252	14	251	5,3	170	130	147,5
7321-4 1T2__1521-1524	Zircon_sample-527.FIN2	582	53	179	28	372	63	3,13	0,611	0,023	0,078	0,002	0,638	0,0574	0,0015	484	14	482	14	527	69	91,5
7321-4 1T2__1521-1524	Zircon_sample-528.FIN2	870	370	325	37	319	21	2,80	0,265	0,021	0,038	0,001	0,393	0,0507	0,0036	238	17	239	8	220	160	108,7
7321-4 1T2__1521-1524	Zircon_sample-530.FIN2	262	14	73	7	129	20	3,60	0,566	0,019	0,072	0,001	0,923	0,0575	0,0022	455	12	446	8,2	507	86	88,0
7321-4 1T2__1521-1524	Zircon_sample-531.FIN2	750	120	251	55	275	52	3,06	0,285	0,010	0,044	0,001	0,063	0,0498	0,0037	254	8,3	274	6,8	170	160	161,3
7321-4 1T2__1521-1524	Zircon_sample-532.FIN2	550	100	194	54	185	40	2,90	0,276	0,039	0,040	0,002	0,457	0,0506	0,0067	247	31	250	11	220	290	113,6
Common-Pb corrected[f]																						
7321-4 1T2__1521-1524	Zircon_sample-263.FIN2	710	110	303	64	760	110	2,37	0,825	0,088	0,105	0,005	-0,579	0,0573	0,0083	610	50	642	29	490	340	131,0
7321-4 1T2__1521-1524	Zircon_sample-277.FIN2	1650	230	390	160	1260	390	4,60	1,390	0,100	0,142	0,008	0,991	0,0708	0,0014	884	43	857	47	950	41	90,2
7321-4 1T2__1521-1524	Zircon_sample-292.FIN2	720	170	268	79	507	93	2,70	0,558	0,025	0,072	0,001	0,188	0,0561	0,0024	450	16	449	12	452	96	99,3
7321-4 1T2__1521-1524	Zircon_sample-320.FIN2	1720	420	320	100	2420	480	5,66	4,840	0,350	0,315	0,027	0,992	0,1113	0,0016	1790	61	1770	130	1820	26	97,3
7321-4 1T2__1521-1524	Zircon_sample-348.FIN2	1080	120	306	63	1926	81	3,67	3,260	0,290	0,235	0,004	-0,207	0,1009	0,0096	1470	68	1362	19	1630	170	83,6
7321-4 1T2__1521-1524	Zircon_sample-359.FIN2	650	170	430	140	680	150	1,54	0,391	0,056	0,050	0,001	0,946	0,0566	0,0087	335	41	317	4	450	340	70,4
7321-4 1T2__1521-1524	Zircon_sample-374.FIN2	456	38	28	3	189	34	16,60	0,520	0,320	0,082	0,003	0,556	0,0460	0,0260	410	210	505	18	930	930	54,3
7321-4 1T2__1521-1524	Zircon_sample-400.FIN2	2870	300	633	79	1040	120	4,63	0,434	0,028	0,059	0,002	0,456	0,0534	0,0029	366	20	369	9,8	340	130	108,5
7321-4 1T2__1521-1524	Zircon_sample-401.FIN2	2147	70	2200	300	2490	170	1,00	0,345	0,025	0,047	0,001	0,593	0,0536	0,0034	301	19	295	5,1	350	140	84,2
7321-4 1T2__1521-1524	Zircon_sample-403.FIN2	1014	75	321	24	2840	230	3,23	9,750	0,450	0,403	0,016	0,963	0,1750	0,0014	2410	43	2180	75	2606	13	83,7
7321-4 1T2__1521-1524	Zircon_sample-471.FIN2	1350	130	380	130	400	130	4,20	0,262	0,019	0,038	0,001	0,551	0,0491	0,0038	236	15	242	5	300	130	80,7
7321-4 1T2__1521-1524	Zircon_sample-513.FIN2	362	83	138	45	210	49	2,71	0,380	0,150	0,049	0,001	0,969	0,0570	0,0210	320	110	306	5,2	1020	480	30,0
7321-4 1T2__1521-1524	Zircon_sample-529.FIN2	531	31	217	7	300	67	2,43	0,281	0,087	0,046	0,001	0,936	0,0440	0,0140	249	70	289	5,3	650	650	44,5

Fig. 7.4 Appendix 4

8 REFERENCES

Anell, I., Faleide, J.-I., & Braathen, A. (2016). Regional tectono-sedimentary development of the highs and basins of the northwestern Barents Shelf. *Norwegian Journal of Geology*, 96 (1), 27-41. https://doi.org/10.17850/njg96-1-04

Anfinson, O. A., Leier, A. L., Embry, A. F., & Dewing, K. (2012). Detrital zircon geochronology and provenance of the Neoproterozoic to Late Devonian Franklinian Basin, Canadian Arctic Islands. *Geological Society of America Bulletin*, *124*(3–4), 415–430. https://doi.org/10.1130/B30503.1

Blaich, O. A., Tsikalas, F., & Faleide, J. I. (2017). New insights into the tectono-stratigraphic evolution of the southern Stappen High and its transition to Bjørnøya Basin, SW Barents Sea. *Marine and Petroleum Geology*, *85*, 89–105. https://doi.org/10.1016/j.marpetgeo.2017.04.015

Bryn, B. K. L., Ahokas, J., Patruno, S., Schjelderup, S., Hinna, C., Lowrey, C., & Escalona, A. (2019). Exploring the reservoir potential of Lower Cretaceous Clinoforms in the Fingerdjupet Subbasin, Norwegian Barents Sea. *Basin Research*, *32*(2), 332–347. https://doi.org/10.1111/bre.12407

Bue, E.P, & Andresen, A. (2013). Constraining depositional models in the Barents Sea region using detrital zircon U–Pb data from Mesozoic sediments in Svalbard. *Geological Society, London, Special Publications*, *386*(1), 261–279. https://doi.org/10.1144/SP386.14

Corfu, F., Andersen, T. B., & Gasser, D. (2014). The Scandinavian Caledonides: Main features, conceptual advances and critical questions. *Geological Society, London, Special Publications*, *390*(1), 9–43. https://doi.org/10.1144/SP390.25

Corfu, F., Polteau, S., Planke, S., Faleide, J. I., Svensen, H., Zayoncheck, A., & Stolbov, N. (2013). U–Pb geochronology of Cretaceous magmatism on Svalbard and Franz Josef Land, Barents Sea Large Igneous Province. *Geological Magazine*, *150*(6), 1127–1135. https://doi.org/10.1017/S0016756813000162

Dalland, A., Worsley, D., Ofstad, K., (1988). A lithostratigraphic scheme for the mesozoic and cenozoic succession offshore Norway north of 62 N. NPD Bulletin. 4,67.

Dewing, K., Mayr, U., Harrison, J.C., and de Freitas, T. (2008). Upper Neoproterozoic to Lower Devonian stratigraphy of northeast Ellesmere Island. *In* Geology of northeast Ellesemere Island adjacent to Kane Basin and Kennedy Channel, Nunavut. *Edited by* U. Mayr. Geological Survey of Canada, Bulletin 592, 31–108

Doré, A. G. (1991). The structural foundation and evolution of Mesozoic seaways between Europe and the Arctic. *Palaeogeography, Palaeoclimatology, Palaeoecology*, *87*(1–4), 441–492. https://doi.org/10.1016/0031-0182(91)90144-G

Faleide, J. I., Vågnes, E., & Gudlaugsson, S. T. (1993). Late Mesozoic–Cenozoic evolution of the southwestern Barents Sea. *Geological Society, London, Petroleum Geology Conference Series*, *4*(1), 933–950. https://doi.org/10.1144/0040933

Faleide, J. I., Bjørlykke, K., & Gabrielsen, R. H. (2010). Geology of the Norwegian Continental Shelf. In K. Bjorlykke, *Petroleum Geoscience* (s. 467–499). Springer Berlin Heidelberg. https://doi.org/10.1007/978-3-642-02332-3_22

Faleide, J. I., Bjørlykke, K., & Gabrielsen, R. H. (2015). Geology of the Norwegian Continental Shelf. In K. Bjørlykke (Red.), *Petroleum Geoscience* (s. 603–637). Springer Berlin Heidelberg. https://doi.org/10.1007/978-3-642-34132-8_25

Faleide, T. S., Midtkandal, I., Planke, S., Corseri, R., Faleide, J. I., Serck, C. S., & Nystuen, J. P. (2019). Characterisation and development of Early Cretaceous shelf platform deposition and faulting in the Hoop area, southwestern Barents Sea—Constrained by high-resolution seismic data. *Norwegian Journal of Geology*, 99(3),1-20. https://doi.org/10.17850/njg99-3-7

Gabrielsen, R. H. (1990). *Structural elements of the Norwegian continental shelf. Part 1: The Barents Sea Region*. Oljedirektoratet.

Gasser, D. (2014). The Caledonides of Greenland, Svalbard and other Arctic areas: Status of research and open questions. *Geological Society, London, Special Publications*, *390*(1), 93–129. https://doi.org/10.1144/SP390.17

Gasser, D., & Andresen, A. (2013). Caledonian terrane amalgamation of Svalbard: Detrital zircon provenance of Mesoproterozoic to Carboniferous strata from Oscar II Land, western Spitsbergen. *Geological Magazine*, *150*(6), 1103–1126. https://doi.org/10.1017/S0016756813000174

Gee, D. (2015). Caledonides of Scandinavia, Greenland, and Svalbard. In *Reference Module in Earth Systems and Environmental Sciences*. Elsevier. https://doi.org/10.1016/B978-0-12-409548-9.09133-8

Gee, D., Fossen, H., Henriksen, N., & Higgins, A. K. (2008). From the Early Paleozoic Platforms of Baltica and Laurentia to the Caledonide Orogen of Scandinavia and Greenland. *Episodes*, *31*(1), 44–51. https://doi.org/10.18814/epiiugs/2008/v31i1/007

Gee, D., & Teben'kov, A. M. (2004). Svalbard: A fragment of the Laurentian margin. *Geological Society, London, Memoirs*, *30*(1), 191–206. https://doi.org/10.1144/GSL.MEM.2004.030.01.16

Gernigon, L., & Brönner, M. (2012). Late Palaeozoic architecture and evolution of the southwestern Barents Sea: Insights from a new generation of aeromagnetic data. *Journal of the Geological Society*, *169*(4), 449–459. https://doi.org/10.1144/0016-76492011-131

Gjelberg, J., & Steel, R. J. (1995). Helvetiafjellet formation (Barremian-Aptian), Spitsbergen: Characteristics of a transgressive succession. *Norwegian Petroleum Society Special Publications*, pp.571–593. Elsevier. https://doi.org/10.1016/S0928-8937(06)80087-1

Gjelberg, J. & Steel, R. (2012). Depositional model for the lower Cretaceous HelvetiafjelletFormation on Svalbard, diachronous vs layer-cake models. *Norwegian Journal of Geology*, 92, 41-54

Glørstad-Clark, E. (2011). Basin analysis in western Barents Sea area: The interplay between accommodation space and depositional system (PhD thesis). University of Oslo, Oslo.

Gradstein, F. M., Anthonissen, E., Brunstad, H., Charnock, M., Hammer, O., Hellem, T., & Lervik, K. S. (2010). Norwegian Offshore Stratigraphic Lexicon (NORLEX). *Newsletters on Stratigraphy*, *44*(1), 73–86. https://doi.org/10.1127/0078-0421/2010/0005

Grantz, A., Hart, P. E., & Childers, V. A. (2011). Chapter 50 Geology and tectonic development of the Amerasia and Canada Basins, Arctic Ocean. *Geological Society, London, Memoirs*, *35*(1), 771–799. https://doi.org/10.1144/M35.50

Grundvåg, S.-A., Marin, D., Kairanov, B., Śliwińska, K. K., Nøhr-Hansen, H., Jelby, M. E., ... Olaussen, S. (2017). The Lower Cretaceous succession of the northwestern Barents Shelf: Onshore and offshore correlations. *Marine and Petroleum Geology*, *86*, 834–857. https://doi.org/10.1016/j.marpetgeo.2017.06.036

Gudlaugsson, S. T., Faleide, J. I., Johansen, S. E., & Breivik, A. J. (1998). Late Palaeozoic structural development of the South-western Barents Sea. *Marine and Petroleum Geology*, *15*(1), 73–102. https://doi.org/10.1016/S0264-8172(97)00048-2

Hadlari, T., Davis, W. J., Dewing, K., Heaman, L. M., Lemieux, Y., Ootes, L., ... Pyle, L. J. (2012). Two detrital zircon signatures for the Cambrian passive margin of northern Laurentia highlighted by new U-Pb results from northern Canada. *Geological Society of America Bulletin*, *124*(7–8), 1155–1168. https://doi.org/10.1130/B30530.1

Hellman, F. J., Gee, D. G., & Witt-Nilsson, P. (2001). Late Archean basement in the Bangenhuken Complex of the Nordbreen Nappe, western Ny-Friesland, Svalbard. *Polar Research*, *20*(1), 49–59. https://doi.org/10.3402/polar.v20i1.6499

Henriksen, E., Ryseth, A. E., Larssen, G. B., Heide, T., Rønning, K., Sollid, K., & Stoupakova, A. V. (2011). Chapter 10 Tectonostratigraphy of the greater Barents Sea: Implications for petroleum systems. *Geological Society, London, Memoirs*, *35*(1), 163–195. https://doi.org/10.1144/M35.10

Higgins, A.K. & Gilotti, J. & Smith, M.P. (2008). The Greenland Caledonides. Evolution of the Northeast Margin of Laurentia. *Geological Society of America Memoir*, 202. https://doi.org/10.1130/MEM202

Hinna, C. H. (2016). Seismic characterization of lower Cretaceous Clinoform packages in the Fingerdjupet sub-basin, southwestern Barents sea (MSc Thesis). University of Stavanger, Stavanger.

Hölttä, P., Heilimo, E., Huhma, H., Juopperi, H, Kontinen, A., Konnunaho, H., ... & Sorjonen-Ward, P. (2012). Archaean complexes of the Karelia Province in Finland. Geological Survey of Finland. Special Paper. 54. 7-20.

Hurum, J., Roberts, A., Dyke, G., Grundvåg, S-A., Nakrem, H., Midtkandal, I., .Olaussen, S. (2016). Bird or maniraptoran dinosaur? A femur from the Albian strata of Spitsbergen. *Palaeontologia Polonica,* 67, 137-147.

Indrevær, K., Gabrielsen, R. H., & Faleide, J. I. (2016). Early Cretaceous synrift uplift and tectonic inversion in the Loppa High area, southwestern Barents Sea, Norwegian shelf. *Journal of the Geological Society*, *174*(2), 242–254. https://doi.org/10.1144/jgs2016-066

Indrevær, K., Gac, S., Gabrielsen, R. H., & Faleide, J. I. (2017). Crustal-scale subsidence and uplift caused by metamorphic phase changes in the lower crust: A model for the evolution of the Loppa High area, SW Barents Sea from late Paleozoic to Present. *Journal of the Geological Society*, *175*(3), 497–508. https://doi.org/10.1144/jgs2017-063

Jakobsson, M., Mayer, L., Coakley, B., Dowdeswell, J. A., Forbes, S., Fridman, B., … Weatherall, P. (2012). The International Bathymetric Chart of the Arctic Ocean (IBCAO) Version 3.0: IBCAO VERSION 3.0. *Geophysical Research Letters*, *39*. https://doi.org/10.1029/2012GL052219

Johansson, Å., Gee, D. G., Björklund, L., & Witt-Nilsson, P. (1995). Isotope studies of granitoids from the Bangenhuk Formation, Ny Friesland Caledonides, Svalbard. *Geological Magazine*, *132*(3), 303–320. https://doi.org/10.1017/S0016756800013625

Kairanov, B., Escalona, A., Mordasova, A., Śliwińska, K., & Suslova, A. (2018). Early Cretaceous tectonostratigraphic evolution of the north central Barents Sea. *Journal of Geodynamics*, *119*, 183–198. https://doi.org/10.1016/j.jog.2018.02.009

Kalsbeek, F., Higgins, A. K., Jepsen, H. F., Frei, R., & Nutman, A. P. (2008). Granites and granites in the East Greenland Caledonides. In *Memoir 202: The Greenland Caledonides: Evolution of the Northeast Margin of Laurentia* (P. 227–249). Geological Society of America. https://doi.org/10.1130/2008.1202(09)

Kalsbeek, F., Nutman, A. P., Escher, J. C., Friderichsen, J. D., Hull, J. M., Jones, K. A., & Schack Pedersen, S. A. (1999). Geochronology of granitic and supracrustal rocks from the northern part of the East Greenland Caledonides: Ion microprobe U–Pb zircon ages. *GEUS Bulletin*, 31–48. https://doi.org/10.34194/ggub.v184.5228

Kirkland, C. L., Pease, V., Whitehouse, M. J., & Ineson, J. R. (2009). Provenance record from Mesoproterozoic-Cambrian sediments of Peary Land, North Greenland: Implications for the ice-covered Greenland Shield and Laurentian palaeogeography. *Precambrian Research*, *170*(1–2), 43–60. https://doi.org/10.1016/j.precamres.2008.11.006

Klausen, T. G., Müller, R., Sláma, J., Olaussen, S., Rismyhr, B., & Helland-Hansen, W. (2017). Depositional history of a condensed shallow marine reservoir succession: Stratigraphy and detrital zircon geochronology of the Jurassic Stø Formation, Barents Sea. *Journal of the Geological Society*, *175*(1), 130–145. https://doi.org/10.1144/jgs2017-024

Korago, E. A., Kovaleva, G. N., Lopatin, B. G., & Orgo, V. V. (2004). The Precambrian rocks of Novaya Zemlya. *Geological Society, London, Memoirs*, *30*(1), 135–143. https://doi.org/10.1144/GSL.MEM.2004.030.01.12

Kośmińska, K., Majka, J., Mazur, S., Krumbholz, M., Klonowska, I., Manecki, M., ... Dwornik, M. (2014). Blueschist facies metamorphism in Nordenskiöld Land of west-central Svalbard. *Terra Nova*, *26*(5), 377–386. https://doi.org/10.1111/ter.12110

Köykkä, J., Lahtinen, R., & Huhma, H. (2019). Provenance evolution of the Paleoproterozoic metasedimentary cover sequences in northern Fennoscandia: Age distribution, geochemistry, and zircon morphology. *Precambrian Research*, *331*, 105364. https://doi.org/10.1016/j.precamres.2019.105364

Lahtinen, R., Huhma, H., Kontinen, A., Kohonen, J., & Sorjonen-Ward, P. (2010). New constraints for the source characteristics, deposition and age of the 2.1–1.9Ga metasedimentary cover at the western margin of the Karelian Province. *Precambrian Research*, *176*(1–4), 77–93. https://doi.org/10.1016/j.precamres.2009.10.001

LOCRA Final Report. (2017). LoCRA: Lower Cretaceous clastic wedges. An under-explored play in the Artic. A multi-university collaboration. University of Stavanger and University Centre in Svalbard, Norway, internal report, 129.

Lorenz, H., Pystin, A. M., Olovyanishnikov, V. G., & Gee, D. G. (2004). Neoproterozoic high-grade metamorphism of the Kanin Peninsula, Timanide Orogen, northern Russia. *Geological Society, London, Memoirs*, *30*(1), 59–68. https://doi.org/10.1144/GSL.MEM.2004.030.01.06

Ludwig, K. R. (1998). On the Treatment of Concordant Uranium-Lead Ages. *Geochimica et Cosmochimica Acta*, *62*(4), 665–676. https://doi.org/10.1016/S0016-7037(98)00059-3

Maher, H. D. (2001). Manifestations of the Cretaceous High Arctic Large Igneous Province in Svalbard. *The Journal of Geology*, *109*(1), 91–104. https://doi.org/10.1086/317960

Majka, J., Be'Eri-Shlevin, Y., Gee, D. G., Czerny, J., Frei, D., & Ladenberger, A. (2014). Torellian (*c*. 640 Ma) metamorphic overprint of Tonian (*c*. 950 Ma) basement in the Caledonides of southwestern Svalbard. *Geological Magazine*, *151*(4), 732–748. https://doi.org/10.1017/S0016756813000794

Majka, J., Czerny, J., Mazur, S., Holm, D. K., & Manecki, M. (2010). Neoproterozoic metamorphic evolution of the Isbjørnhamna Group rocks from south-western Svalbard: Neoproterozoic metamorphism in southern Svalbard. *Polar Research*, *29*(3), 250–264. https://doi.org/10.1111/j.1751-8369.2010.00186.x

Malone, S. J., McClelland, W. C., von Gosen, W., & Piepjohn, K. (2017). The earliest Neoproterozoic magmatic record of the Pearya terrane, Canadian high Arctic: Implications for Caledonian terrane reconstructions. *Precambrian Research*, *292*, 323–349. https://doi.org/10.1016/j.precamres.2017.01.006

Marín, D., Escalona, A., Grundvåg, S.-A., Olaussen, S., Sandvik, S., & Śliwińska, K. K. (2018). Unravelling key controls on the rift climax to post-rift fill of marine rift basins: Insights from 3D seismic analysis of the Lower Cretaceous of the Hammerfest Basin, SW Barents Sea. *Basin Research*, *30*(4), 587–612. https://doi.org/10.1111/bre.12266

Marin, D., Escalona, A., Śliwińska, K. K., Nøhr-Hansen, H., & Mordasova, A. (2017). Sequence stratigraphy and lateral variability of Lower Cretaceous clinoforms in the southwestern Barents Sea. *AAPG Bulletin*, *101*(09), 1487–1517. https://doi.org/10.1306/10241616010

McClelland, W. C., von Gosen, W., & Piepjohn, K. (2019). Tonian and Silurian magmatism in Nordaustlandet: Svalbard's place in the Caledonian orogen. In Piepjohn K.,, Strauss, J.V., Reinhardt, L. & McClelland, W.C. *Circum-Arctic Structural Events: Tectonic Evolution of the Arctic Margins and Trans-Arctic Links with Adjacent Orogens*. Geological Society of America. https://doi.org/10.1130/2018.2541(04)

Midtkandal, I., & Nystuen, J. P. (2009). Depositional architecture of a low-gradient ramp shelf in an epicontinental sea: The lower Cretaceous of Svalbard. *Basin Research*, *21*(5), 655–675. https://doi.org/10.1111/j.1365-2117.2009.00399.x

Midtkandal, I., Nystuen, J.P., Nagy, J. & Mørk, A., 2008. Lower Cretaceous lithostratigraphy across a regional subaerial unconformity in Spitsbergen: the Rurikfjellet and Helvetiafjellet formations. *Norwegian Journal of Geology*, 88, 287-304.

Midtkandal, I., Faleide, T. S., Faleide, J. I., Planke, S., Anell, I., & Nystuen, J. P. (2019). Nested intrashelf platform clinoforms—Evidence of shelf platform growth exemplified by Lower Cretaceous strata in the Barents Sea. *Basin Research*, *32*(2), 216–223. https://doi.org/10.1111/bre.12377

Midtkandal, I., Svensen, H. H., Planke, S., Corfu, F., Polteau, S., Torsvik, T. H., ... Olaussen, S. (2016). The Aptian (Early Cretaceous) oceanic anoxic event (OAE1a) in Svalbard, Barents Sea, and the absolute age of the Barremian-Aptian boundary. *Palaeogeography, Palaeoclimatology, Palaeoecology*, *463*, 126–135. https://doi.org/10.1016/j.palaeo.2016.09.023

Midtkandal, I., Nystuen, J.P., Nagy, J., Mørk, A., (2008). Lower Cretaceous lithostratigraphy across a regional subaerial unconformity in Spitsbergen: the Rurikfjellet and Helvetiafjellet formations. *Norwegian Journal of Geology*. 88, 287-304.

Mørk, A., Dallmann, A., Dypvik, H., Johannessen, E., Larssen, G., Nøttvedt, N., ... Worsley, D. (1999), Mesozoic lithostratigraphy, in W. K. Dallmann, ed., Lithostratigraphic lexicon of Svalbard. Upper Palaeozoic to Quaternary bedrock. Review and recommendations for nomenclature use: Tromsø, Norway, Norsk Polarinstitut, 127–214.

Norwegian Petroleum Directorate (NPD). (2020). Factpages (online). Available 4.05.2020.

Nøhr-Hansen, H., Piasecki, S., & Alsen, P. (2019). A Cretaceous dinoflagellate cyst zonation for NE Greenland. *Geological Magazine*, 1–35. https://doi.org/10.1017/S0016756819001043

Onderdonk, N., & Midtkandal, I. (2010). Mechanisms of collapse of the cretaceous helvetiafjellet formation at Kvalvågen, eastern Spitsbergen. *Marine and Petroleum Geology*, *27*(10), 2118–2140. https://doi.org/10.1016/j.marpetgeo.2010.09.004

Patruno, S., Hampson, G. J., & Jackson, C. A.-L. (2015). Quantitative characterisation of deltaic and subaqueous clinoforms. *Earth-Science Reviews*, *142*, 79–119. https://doi.org/10.1016/j.earscirev.2015.01.004

Patruno, S., & Helland-Hansen, W. (2018). Clinoforms and clinoform systems: Review and dynamic classification scheme for shorelines, subaqueous deltas, shelf edges and continental margins. *Earth-Science Reviews*, *185*, 202–233. https://doi.org/10.1016/j.earscirev.2018.05.016

Pease, V. (2011). Chapter 20 Eurasian orogens and Arctic tectonics: An overview. *Geological Society, London, Memoirs*, *35*(1), 311–324. https://doi.org/10.1144/M35.20

Pease, V., Drachev, S., Stephenson, R., & Zhang, X. (2014). Arctic lithosphere—A review. *Tectonophysics*, *628*, 1–25. https://doi.org/10.1016/j.tecto.2014.05.033

Pettersson, C. H., Tebenkov, A. M., Larionov, A. N., Andresen, A., & Pease, V. (2009). Timing of migmatization and granite genesis in the Northwestern Terrane of Svalbard, Norway: Implications for regional correlations in the Arctic Caledonides. *Journal of the Geological Society*, *166*(1), 147–158. https://doi.org/10.1144/0016-76492008-023

Petrov, O.V., Sobolev, N.N., Koren, T.N., Vasiliev, V.E., Petrov, E.O., Larssen, G.B. & Smelror, M. (2008). Palaeozoic and Early Mesozoic evolution of the East Barents and Kara Seas sedimentary basins. *Norwegian Journal of Geology*, 88, 227-234.

Petrov, O., Morozov, A., Shokalsky, S., Kashubin, S., Artemieva, I., Sobolev, N., ... Smelror, M. (2016). Crustal structure and tectonic model of the Arctic region. *Earth-Science Reviews,* 154, 29-71.

Piepjohn, K., & von Gosen, W. (2017). Structural transect through Ellesmere Island (Canadian Arctic): Superimposed Palaeozoic Ellesmerian and Cenozoic Eurekan deformation. *Geological Society, London, Special Publications*, *460*(1), 33–56. https://doi.org/10.1144/SP460.5

Porębski, S. J., & Steel, R. J. (2003). Shelf-margin deltas: Their stratigraphic significance and relation to deepwater sands. *Earth-Science Reviews*, *62*(3–4), 283–326. https://doi.org/10.1016/S0012-8252(02)00161-7

Ritzmann, O., & Faleide, J. I. (2009). The crust and mantle lithosphere in the Barents Sea/Kara Sea region. *Tectonophysics*, *470*(1–2), 89–104. https://doi.org/10.1016/j.tecto.2008.06.018

Roberts, D., & Gee, D.G. (1985). An introduction to the structure of the Scandinavian Caledonides, in Gee, D.G., and Sturt, B.A., editors., The Caledonide Orogen—Scandinavia and related areas (pp.55–68). Chichester: John Wiley & Sons.

Røhr, T. S. & Andersen, T. (2009). Detrital zircons from the high Arctic; evidence for extensive recycling of sediment from Devonian through Mesozoic times. In: Røhr, T. S. (ed.) Sedimentary Provenance Analysis of Lower Cretaceous Sedimentary Successions in The Arctic; Constraints From Detrital Zircon data. PhD thesis, Faculty of Mathematics and Natural Sciences, University of Oslo, Oslo, 55–105.

Røhr, T. S., Andersen, T., & Dypvik, H. (2008). Provenance of Lower Cretaceous sediments in the Wandel Sea Basin, North Greenland. *Journal of the Geological Society*, *165*(3), 755–767. https://doi.org/10.1144/0016-76492007-102

Røhr, T. S., Andersen, T., Dypvik, H., & Embry, A. F. (2010). Detrital zircon characteristics of the Lower Cretaceous Isachsen Formation, Sverdrup Basin: Source constraints from age and Hf isotope data. *Canadian Journal of Earth Sciences*, *47*(3), 255–271. https://doi.org/10.1139/E10-006

Sandelin, S., Tebenkov, A. M., & Gee, D. G. (2001). The stratigraphy of the lower part of the Neoproterozoic Murchisonfjorden Supergroup in Nordaustlandet, Svalbard. *GFF*, *123*(2), 113–127. https://doi.org/10.1080/11035890101232113

Seldal, J. (2005). Lower Cretaceous: The next target for oil exploration in the Barents Sea? *Geological Society, Petroleum Geology Conference Series*, *6*(1), 231–240. https://doi.org/10.1144/0060231

Serck, C. S., Faleide, J. I., Braathen, A., Kjølhamar, B., & Escalona, A. (2017). Jurassic to Early Cretaceous basin configuration(s) in the Fingerdjupet Subbasin, SW Barents Sea. *Marine and Petroleum Geology*, *86*, 874–891. https://doi.org/10.1016/j.marpetgeo.2017.06.044

Smelror, M., Mørk, A., Monteil, E., Rutledge, D., & Leereveld, H. (1998). The Klippfisk Formation - a new lithostratigraphic unit of Lower Cretaceous platform carbonates on the Western Barents Shelf. *Polar Research*, *17*(2), 181–202. https://doi.org/10.1111/j.1751-8369.1998.tb00271.x

Smelror, M., Petrov, O., Larssen, G-B & Werner, S.C.. (2009). ATLAS: Geological History of the Barents Sea. Geological Survey of Norway.

Smith, M. P., & Rasmussen, J. A. (2008). Cambrian–Silurian development of the Laurentian margin of the Iapetus Ocean in Greenland and related areas. I *Memoir 202: The Greenland Caledonides: Evolution of the Northeast Margin of Laurentia* (pp.137–167). Geological Society of America. https://doi.org/10.1130/2008.1202(06)

Steel, R., Mellere, D., Plink-Bjorklund, P., Crabaugh, Deibert, J., Loeseth & Shellpeper. (2000). Deltas vs. Rivers on the Shelf Edge: Their Relative Contributions to the Growth of Shelf-Margins and Basin-Floor Fans (Barremian and Eocene, Spitsbergen). GCSSEPM Special Publication. 20. 981-1009. 10.5724/gcs.00.15.0981.

Torsvik, T.H., Carlos, D., Mosar, J., Cocks, L.R.M. & Malme, T. (2002). Global reconstructions and North Atlantic palaeogeography 400 Ma to Recent. In: Eide, E.A. (coord.). BATLAS – Mid Norway plate reconstructions atlas with global and Atlantic perspectives. Geological Survey of Norway, 18-39.

Torsvik, T. H., Van der Voo, R., Preeden, U., Mac Niocaill, C., Steinberger, B., Doubrovine, P. V., ... Cocks, L. R. M. (2012). Phanerozoic polar wander, palaeogeography and dynamics. *Earth-Science Reviews*, *114*(3–4), 325–368. https://doi.org/10.1016/j.earscirev.2012.06.007

Trettin, H. P. (Red.). (1991). Geology of the Innuitian Orogen and Arctic Platform of Canada and Greenland. *Geological Society of Americ,* 3, 569. https://doi.org/10.1130/DNAG-GNA-E

Vickers, M. L., Price, G. D., Jerrett, R. M., & Watkinson, M. (2016). Stratigraphic and geochemical expression of Barremian–Aptian global climate change in Arctic Svalbard. *Geosphere*, *12*(5), 1594–1605. https://doi.org/10.1130/GES01344.

Vigran, J. O. (2014). *Palynology and geology of the Triassic succession of Svalbard and the Barents Sea*. Norges geologiske undersoekelse.

Witt-Nilsson, P., Gee, D. G. & Hellman, F. J. (1998). Tectonostratigraphy of the Caledonian. Atomfjella Antiform of northem Ny Friesland, Svalbard. *Norwegian Journal of Geology*, 78, 67-80. Oslo.

Worsley, D. (2008). The post-Caledonian development of Svalbard and the western Barents Sea. *Polar Research*, *27*(3), 298–317. https://doi.org/10.1111/j.1751-8369.2008.00085.x

Worsley, D., Agdestein, T., Gjelberg, J., Kirkemo, K., Mørk, A., Nilsson, I., ... Nilsson, A. (2001). The geological evolution of Bjørnøya, Arctic Norway: Implications for the Barents Shelf. *Norwegian Journal of Geology,* 81, 195-234.

Århus, N., Kelly, S. R. A., Collins, J. S. H., & Sandy, M. R. (1990). Systematic palaeontology and biostratigraphy of two Early Cretaceous condensed sections from the Barents Sea. *Polar Research*, *8* (2), 165–194. https://doi.org/10.1111/j.1751-8369.1990.tb00383.x